THE APPLICATION OF INVERSE METHODS TO PROBLEMS IN OCEAN CIRCULATION

by

DEAN HOWARD ROEMMICH

B.A., Swarthmore College
(1970)

SUBMITTED IN PARTIAL FULFILLMENT
OF THE REQUIREMENTS FOR THE
DEGREE OF

DOCTOR OF PHILOSOPHY

at the

MASSACHUSETTS INSTITUTE OF TECHNOLOGY

and the

WOODS HOLE OCEANOGRAPHIC INSTITUTION

October, 1979
(i.e. February, 1980)

Signature of Author _____
Joint Program in Oceanography, Massachusetts Institute of Technology - Woods Hole Oceanographic Institution, and Department of Earth and Planetary Sciences, and Department of Meteorology, Massachusetts Institute of Technology, October, 1979.

Certified by _____
Thesis Supervisor

Accepted by _____
Chairman, Joint Oceanography Committee in Earth Sciences, Massachusetts Institute of Technology - Woods Hole Oceanographic Institution

THE APPLICATION OF INVERSE METHODS TO PROBLEMS IN OCEAN CIRCULATION

by

DEAN HOWARD ROEMMICH

Submitted to the Massachusetts Institute of Technology - Woods Hole Oceanographic Institution Joint Program in Oceanography on October 24, 1979 in partial fulfillment of the requirements for the Degree of Doctor of Philosophy

ABSTRACT

The inverse method of estimating ocean circulation from hydrographic data (Wunsch, 1977, 1978) is examined with particular attention to the problem of scale resolution. The method applies conservation constraints, which may be imposed on mass, salt, or other quantities, in a number of distinct layers separated by surfaces of constant potential density. These constraints are used to find a geostrophic flow field which is the product of a known linear resolution operator on the unknown hydrographic station grid scale field of absolute velocity. One may apply this operator to a single reference level, and then combine the smooth reference level field with grid scale relative velocity, or apply the operator at all levels to obtain a unique smooth field. Two simple hypothetical examples are analyzed in detail in order to ilustrate why some features of a flow field are uniquely determined, and to explain how such features can be anticipated and identified in real problems.

Three applications of the method are presented, using historical hydrographic data from the Atlantic Ocean. The Caribbean Sea provides a well resolved problem because of the high quality data set and strong constraints imposed by topography in the basin and adjoining passages. The resolution operator is local in space (compact resolution), conserves transport, and has fairly low sensitivity to noise. Scales as fine as about 50 kilometers are resolved in the Windward Passage and the Florida Straits, with coarser resolution of several hundred kilometers in the interior of the Caribbean. The estimated transport of 29 x $10^6 m^3$/sec leaving the western Caribbean is in agreement with direct measurements. Out of this total, 22 x $10^6 m^3$/sec flows across the eastern Caribbean and the remaining 7 x $10^6 m^3$/sec enters through the Windward Passage.

In the second application, the Wunsch type inverse is applied to an area formed by the perimeter of the Gulf Stream '60 hydrographic data. The resolution is inadequate to determine the deep structure and transport of the Gulf Stream and nearby energetic features. A second calculation is made using additional vorticity conservation constraints on the entire three dimensional data set in order to obtain a more highly resolved problem. Some crude approximations are necessary in the vorticity balance because the data do not adequately resolve the energetic features and contain no information in the time domain. The

resulting snapshot of horizontal velocity shows a Gulf Stream that does not, in general, penetrate to the bottom below the high velocity core. There are, however, energetic deep features nearby, with eastward velocities of order 20 cm/sec at 4000 meters, whose identification as part of the Gulf Stream or as local eddies is ambiguous.

The final problem is to estimate the meridional heat flux in the North Atlantic at 24°N, 36°N, and 48°N. As anticipated, the resolution is rather coarse and spatially variable, with typical scales of 2000 kilometers or more. At 24°N, the resolution is compact. The net geostrophic transport of individual layers is well determined at this latitude to within about $2 \times 10^6 m^3/sec$, and it is found that the layer transports serve to determine the geostrophic heat flux, which is estimated to be 90×10^{13} watts. Solutions at 36°N and 48°N are more poorly resolved. The essential difference at 24°N is the confinement of the Florida Current to the shallow Straits of Florida, with a known volume transport.

Thesis advisor: Carl Wunsch
Chairman, Department of Earth and Planetary Sciences
Massachusetts Institute of Technology

Table of Contents

Chapter I

A. Introduction

This thesis examines the applicability of linear inverse theory to problems in ocean circulation through a series of examples. The method was proposed as being appropriate to the study of ocean circulation by Wunsch(1977,1978), who used it on a hydrographic dataset from the northwest Atlantic. Wunsch's study established that a multiplicity of solutions were consistent with the hydrography that he used, with some examples to illustrate the diversity of possible solutions.

A number of important questions about the method formed the motivation for this work. First, how much more information could be drawn from the data, either by refined data handling techniques or through the imposition of additional constraints? Second, given the strongly underdetermined nature of the problem studied by Wunsch (1978), were there areas where a better determination could be obtained? One might imagine (and later in this chapter a simple example will be given) that hydrography and topography could combine to restrict the admissible solutions to a fairly narrow range. One would like to know to what extent the range of admissible solutions can be decreased through the addition of data in a given area or through coupling to other areas. A most important problem, which will be dealt with in each of the applications, is to identify and interpret quantities that are fully determined by the constraints. This work is about ocean circulation, and an evaluation of the success of the method rests on how much is learned about the ocean.

Chapter I gives a brief review of classical techniques of analysis of ocean circulation followed by a summary of the inverse method formalism as it applies to this problem. This summary is given for the sake of completeness, and it repeats results that are described more fully in other work on inverse methods such as Wiggins (1972) and Wunsch (1978). The linear algebra may be unfamiliar to some readers and it is hoped that this will not obscure the underlying simplicity of the technique. Two simple examples are analyzed in some detail, with the intent of demonstrating the principles that can be applied to the more complex problems of the real ocean.

The applications are presented in chapters II, III, and IV in the order in which they were computed. The Caribbean Sea was considered first because it was felt that this region, with its strong topographic constraints and an excellent dataset, would give a clean, unambiguous result. Chapter II describes the solution in that area. Next, it was decided to test the limits of resolution which could be obtained by imposing additional dynamical constraints. Chapter III uses the dense Gulf Stream '60 hydrographic survey for this purpose and a formulation of the inverse problem which is much like the β-spiral method of Stommel and Schott (1977). Chapter IV goes to the opposite extreme in spatial scales. Zonal sections of the Atlantic from the IGY are used to estimate the net transport of heat in the ocean across latitude circles. The three problems are quite distinctive and each presents some unique features of interest.

B. Background

Classical methods of studying the general circulation using hydrographic data can be roughly divided into two main categories. One of these is water mass analysis or property analysis. It involves mapping properties such as temperature, salinity, or dissolved oxygen in ways that are held to reveal the pattern of flow. Wust's core method is one such technique, in which property extrema indicate the 'cores' of various water masses. For instance, the core of Antarctic Intermediate Water is marked by an intermediate salinity minimum, Upper North Atlantic Deep Water by an intermediate salinity maximum, and so on. Wust (1935) mapped salinity, temperature, and oxygen along a number of core layers in the Atlantic, and used these maps to infer the spreading of water masses. A related method is isentropic analysis, in which properties are mapped along surfaces of constant density. Montgomery (1938) used isentropic analysis to infer the flow pattern of upper waters in the southern North Atlantic. Although these property analysis methods give an indication of patterns of flow, they cannot alone provide estimates of flow volume.

The second type of analysis is the dynamic method. The lowest order dynamical balance for large scale ocean circulation permits the calculation of vertical shear in horizontal velocity from the horizontal gradient of density. However, integration of shear to get velocity leaves an arbitrary constant, a reference level velocity, unspecified. Many authors have used the dynamic method with some assumption about reference level velocity.

Historically, the problem evolved as an attempt at specifying some surface along which velocity, or a component of velocity, was thought to

be near zero. It was thus referred to as the level of no motion problem. Sverdrup, Johnson, and Fleming (1942) list four methods (given below) of determining such a level, of which the first three are largely intuitive.

i) Assume that currents are negligible at great depth and therefore compute current relative to the bottom or to a depth near the bottom. Worthington (1976) found that this assumption led to gross violations of mass conservation in the Northwest Atlantic and therefore did not make geostrophic calculations in the Gulf Stream recirculation region. Instead, he used water mass arguments to close his circulation scheme.

ii) Assign zero velocity to the mid-depth minimum in dissolved oxygen. There is no dynamical or observational support for this method.

iii) (Defant's method) Place the zero velocity surface in a finite thickness layer of minimum shear. Defant (1941) was able to trace this layer over most of the North Atlantic.

iv) Use conservation of mass as a constraint to determine the reference level. Considering the Atlantic as an enclosed basin, any section that spans the width of the ocean should have zero net transport. The average level of no motion is that depth for which the northward and southward relative transports are equal. Using a pair of Meteor stations near opposite coasts in the South Atlantic, Sverdrup et. al. (1942) found the level of no motion to be 1325 meters.

In other important work, mid-depth levels of no motion were assumed. Iselin (1936) employed a 2000 meter reference level in his paper on the

circulation of the North Atlantic. Stommel's (1965) monograph on the Gulf Stream has dynamic calculations based on a 1600 meter reference surface.

Authors have sometimes used both water mass analysis and the dynamic method, as in Iselin (1936), Montgomery (1938), Worthington (1976), and others. In most cases, the two methods were applied separately, with the results of one being invoked to support, quantify, or question the results of the other method. The inverse method is in a sense a marriage of the two classical methods because it imposes property conservation constraints in any number of individual water masses, together with dynamic calculations, to estimate a profile of absolute velocity.

Along with the studies mentioned above which apply the dynamic method in order to describe ocean circulation, a number of other attempts have been made to determine the appropriate reference level for such calculations. Hidaka (1940) selected four stations in the North Atlantic, and by conserving mass and salt in three triangular areas defined by these statons (figure 1.1), was able to write a system of six equations in six unknown reference velocities. Defant (1961) noted that these equations were nearly singular because of the tight T/S relationship, and the solutions were therefore dominated by noise. This objection would reduce Hidaka's system to three equations in six unknowns. There are other problems with the method. One can see, for example, that once three of the reference level velocities are specified, then in order to avoid a discontinuity in pressure, the other three can be deduced. On similar grounds, a further reduction in the number of equations can be made.

Stommel (1956) used Ekman dynamics in the surface layer and potential vorticity conservation in the interior to estimate a profile of meridional velocity from stations in the Sargasso Sea. The vertical velocity at the base of the Ekman layer was computed from measurements of wind stress. This vertical velocity implies a net stretching or shrinking of the underlying water column. In response, the column must move poleward (for stretching) or equatorward (for shrinking) in order to conserve potential vorticity. He found a level of no meridional motion which produces the correct net meridional transport. The method left the zonal velocity undetermined, was applicable only in interior regions where the steady linear potential vorticity equation was thought to be applicable, and ignored vortex stretching due to topography and bottom friction. Sudo (1965) refined the technique by adding a lower boundary condition of no flow across a material surface. Leetmaa, Niiler, and Stommel (1977) used wind stress curl to calculate meridional transport at several latitudes in the North Atlantic. They applied a longitudinal smoothing to remove eddy noise.

Stommel and Schott (1977) obtained an overdetermined system of equations for horizontal velocity under assumptions of mass conservation, steady linear potential vorticity conservation, and no flow across density surfaces. Some examples given by Schott and Stommel (1978) showed a sensitivity to noise. A more detailed description of this method is given in the next section and in Chapter IV.

Many investigators have made direct measurements of current in order to fix a reference level velocity (c.f. Warren and Volkmann, 1968). Current meters and neutrally buoyant floats have been deployed for this

purpose. However, care must be taken in combining point measurements with spatially averaged valves of shear. One needs a spatially coherent array of point measurements and one must decide on the appropriate time scale to sample if the measurements are to be used in conjunction with hydrography.

A possible technique for the future is the use of satellite altimetry for the measurement of sea surface height. The slope of the sea surface relative to the geoid is proportional to the geostrophically balanced part of the surface current. At present, errors such as inaccuracies in the estimated geoid are comparable to or larger than the oceanographic signal. If the problems can be overcome, satellite altimetry together with hydrographic data could give absolute velocities over broad spatial scales with global coverage.

C. The Inverse Method

In this section a derivation of the Wunsch inverse formulation is given followed by a comparison with the related beta-spiral method of Stommel and Schott (1977). These are both inverse methods in the following sense. The problem of determining horizontal density gradients from a known geostrophic velocity field can be easily solved by taking a vertical derivative of velocity and then using the thermal wind equation. This is the forward problem. The corresponding inverse problem is to use a known field of horizontal density gradients to compute geostrophic velocity. Unlike the forward problem, the inverse is non-trivial because of the unknown integration constant.

a). Wunsch's Method

The technique applied by Wunsch (1977, 1978) to the Northwest Atlantic uses property conservation constraints to estimate the unknown reference level velocity and can be thought of as a generalization of the work by Hidaka (1940) and the fourth method given by Sverdrup, Johnson, and Fleming (1942). It allows the constraints to be applied to many layers instead of a single layer and permits stable solutions to be calculated in the presence of noisy data.

To begin with, the fluid is assumed to be incompressible and steady so that conservation of mass is given by

$$\nabla \cdot \bar{u} = 0 \tag{1.1}$$

where $\bar{u} = (u,v,w)$ is the vector velocity. Consider a closed volume V, bounded on top and bottom by isopycnal surfaces (Wunsch used isotherms) and on the sides by an arbitrary vertical surface S. Integrate 1.1 over this volume and apply the divergence theorem

$$0 = \iiint_V \nabla \cdot \bar{u}\, dV' = \iint_S \bar{u} \cdot \hat{n}\, dA + \iint_{top} \bar{u} \cdot \hat{n}\, dA + \iint_{bottom} \bar{u} \cdot \hat{n}\, dA \tag{1.2}$$

$\hat{n}$ is a unit vector prependicular to the boundary of V and directed outward. The net flow across isopycnal surfaces is assumed to be negligible so that the second and third terms on the right may be ignored. The flow perpendicular to the boundary surface S is assumed to be geostrophically and hydrostatically balanced. It can then be rewritten as the sum of an unknown reference level velocity and a

relative velocity computed from the thermal wind equation.

$$\bar{u} \cdot \hat{n} = \bar{u}_o \cdot \hat{n} = \bar{u}' \cdot \hat{n} \tag{1.3}$$

where

$$\bar{u}'_o = \frac{-g}{\rho f^2} \left(\bar{f} \times \int_{z_o}^{z} \nabla\rho \, dz'\right) \tag{1.4}$$

so that 1.2 becomes

$$\iint_S \bar{u}_o \cdot \hat{n} \, dA = - \iint_S \bar{u}' \cdot \hat{n} \, dA \tag{1.5}$$

Equation 1.5 expresses the fact that no net transport is allowed across the vertical surface S, so that transport due to relative (sheared) velocity is balanced by an equal and opposite transport due to depth-independent velocity. Ageostrophic transport across S, transport across isopycnal surfaces and transient mass storage within the enclosed volume are assumed negligible. Equations of the type 1.5 may be written for each of a number of layers, or water masses, in a vertical column of ocean. Because the ocean is discretely sampled by hydrographic stations, a discrete form of 1.5 is appropriate for computation. Define the relative transport in layer i as Γ_i. If there are N station pairs of width Δx_j,

$$\Gamma_i = \sum_{j=1}^{N} \left(\int_{z_{i-1}}^{z_i} \bar{u}' \cdot \hat{n} \, dz' \right) \Delta x_j \tag{1.6}$$

Let x_j be the unknown reference level velocity normal to S at station pair j.

$$x_j = (\bar{u}_o \cdot \hat{n})_j$$

The area of layer i at station pair j is a_{ij}.

$$a_{ij} = (\text{separation of pair j}) \times (\text{layer thickness})_{ij}$$

Then, the discrete form of 1.5 is

$$\sum_{j=1}^{N} a_{ij} x_j = -\Gamma_i \tag{1.7}$$

If there are M layers, and therefore M equations of this type, the system can be written in matrix form as

$$A_{MXN} x_{NX1} = -\Gamma_{MX1} \tag{1.8}$$

or

$$\begin{pmatrix} a_{11} & a_{12} & \cdots & a_{1N} \\ a_{21} & a_{22} & \cdots & a_{2N} \\ \cdot & \cdot & \cdot & \cdot \\ \cdot & \cdot & \cdot & \cdot \\ a_{M1} & a_{M2} & \cdots & a_{MN} \end{pmatrix} \begin{pmatrix} x_1 \\ \cdot \\ \cdot \\ \cdot \\ x_N \end{pmatrix} = \begin{pmatrix} -\gamma_1 \\ \cdot \\ \cdot \\ \cdot \\ -\gamma_M \end{pmatrix}$$

In addition, adjacent volumes of ocean with common bounding surfaces can easily be included in coupled systems of equations. If the data were perfect and the physical assumptions were precisely correct, then one could imagine increasing the number of water masses until the number of equations was about equal to the number of unknowns. However, small

amounts of noise obscure differences between equations that are almost linearly dependent, and reduce the effective number of equations (rank of A).

b. The method of Stommel and Schott

The beta-spiral inverse of Stommel and Schott (1977) is given in differential form. As noted by Davis (1978), the physical assumptions are much the same as in Wunsch's integral formulation. One assumes continuity (1.1), geostrophic and hydrostatic balance, and no flow across isopycnal surfaces written as

$$u\, h_x + v\, h_y = w \quad \text{where for example} \quad h_x = \left(\frac{\partial z}{\partial x}\right)_\rho = \frac{-\rho_x}{\rho_z} \tag{1.9}$$

Then, the further explicit assumption of a linear steady potential vorticity balance is

$$\beta\, v = f\, w_z \tag{1.10}$$

These assumptions are presumed to be valid for large scale (O(1000 km)) flows in the ocean interior, so the data should be appropriately smoothed. The equations are combined to give

$$u_o\, h_{xz} + v_o\, (h_{yz} - \beta/f) = -u'\, h_{xz} - v'\, (h_{yz} - \beta/f) \tag{1.11}$$

When written with data from many depths, the system of equations is formally overdetermined. For comparison, a differential form without using 1.10(equivalent to the Wunsch formulation) is obtained by taking a z-derivative of 1.9 and then substituting for w_z from 1.1.

$$u_o\, h_{xz} + v_o\, h_{yz} + u_{ox} + v_{oy} = -(u'h_{xz} - v'h_{yz} - u'_x - v'_y)$$

Note that there are four unknowns, u_{ox}, v_{oy}, u_o, and v_o rather

than 2 as in 1.11. Writing this equation with data from many depth produces the following coefficient matrix A.

$$\begin{pmatrix} h_{xz}(z_1) & h_{yz}(z_2) & 1 & 1 \\ \cdot & \cdot & \cdot & \cdot \\ \cdot & \cdot & \cdot & \cdot \\ \cdot & \cdot & \cdot & \cdot \\ h_{xz}(z_m) & h_{yz}(z_m) & 1 & 1 \end{pmatrix}$$

One can see that this matrix is at most of rank 3 since the third and fourth columns are identical. The system of equations is underdetermined without the vorticity balance. However, computation of $u'_x + v'_y$ using geostrophy gives $\frac{\beta v'}{f}$, and for consistency one should set $u_{ox} + v_{oy}$ equal to $\frac{\beta v_o}{f}$. The result is of course the beta-spiral equation 1.11. This is Davis' (1978) point. In the mid-ocean case, with no topography, the two methods are equivalent if the implicit use of 1.10 is recognized.

It will now be shown that in a more general application of the integral formulation, the equivalence does not hold. The key step is the use of the divergence theorem. Note that in the interior of the volume V, only continuity (1.1) is assumed. Any vorticity balance is permitted. The use of the steady linear vorticity balance is only implicit only if the hydrographic sections completely enclose the area and if there is no topography. If there are land boundaries or topography, then the argument advanced in the last paragraph no longer applies. Indeed, deviations from the steady linear balance, 1.10, will contribute to the signal, as we shall see.

An example makes the point clearly. Consider a 2-layer representation of a zonal section of the North Atlantic, as in Stommel, Niiler, and Anati (1978). They note that the thermocline is deeper at the eastern boundary than at the western boundary. This implies (in the 2-layer model) a net northward flow of the upper layer relative to the lower layer. Examination of isopycnal surfaces ranging from σ_θ = 27.1 to 27.7 in the IGY section at 30°N shows an average net drop of roughly 200 meters from west to east. Isotherms drop by much more, because of variations in TS characteristics approaching the Mediterranean outflow. Considering the North Atlantic as a closed basin, one could trace the σ_θ =27.4 surface along the boundary from Spain around to North America and find a net upward slope. Pressure gradients along the coast in one or both layers must accompany this slope. With no steady flow into the coast, these very small pressure gradients are not geostrophically balanced. They reflect the accumulation of small non-geostrophic terms in the momentum balance.

Scale analysis shows that this is not unreasonable, since effects of the proper magnitude can be produced by a low Rossby number flow. For instance, suppose part of the alongshore pressure gradient is balanced by deceleration of the western boundary current above a lower layer at rest, with the pycnocline slope along shore compensating for slope of the sea surface. Assume, for scale purposes, a pycnocline height change of 10^2 meters in a distance alongshore of order 10^6 meters, with a characteristic current speed of 1 m/sec and a density difference $\frac{\Delta\rho}{\rho}$ of 1 x 10^{-3}. Then the ratio of advective acceleration to Coriolis acceleration is very small.

$$\frac{U\,U_x}{fU} \sim \frac{g\Delta\rho}{\rho f U}\,\frac{\Delta h}{L} = .01$$

The point here is not to quantify the vorticity balance, which may vary in a complicated way in space and time, but merely to observe that other balances besides 1.10 are consistent with the integral formulation of the inverse. Without the net pycnocline slope in the preceding example, there would be no imbalance in the baroclinic mass flux and one could not then infer a barotropic circulation, as is done in Stommel et al. (1978) and more generally in the Wunsch type of inverse problem. Resolution is greatly improved by the use of an appropriate vorticity equation as in Stommel and Schott (1977). An example of this increased resolution is given in chapter IV using the dense sampling of the Gulf Stream '60 experiment.

The question of how much information to include in a problem, whether the information is in the form of data or physical relationships, is one of resolution versus stability. As one includes more independent information, problem resolution improves. If, however, the added information differs from other information only in noise content (data noise or inappropriate physics) then no additional resolution is achieved, and to force the problem to be more highly resolved simply decreases the stability of the solution. This tradeoff is really the key to the whole problem and is discussed in more detail in the subsequent sections on resolution, weighting, and noise.

The matrix equation 1.8 can be solved by a singular valve decomposition (SVD) of the A matrix. Good discussions of this technique

may be found in Lanczos (1961), Wiggins (1972), Wunsch (1978), and other sources. One can always write the matrix A as the product of three matrices

$$A_{MXN} = U_{MXK}\ L_{KXK}\ V^T_{KXN} \quad (M < N) \tag{1.12}$$

The columns of the U and V matrices are orthonormal.

$$U^TU = I \quad \text{and} \quad V^TV = I \quad \text{but, in general} \quad VV^T \neq I \quad \text{and} \quad UU^T \neq I$$

The matrix L is a diagonal matrix of the non-zero 'singular values'. U and V are the respective eigenvector matrices for the eigenvalue problems

$$(A\ A^T)\ u = l^2 u \qquad \text{and} \qquad (A^TA)\ v = l^2 v$$

The non-zero eigenvalues, l^2, are the same for both of these problems and they are the squares of the 'singular values' in matrix L. Since standard numerical routines are available to compute eigenvalues and eigenvectors of square matrices, the SVD of the rectangular matrix A can be computed as follows. M is usually much smaller than N, so it is easier to solve the first of the above eigenvalue problems than the second. This gives U and L, and V is calculated from 1.12

$$V^T = L^{-1}U^TA$$

The SVD solution to 1.8 is obtained by left-multiplying 1.8 by $VL^{-1}U^T$

$$V\ L^{-1}U^TA\ x = V\ V^Tx = -V\ L^{-1}U^T\ \Gamma \tag{1.13a}$$

Define $b = VV^Tx$ and note that

$$A\ V\ V^Tx = A\ b = U\ L\ \ V^TV\ V^Tb = A\ x = -\ \Gamma \tag{1.13b}$$

Therefore b (the SVD solution) is in fact a solution to 1.8. The 'correct solution', that is the solution that would be obtained if the resolution was perfect (i.e. if rank(A)=N so that $VV^T=I$) ,is denoted by x, whereas the estimate of x is called b. Of the infinity of possible solutions to 1.8, the SVD solution is the smoothest in the sense of introducing no structure that is not necessary to satisfy the constraints. In the ocean circulation problem, this means that the largest available scales in the data are used and the reference level velocity is smoothed over these scales.

If the matrix A has K linearly independent rows (rank (A) = K), then only K of the singular values are non-zero. In practice, because of noise in the A matrix, singular values that should be zero are instead small positive numbers. One must rank the singular values from largest to smallest and decide beyond what value they should be considered to be equal to zero. Wiggins (1972) discusses several techniques for making this decision. One may either take what he refers to as a sharp cutoff or a tapered cutoff approach. In the former, small singular values (and their corresponding eigenvector coefficients) are excluded from the solution in order to hold down the problem variance. In the latter, the effect of small eigenvalues is damped by replacing 1.8 by

$$Ax + n = -\Gamma \tag{1.14}$$

where $\langle n_i n_j \rangle = \sigma^2 \delta_{ij}$, $\langle n_i \rangle = 0$ and σ^2 is referred to as the

problem variance. The tapered cutoff solution to 1.14 is

$$b = A^T (AA^T + \bar{\sigma}^2 I)^{-1} (-\Gamma) \tag{1.15}$$

Here, $\bar{\sigma}^2$ is the ratio of the problem variance to the solution variance. Wiggins(1972) shows that the effect of $\bar{\sigma}^2$ is to eliminate the effects of the smallest eigenvalues. Hoerl and Kennard (1970 a,b) studied the behavior of the length of the solution vector as $\bar{\sigma}^2$ is varied, a technique termed ridge analysis. A discussion of this inverse and its relationship to the SVD inverse is given by Wunsch(1978).

The examples in chapters II, III, and IV use both the sharp and tapered cutoff methods. For sharp cutoff, the decision on the smallest non-zero singular value was made by studying estimated error variance, length of solution and residual vectors and smoothness of the VV^T matrix (discussed in the next section) for several choices of K. Usually the smallest singular value was about 2 orders of magnitude less than the largest. The solutions tend to be very stable with respect to small changes in K.

D. Resolution

The non-uniqueness of solutions to the problem 1.8 leads to the question of how to interpret a particular solution $b_{j = 1,N}$. The infinity of possible solutions are all compatible with the imposed physics. All must be considered possible states of the real ocean until additional data or further constraints are introduced. However, a set of K independent linear equations does give a unique determination of K linear combinations of the solution elements. It is the purpose of this

section to show that in some problems, these well determined quantities have a simple and physically useful interpretation.

An example brings out the main points. Consider a 2-layer ocean bounded by land on the north and south. Two hydrographic sections containing 2 and 1 station pairs traverse the ocean. Figure 1.2 shows the geometry, with areas of upper and lower layers marked at each station pair. Let the A-matrix be composed of areas of the upper-layer (1st row) and of the total water column (2nd row).

$$A = \begin{pmatrix} .5 & .4 & .4 \\ 1.0 & .9 & .4 \end{pmatrix}$$

For now, ignore the question of weighting and assume A is noise free so that its rank is 2. The singular value decomposition of A is given by

$$A = ULV^T = \begin{pmatrix} .4659 & .8848 \\ -.8848 & .4659 \end{pmatrix} \begin{pmatrix} 1.583 & 0 \\ 0 & .1814 \end{pmatrix} \begin{pmatrix} .7060 & .6207 & .3411 \\ .1311 & .3589 & -.9241 \end{pmatrix} \quad (1.16)$$

Define a matrix R, called the resolution matrix

$$R \quad VV^T = \begin{pmatrix} .5156 & .4853 & .1197 \\ .4853 & .5141 & -.1199 \\ .1197 & -.1199 & .9703 \end{pmatrix} \quad (1.17)$$

Wiggins (1972) shows that the columns of the resolution matrix represent the best approximation, in a least square error sense, to a set of delta functions, δ_{ij}. The columns measure the degree to which individiual station pairs can be resolved using linear combinations of the eigenvectors. They cannot ,in general be perfectly resolved because the V-eigenvectors only span the observation (row) space of A and not the solution (column) space, which is of higher dimension.

The indeterminacy can be examined directly by computing the vector which is orthonormal to the two V eigenvectors in 1.16. In general there are N-K such vectors. They are called the null-space eigenvectors, or annihilator of A, because they are normal to the rows of A. In the example, the null-space eigenvector is

$$\bar{v}_3 = (.70,-.70,-.17)$$

The infinity of possible solutions will differ from each other by multiples of $\bar{v}_3$. That is, given any solution, an arbitrary multiple of $\bar{v}_3$ may be added to that solution and the result will still satisfy the constraints since $\bar{v}_3$ has no effect on the constraints. One can see that $\bar{v}_3$ is primarily a recirculation between station pairs 1 and 2 ($v_{13} = -v_{23}$). The extent of this possible recirculation is the undetermined quantity in the problem.

A second interpretation of R follows from 1.13. Suppose, hypothetically, that the reference level velocities in the ocean were somehow known at each station pair. This set of velocities will be referred to as the 'perfectly resolved' solution. Then, according to 1.15, multiplication of these velocities by R would produce the SVD solution, b. The resolution matrix is a linear operator which maps the perfectly resolved solution (as well as every other possible solution) into a particular solution b. It is a filter for which the real ocean is the unknown input and the b's are the computed output.

In the example, 1.16, if the perfectly resolved solution was 1 at station pair 1 and 0 at pairs 2 and 3, then the computed solution, given

by the first column of R, would be $b_1 = .5156$, $b_2 = .4853$, $b_3 = .1197$. Similarly, the second and third columns of R give the computed solutions which would result if the perfectly resolved solutions were (0,1,0) and (0,0,1) respectively. Because the system is linear, such solutions may be added. It is obvious that station pair 3 is well resolved by itself. Pairs 1 and 2 are not well resolved individually, but are well resolved as a group. Any velocity in either of these pairs is simply smoothed over both, with minor 'spillage' into pair 3. In this case, R is a good spatial averaging filter, with the averaging pretty well confined to the separate sections. In such instances, where physically adjacent groups of stations are resolved, the resolution is said to be compact. A problem with non-compact resolution can be constructed trivially by considering station pair 2 to be one section and pairs 2 and 3 combined to form the other. The resolution matrix is unchanged, but now, since pairs 1 and 2 are no longer physically adjacent, the resolution is not compact.

The resolution of volume transport is often a more useful quantity than the resolution of velocity because the constraints are written in terms of transport. Whereas velocity need not be preserved by the operator R, as in the case of groups of stations of very different widths, transport must be conserved for the constraints to be satisfied. A matrix for resolution of volume transport due to the reference level velocity, say in the ith layer, can be obtained by multiplying the corresponding velocity resolution elements by the appropriate water mass area (element of the A-matrix) and then normalizing.

Suppose, for example, that one wants to know the amount of transport that will appear at station pair 2 because of the failure to perfectly resolve station pair 1. Let row i of the A matrix represent the total transport constraint. The velocity resolution element r_{21} gives the velocity at station pair 2 that results from imperfect resolution of a velocity of 1 at station pair 1. Then $r_{21}a_{i2}$ converts this to a transport at pair 2. Finally $(r_{21}a_{i2})/a_{i1}$ is the transport at pair 2 due to the imperfectly resolved transport (instead of velocity) of 1 at pair 1. More generally,

$$t_{pj} = \frac{r_{pj}\, a_{ip}}{a_{ij}} \tag{1.19}$$

In the example, the resolution matrix for total transport is

$$T = \begin{pmatrix} .5156 & .5392 & .2993 \\ .4368 & .5141 & -.2698 \\ .0479 & -.0533 & .9703 \end{pmatrix} \tag{1.20}$$

Note that the sum in any column is 1 so transport is conserved. Inspection of this matrix suggests that computed net volume transport in each section will probably agree with the real transports to within about 5%.

Although the example problem is formally underdetermined, good estimates have been obtained of net transport through each section and of the smoothed reference level velocities. Indeed, the only thing not determined is the extent of the possible recirculation between station pairs 1 and 2. With good hindsight, one can look back at the A matrix

and see that the resolution agrees well with intuition. Station pairs 1 and 2 have nearly the same proportions of shallow and deep water. It is this purely geometrical similarity which leads to their being grouped together. They are geometrically almost indistinguishable, and therefore they will be assigned nearly the same solution elements. Station pair 3 is distinctly different by virtue of having no deep water. It is therefore well resolved by itself.

What if, because of noise, the rank of A is found to be 1 rather than 2? With only one independent equation, all three station pairs should be grouped together.

$$R_{K=1} = \begin{pmatrix} .50 & .44 & .24 \\ .44 & .39 & .21 \\ .24 & .21 & .12 \end{pmatrix} \qquad T_{K=1} = \begin{pmatrix} .50 & .49 & .60 \\ .39 & .39 & .48 \\ .10 & .09 & .12 \end{pmatrix}$$

The relatively small velocities and transports at station pair 3 are due to its small area in the unweighted problem. Notice that the sum of the columns in the transport matrix is not as close to 1 as in the K = 2 case. As the constraints are relaxed, transport is not as well conserved by the smoothing operator.

The kind of reasoning applied to this simple problem can also be used in real problems to anticipate resolution. That is a central question of Chapter II. In general, station pairs with similar ratios of layer depths will be grouped together in the solution. More precisely, groups are formed from station pairs whose corresponding columns in the A-matrix are most nearly linearly dependent. If the station pairs are physically adjacent, then the resolution is compact, the solution is a spatially smoothed version of the real reference level velocity field. Salt

advection, heat advection, etc. (assuming a tight T/S curve) can be estimated for the groups. If the resolution is not compact, interpretation is far more perilous.

The essential difference between compactness and non-compactness is easily illustrated. Consider a slice of ocean bounded by two hydrographic sections that run from a coastline to a common point in mid-ocean (Figure 1.3a). Suppose that each section has many station pairs but that out of all station pairs, two have identical depths and layer thicknesses. The corresponding two columns of the A-matrix will be equal and the solution elements for the two stations will be equal in terms of the mass flux constraints. That is, if the two station pairs are in opposing sections, the determined velocities will be equal and opposite (Figure 1.3b). If they are in the same section (say side by side), the determined velocities will be equal and of the same sign (Figure 1.3c). The indeterminate part of the flow is any flow that does not affect the mass flux constraints. This null space of A admits, in the first case, the possibility of an arbitrarily large mass flux through the system, so long as it is the same at the two station pairs (Figure 1.3d). In the second case, the undetermined quantity is simply a small scale recirculation in the adjacent pairs (Figure 1.3e). An example of the first type will be shown in Chapter IV using Gulf Stream '60 data and one of the second type in Chapter II on the Caribbean Sea.

We have shown that, in the compact resolution case, the b's represent a spatially smoothed version of the reference level velocities. However, the choise of reference level is somewhat arbitrary, and further, a display of the smooth b's together with unsmoothed relative velocities

entails a mismatch in scales. The relative velocities each represent an average over a single station pair while the b's are typically averaged over many station pairs. The mismatch is removed simply by applying the same filter to the relative velocities as was applied to the reference velocities. At each level,

$$(VV^T)_{NXN}\ (v^r)_{NX1} = \tilde{v}^r_{NX1}$$

The total smoothed velocity is then

$$(\tilde{v}^r + b) = V\ V^T(v^r + x) \qquad (1.21)$$

The smoothed field is independent of the initial reference level, since every level has been filtered by the same operator. In this sense the smoothed field is unique. Further, the smoothed field gives, at every level, the b field which would result if that level were chosen as the initial reference level in the computation of an unsmoothed solution. This means that one need not recompute the SVD solution for each choice of initial reference level. A single computation of the smoothed field gives the b's corresponding to each initial reference level. The formulation of the smoothed field (1.21) is equivalent to the more complicated appearing form given by Wunsch (1978).

E. Weighting

In the applications discussed in Chapters II, III, and IV, the unweighted problem, 1.5, is replaced by the weighted problem.

$$A'b' = -\Gamma \ , \ A' = AW^{-1/2} \quad b' = W^{+1/2}b \tag{1.22}$$

There are two purposes for this substitution. One is to remove any unintentional bias in the solution. The other is to impose a bias by controlling the solution variance or influencing the problem resolution.

Hidden bias in the ocean circulation problem is the result of different station pairs having different areas (product of mean depth times station separation). Consider two adjacent station pairs with the same mean depth and the same layer thicknesses, but whose station separations differ by a factor of α. The solution should not be sensitive to the placement of the center hydrostation (i.e. to the value of α) and should clearly be the same at the two station pairs. The matrix A will show two columns that differ only by a factor of α. If the station pairs are at positions j and j+1 in the A matrix,

$$A = \begin{pmatrix} a_{ij} & \alpha a_{ij} \\ a_{2j} & \alpha a_{2j} \\ \vdots & \vdots \\ a_{mj} & \alpha a_{mj} \end{pmatrix}$$

The V eigenvectors, which span the rows of A will have elements that differ by a factor of α

$$V^T = \begin{pmatrix} V_{j1} & \alpha V_{j1} \\ V_{jk} & \alpha V_{jk} \end{pmatrix}$$

The corresponding columns of the resolution matrix also differ by the factor α

$$r_{ij+1} = \sum_{p=1}^{K} V_{i1}\, V_{j+11} = \sum_{p=1}^{K} \alpha V_{i1}\, V_{j1} = \alpha\, r_{ij}$$

$$R = \begin{pmatrix} r_{1j} & \alpha r_{1j} \\ r_{2j} & \alpha r_{2j} \\ r_{nj} & \alpha r_{nj} \end{pmatrix}$$

The solution elements, which by symmetry should be equal, show the same bias.

$$b^T = (\,.. b_j,\ \alpha b_j, ..\,)$$

The symmetry argument is not quite as compelling when applied to depth. Suppose two station pairs have the same separation and the same ratios of layer thickness to total depth for each layer, but that the depths differ by a factor of α. Once again the solutions are biased as above. However, it is not obvious that the same solution should be assigned at both station pairs. For one thing, this hypothetical situation does not occur in the real ocean, where shallow stations may show less of the dense layers without having thinner upper layers. Nevertheless, it is undesirable to assign a large velocity to a deep station merely because it is deep, so removal of all bias based on the area of station pairs seems reasonable. This is accomplished by setting

$$W_{ij}^{-1} = \delta_{ij}\, (d_i\, \Delta x_j)^{-1} \qquad (1.23)$$

In the weighted problem,

$$A' = \begin{pmatrix} a'_{ij} & \alpha^{1/2} a_{ij} \\ a'_{mj} & \alpha^{1/2} a'_{mj} \end{pmatrix} \quad \text{and} \quad R' = \begin{pmatrix} r'_{lj} & \alpha^{1/2} r_{lj} \\ r'_{nj} & \alpha^{1/2} r'_{nj} \end{pmatrix}$$

Next, the weighting is removed from the resolution matrix in order to derive an expression analagous to 1.13. Let

$$A' = U\, L\, V^T$$

$$VV^T X' = VL^{-1}\, U^T A' X' = VL^{-1}\, U^T\, \Gamma = b'$$

so $$b = (W^{-1/2} V\, V^T\, W^{+1/2})\, X$$

Define, $$R = W^{-1/2}\, V\, V^T\, W^{+1/2} \qquad (1.24)$$

R can be called the deweighted resolution matrix. It is easily verified that in any column of this matrix, the two elements corresponding to the two hypothetical station pairs are equal, i.e.

$$r_{j+1\ i} = r_{ji}$$

Application of the weighting scheme 1.22 to the earlier example 1.16 improves the resolution of station pair 3 (the smallest in area) by cutting down its side lobes. Compare to 1.17 and 1.20.

$$R = \begin{pmatrix} .48 & .47 & .05 \\ .52 & .53 & -.05 \\ .13 & -.12 & .99 \end{pmatrix} \qquad T = \begin{pmatrix} .48 & .52 & .13 \\ .47 & .53 & -.12 \\ .05 & -.05 & .99 \end{pmatrix} \qquad \left(t_{pj} \equiv \frac{r_{pj}\, a_{ip}}{a_{ij}}\right) \quad (1.25)$$

The weighted problem is also useful if there is anything known about correlation length scales of the velocity field or if it is desired to force certain solution elements to be correlated. The weight matrix W is

the covariance matrix of the solution elements, b (Wiggins, 1972). The use of non-zero off-diagonal elements in this matrix causes corresponding solution elements to be correlated.

Refer again to example 1.16. Suppose that the mass imbalance is given by

$$\Gamma = \begin{pmatrix} 10 \\ 10 \end{pmatrix}$$

The lower layer is balanced, but the upper layer (and therefore the total water columnn also) has a mass surplus. There are two ways of balancing the system. An outflow velocity at station pair 1 coupled with an equal inflow velocity at station pair 2 gives a net outflow of upper water and no net flux of deep water. Alternatively, an outflow at station pair 3, which has no deep water, accomplishes the same end. Solutions consistent with these two extremes are

$$\text{i)} \quad b = \begin{pmatrix} 100 \\ -100 \\ 0 \end{pmatrix} \qquad \text{ii)} \quad b = \begin{pmatrix} 0 \\ 0 \\ 25 \end{pmatrix} \tag{1.26}$$

Using the simple diagonal weight matrix, 1.23, the SVD solution is

$$b = W^{1/2} U'^{T} S'^{-1} V' \Gamma = \begin{pmatrix} 1.3 \\ -1.3 \\ 24.7 \end{pmatrix} \tag{1.27}$$

The second alternative is favored by the SVD solution since it gives a much lower value of $b^T b$. However, the SVD solution can be driven closer to either 1.26i or 1.26ii by imposing non-zero covariances. If an off-diagonal element of $W^{-1/2}$ is set equal to a diagonal element of the

same row, the corresponding two solution elements are perfectly correlated. In other words, if

$$W_{12} = W_{11} \quad \text{and} \quad W_{21} = W_{22}$$

then, this is equivalent to the additional constraint

$$b_1 = b_2$$

Similarly

$$W_{12} = -W_{11} \quad \text{and} \quad W_{21} = -W_{22}$$

leads to

$$b_1 = -b_2$$

The former leads to solution 1.26ii and the latter to 1.26i. As the off-diagonal elements go from zero to plus or minus the value of the diagonal elements, the whole range of solutions between 1.27 and 1.26ii or 1.26i is accessed.

Similar alternatives exist in real problems where large eigenvalues are associated with broad flows that account for most of the mass balance, and smaller eigenvalues bring in smaller scales, particularly small scale recirculations that make minor adjustments in the net flux of mass. An approach advocated by Jordan and Franklin (1968) attempts to enhance the resolution of the broad scales by solving the problem first with a diagonal weight matrix to determine what solution elements tend to be grouped in resolution, and then repeating the problem with positive covariances between members of each group. According to Wiggins (1972),

this will cause the eigenvalues to become more polarized, with large ones becoming larger and small ones becoming smaller. The intended effect is to put more emphasis on the best determined, least noise sensitive components of the solution.

It is quite possible to become bogged down in details of a weighting scheme, and some perspective is useful. One can never obtain the velocity field with perfect resolution. Rather, one can derive a filter, R, and also the unique output of this filter after it acts on the true velocity field. Interpretation of the output relies on the filter having some relatively simple characteristics. It should perform a local spatial smoothing. The weight matrix is the means of manipulating the filter (to a limited extent) to perform the desired function.

In addition to the column weighting, it is also posssible to perform a row weighting in order to vary the weight placed on each constraint in the problem. Let

$$A'' = S^{1/2} A', \quad \Gamma'' = S^{1/2} \Gamma'$$

so that

$$A'' \, b' = - \Gamma''$$

If

$$A'' = U \, L \, V^T \, \Gamma$$

then the singular value decomposition solution is

$$b' = -V \, L^{-1} \, U^T \, S^{1/2} \, \Gamma$$

and

$$b = -W^{-1/2} V L^{-1} U^T S^{1/2} \Gamma$$

Wunsch (1978) discusses this row scaling. The matrix S^{-1} is the covariance matrix of the observations.

F. Errors

Error estimates for problem 1.8 are made either by considering the size of errors in the observations or from a study of problem residuals (goodness of fit). The two should be comparable in magnitude. If they are not, then either the observational errors are incorrectly assessed or the physical model is insufficient to describe the data. The following begins with a discussion of errors in the data. Some comments on likely errors in the model are made, and then briefly, the propagation of data errors through to the solution is considered.

1. Data Errors

A hydrographic station in deep water normally consists of two Nansen bottle casts. A shallow cast is made with about 12 to 15 bottles at 100 meter intervals (or closer near the surface). The bottles should be placed to be as close to standard depths as possible in order to minimize interpolation errors in dynamic computation. Except in regions of high shear (resulting in large drag on the wire), the bottles can usually be placed within 10 to 20 meters of optimal depth. In the deep cast, bottle spacing may be 200 to 300 meters or even greater at very deep stations. Interpolation errors are small below the thermocline where the vertical

profiles of temperature and salinity become almost linear. The 'artistry' of a deep cast is in placing the bottom bottle as close as possible to the ocean floor.

There are measurement errors in temperature, salinity, pressure, and geographical position (navigation). The magnitudes of the first three, for carefully made Nansen casts, is roughly .02°C in temperature, .005‰ in salinity and 5 decibars in pressures up to 1000 decibars and about .5% at greater pressure. Navigation errors depend on the method used (e.g. Loran, satellite, etc.) but are usually negligible in relation to the other errors. An equivalent error in the pressure of a given isopycnal can be estimated by multiplying the position error by isopycnal slope. An error of 1 kilometer, even with a relatively large isopycnal slope, say 1×10^{-3}, is equivalent to only 1 decibar in pressure.

The interpolation procedure for temperature and salinity is discussed in the Appendix along with other details of computation. Some tests of the interpolation routine using CTD data with dummy 'observed' depths showed that in most cases the interpolation errors were smaller than, or the same size as, the measurement errors. Exceptions were at depths where there is both large curvature in the vertical profiles (usually the upper 1200 meters) and where the interpolated depth was nearly midway between observed values. Then rms errors of about .08°C in temperature and .015‰ in salinity were found. Internal waves with displacements of order 10 meters give rise to errors of equal or smaller magnitude than those due to measurement and interpolation.

The equation of state gives specific volume as a function of salinity, temperature, and pressure. Given specific volume at two adjacent stations, A and B, vertical shear is computed from the

geostrophic relationship (see for example, Sverdrup, Johnson, and Fleming (1942), p. 448).

$$v_1 - v_2 = \frac{10}{2\Omega(\sin \Phi)L} \left[\left(\int_{p_1}^{p_2} \alpha \, dp \right)_A - \left(\int_{p_1}^{p_2} \alpha \, dp \right)_B \right]$$

The rotation rate of the earth is Ω, Φ is latitude, L is distance between the stations (in meters), α is specific volume, p is pressure in decibars, and v is velocity in meters per second. The error in estimated shear (discounting the finite integration steps, which may contribute significantly) is

$$\varepsilon_v \sim \frac{10}{2(\sin \Phi)L\Omega} \Delta p \, \varepsilon_\alpha$$

Table 1.1 shows the size of errors in specific volume at several depths from Crawford station 889 (in the Sargasso Sea), computed by assuming the measured temperature, salinity, and pressure to be in error by .02°C, .005‰ and 5 decibars or .5% (whichever is greater) respectively. From this, a rough estimate of error in relative velocity is obtained for a station pair at mid-latitude with a separation of 100 kilometers, a depth of 4000 meters and a typical specific volume error of 1×10^{-5} $cm^3 gm$. The error in relative velocity accumulates with the number of integration steps away from the reference level to O(1 cm/sec). The corresponding uncertainty in the relative volume transport is about $2 \times 10^6 m^3/sec$. Thompson and Veronis (1978) calculated the error in relative transport assuming random errors in the measurements with standard deviation .005% in salinity, .02°C in temperature, and .5% in

pressure for a data set in the Tasman and Coral Seas. The estimate of 4 x 10^6 m^3/sec was mainly in the deep water.

In the preceding, there are several important points which are somewhat obscured by the numbers. First, transport errors are latitude dependent, with a singularity at the equator. Errors in adjacent layers may be strongly correlated. That is, an error at any standard depth is carried over into all subsequent standard depths. Finally, since the relative total transport through a section is dependent only on the end stations, the estimated error is the same for any section (except for the latitude dependence) regardless of length and number of station pairs, and is equal to that for a single station pair.

Aside from the errors which result from measurement and interpolation, there are additional errors in the presence of a sloping bottom, due to the lack of data along the bottom. Below the deepest bottle of the shallower of two stations, there is no accurate way of determining shear. Historically, methods such as those of Helland-Hansen (1934) and Jacobson and Jensen (1926) were devised to estimate shear (and sometimes absolute velocity) along a sloping bottom. The physical assumptions of these methods are difficult to justify. Wunsch (1977) filled in values for shear below the deepest common standard depth by a linear vertical extrapolation of shear. This proved unsatisfactory in cases where the shallow station was in the thermocline and the deep station much deeper, resulting in unreasonably large values of relative velocity. Some experimentation with simple horizontal and vertical extrapolations of the measured fields showed the former to be slightly more stable. However, a vertical procedure, in which isopycnal slope was

held constant below the deepest common standard depth, was settled on here. It seems clear from studying open ocean sections of temperature and salinity that the vertical coherence of the fields over several hundred meters is visibly greater than horizontal coherence over station spacing scales (20 - 100 kilometers). Thompson and Veronis (1978) also used a vertical method, requiring shear to diminish linearly to zero at the bottom.

Lacking sufficient observations to predict the behavior of the density field near sloping boundaries, any method is prone to significant errors. The errors are probably comparable to the actual shear, and therefore range from a few tenths of a centimeter per second for depth differences of a few hundred meters in deep water to tens of centimeters per second for depth differences of a couple thousand meters in energetic regions. The resulting error in relative transport depends largely on whether or not the reference level is the bottom. If the reference level is above the deepest common standard depth, then the shear error contributes to transport error only below the deepest common standard depth. If the reference level is the bottom, then the deep shear error leads to a relative velocity error in the whole water column. For example, suppose station A has a depth of 1000 meters and station B has a depth of 2000 meters. Let the velocity error be linear from 1000 to 2000 meters and equal to 5 cm/sec at 1500 meters. If the station separation is 25 km (stations are normally fairly close over steep slopes), then a bottom reference level leads to a transport error of about 3 x $10^6 m^3$/sec while a reference level at 1000 meters gives an error of only .6 x $10^6 m^3$/sec. There are pathological examples where depth

changes of 2000 meters and station separations of 100 km could produce very large errors. Unlike the measurement and interpolation errors, these errors accumulate with the length of a section and, of course, with roughness of topography. The only way to reduce them is to decrease station spacing to give better resolution of topographic features and to sample all the way to the bottom.

So far, the discussion has been confined to errors in the calculation of vertical shear, and therefore of transport (the Γ matrix in problem 1.8). The same measurement errors also affect the A matrix of water mass areas through interpolation to locate the depths of isopycnal surfaces. Table 1.1 converts the measurement errors into equivalent errors in the depth of an isopycnal surface at Crawford station 889. Recall that interpolation error may be larger than the measurement errors by up to a factor of 4 where there is large curvature in the vertical profiles. The errors are at best on the order of 10 meters and become much larger when the vertical derivative of potential density is small. This occurs in well mixed layers like 18° water in the Northwest Atlantic and in the deep water. When initiating a problem, dividing surfaces in strong linear gradients should be used when possible. If some bounding surfaces have much larger expected errors than others, the corresponding layers may be downweighted in the problem.

In estimating water mass areas, the isopycnals are approximated by linear segments between hydrographic stations. Unlike the shear estimate, which gives the horizontally averaged shear between stations, independent of the structure, the area of a bounded water mass can be significantly affected by curvature of the isopycnals. Station spacing

should be fine enough to adequately sample any very energetic features in the density field. Similarly, curvature of the bottom adds to errors in the area of the deepest layer and the total water column. It is not uncommon to find topographic features of at least several hundred meters amplitude between stations.

A final data error results when non-simultaneous hydrographic sections are used. In the Caribbean, for example, one expects variations in the total transport of 10-20%, based on the measurements in the Florida Straits by Niiler and Richardson (1973). Therefore, hydrographic sections made at different times may yield inconsistencies of this magnitude. A more serious inconsistency can result if non-simultaneous sections intersect. An eddy in one of the sections could certainly produce a spurious imbalance on the order of $10 \times 10^6 m^3/sec$. Wunsch (1978) abandoned some sections for this reason.

2. Model Errors

Even in the presence of perfect, error free, simultaneous data, the conservation constraints 1.8 are not expected to hold exactly since the assumptions necessary to derive them are not precisely correct. There may be real transient mass storage in one or more layers. Corrections to the geostrophically derived transports can be locally significant. For example, in a western boundary current the ratio of advective acceleration to Coriolis acceleration might be expected to be as high as .1 near the surface. The correction for Ekman transport due to wind stress might be 2 to $3 \times 10^6 m^3/sec$ for a long zonal sectional at mid-latitude. Flow across isopycnal surfaces is perhaps also appreciable

if very large areas are considered. For perspective, note that a mean cross isopycnal velocity of 10^{-4} cm/sec is necessary over an area 1000 km on a side to give a net flux of 1×10^{6} m^3/sec.

Errors in the model are, of course, not random and the model can be adjusted to accommodate a higher order balance. The beta spiral calculations of Stommel and Schott (1977) are an example of this, and an application of a similar method is described in Chapter IV. One should be careful, however, that the data are of sufficient quality and coverage to justify carrying extra terms.

3. Solution Errors

Formal estimates of solution errors due to random errors in the data are made as in Wiggins (1972) and Wunsch (1978). The relative variance, defined as the ratio of the solution variance, $\langle b'^2_j \rangle$, to the problem variance, σ^2, is

$$\frac{\langle b'^2_j \rangle}{\sigma^2} = \sum_{i=1}^{k} \frac{v^2_{ji}}{l^2_i} \tag{1.28}$$

Some examples of the relative variance are shown in Wunsch (1978). Sometimes, one would prefer to know the actual solution variance, and this can be obtained by first estimating the problem variance. From the previous discussion on measurement errors, one would expect the problem variance to be of order 1 to 10×10^{12} m^6/sec^2. An estimate can be made from the problem residuals, that is from the goodness of fit of the solution to the constraints.

$$\sigma^2 = \frac{\sum_{i=1}^{M} (A b - \Gamma)^2_i}{M - K} \tag{1.29}$$

Recall that M is the total number of constraints and K is the number of independent constraints. The estimated solution variance, from 1.28 and 1.29 applies to the weighted problem, and the deweighted solution variance is obtained by dividing by the appropriate weights.

$$\langle b_i^2 \rangle = \langle b'^2_i \rangle / W_{ii}$$

As an example, figure 1.4 shows the deweighted solution variance for the 41 station pairs in the first of the two Gulf Stream '60 calculations discussed in Chapter III. The problem variance, using 1.29, was estimated at $.33 \times 10^{12}$ m^6/sec^2. The best resolved station pairs tend to have the highest variance because of their dependence on the smaller eigenvalues.

A brief examination of the non-random errors in the geostrophic calculations gives an indication of why the estimate of problem variance from 1.29 is smaller than the a priori guess. One calculates relative velocities as a sum of shear estimates, and a shear error at any depth contributes a uniform error at each subsequent depth in the integration. It was noted that fairly large shear errors resulted from attempts to estimate shear below the deepest common standard depth of a station pair, and that these caused large expected errors in transport relative to the bottom. The effect of depth independent velocity errors is easily understood. Refer once again tto the example problem 1.16. Suppose there is a uniform velocity error of 1 at station pair 1. The error in initial transport is then

$$\epsilon_\Gamma = \begin{pmatrix} .5 \\ 1.0 \end{pmatrix}$$

and the solution error is , in the unweighted problem,

$$\varepsilon_b = - V L^{-1} U^T \Gamma$$

$$\varepsilon_b^T = (-.52, -.48, -.12)$$

But this is just column 1 of the resolution matrix, 1.17, multiplied by -1. Depth independent errors are compensated by smoothing through the VV^T filter because such errors are parallel to columns of the matrix A. No imbalance in the solution transports results from such errors. Whether or not the errors are compensated locally depends on the scale and compactness of the resolution. Velocity errors which are uniform over part of the ocean depth will be parallel to the corresponding part of a column of the A matrix and will be partially compensated in the solution transports.

Similar consideratons apply to depth independent or partly depth independent errors in the model. For example, consider the problem of seasonal variability in the Caribbean. Suppose a section of the western Caribbean, made when the volume transport was 27×10^6 m^3/sec, is combined with a Florida Straits section made when the volume transport was 33×10^6 m^3/sec. In this case, if the model requires the two transports to balance, there is a model 'error' of 6×10^6 m^3/sec. Niiler and Richardson (1973) found that the seasonal signal is nearly depth independent in the Florida Straits. It will effect only about the upper 700 meters in the western Caribbean, but not the deep water, for

which there is no outlet. Because this 'error' is parallel to the A matrix columns from the Florida Straits section, this is where most of the compensation will occur. Assuming compact resolution, the solution will show a transport closer to 27 than to 33 x 10^6 m^3/sec. In cases where the model error is equally parallel to station pairs of to two or more sections, for instance a high transport section of the western Caribbean combined with a low transport section of the eastern Caribbean, the solution will be closer to a mean value, again, if the resolution is compact.

Chapter II

A. Introduction

The Caribbean Sea was chosen as the first example in this work. As a partially enclosed basin with a good selection of hydrographic data available, it would serve as a prototype for calculations involving larger datasets in the open ocean. Further, it was seen in chapter I that the presence of land boundaries and large topographic variability tends to enhance problem resolution. It was felt that the Caribbean, with its shallow passages and steep relief, would produce a better determined solution than the examples shown by Wunsch (1978) in the northwest Atlantic. Outflow through the relatively shallow Straits of Florida is confined to water above about $7^{\circ}C$. There can be no net mass flux of colder water through the Caribbean. This fact helps justify, a priori, the choice of a deep initial reference level, and it will be shown that the powerful constraints yield similar solutions from any initial choice. The problem is, however, still formally underdetermined. Therefore, beyond simply presenting the solution, a major focus of this chapter will be to show what is determined in the problem and what is not.

A further reason for using the Caribbean as an example is that it is a relatively well studied area. The general circulation of the area and the flow through adjacent passages has received considerable attention, and results can be compared with earlier work.

B. Background

The earliest American oceanographic observations were made in the Caribbean Sea and adjacent regions. Bartlett, Sigsbee, and Pillsbury of the U. S. Coast and Geodetic Survey made early observations from the USS Blake, according to Wust (1964), 'particularly in the depths of the Caribbean and its passages' in the years 1867-69. This early work focused on the role of the Caribbean as the 'source' of the Gulf Stream. Direct measurements of current were made by Pillsbury (1890) in the Florida Straits. This data, taken from the Blake while at anchor, extended to a depth of 230 meters. Schmitz and Richardson (1968) calculated transport using Pillsbury's data extrapolated to the bottom, and found a total of 25.1 x 10^6 m^3/sec (linear extrapolation) to 29 x 10^6 m^3/sec (non-linear extrapolation) flowing northward. The near surface data of Pillsbury (see Sverdrup, Johnson, and Fleming (1942), p. 674) compare well with velocity sections made by Richardson, Schmitz, and Niiler (1969) using transport floats.

The first comprehensive hydrographic survey of the Caribbean was made from the Atlantis in the early 1930's and is discussed by A. E. Parr (1937). After the advent of the Schleicher-Bradshaw conductivity salinometer to replace the less accurate and more tedious titration method, the Atlantis survey was repeated during the International Geophysical Year by W. G. Metcalf aboard the Crawford (Metcalf, 1959). Wust (1964) found a total of 1725 stations to depths greater than 200 meters in the Caribbean taken between 1877 and 1961. More recently, the CICAR observations have extended the spatial coverage as well as including the time domain through repeated occupation of 10 standard

sections in the Caribbean and adjacent waters. A CICAR status report prepared by the National Oceanographic Data Center in 1977 showed 2326 stations taken between 1969 and 1975 (not including a number of cruises which hadn't yet reported) by ships of 9 nations. For our purposes, it is unfortunate that many of these stations do not go to the bottom and some of the sections stop before reaching shallow water.

The transport through the Florida Straits and thus the outflow from the western Caribbean is one of the best known quantities in physical oceanography. The measurement technique (transport floats) is discussed in Richardson and Schmitz (1965). Schmitz and Richardson (1968) found a mean transport of $32 \pm 3 \times 10^6$ m ^{3}/sec northward. With additional data, Niiler and Richardson (1972) calculated a mean of 29.5×10^6 m ^{3}/sec and annual variability of amplitude 4.1×10^6 m ^{3}/sec. They also found large variability (about 10 to 20%) on time scales as short as a few weeks. A small number of measurements by Stalcup and Metcalf (1972) using moored current meters and transport floats in the passages of the Southern Lesser Antilles suggested that most (about 26×10^6 m ^{3}/sec) of the inflow occurred through these passages. Subsequently, geostrophic calculations by Gordon (1967) and by Morrison (1977) in the eastern and western basins of the Caribbean reinforced the idea that nearly all of the water enters by the eastern passages.

Wust (1964), in his monograph on the Caribbean, used the 'core method' to study the origins of Caribbean waters as well as circulation and mixing in the region. He identified a number of core layers for

study, using property extrema to trace the path of a core. These include surface water (temperature maximum), Subtropical Underwater (salinity maximum at 50-200 meters), the cold water-warm water boundary (oxygen minimum at 400-600 meters), Subantarctic Intermediate Water (salinity minimum at 700-800 meters), North Atlantic Deep Water (oxygen maximum at 1800-2500 meters) and Caribbean Bottom Water (minimum potential temperature). Morrison (1977) took a similar approach, following property extrema along potential density surfaces, and identified several additional cores.

One difficulty of this method is that the anomalous water of a core need not be a major contributor to a current, in terms of volume transport, and in such a case a trace of the core does not accurately portray the circulation of the layer. An example of this is the subtropical underwater salinity maximum. Wust (1964) traced this water from its origin in a convergence zone near 55^{o}W, 21^{o}-23^{o}N, to several tongues entering the Caribbean mainly by way of the northeastern passages. Morrison (1977) found two axes for the salinity maximum in the eastern Caribbean and used this to support a hypothesis of a dual axial Caribbean Current. However, Stalcup and Metcalf (1972) used oxygen to show that most of the water in the current region is of North Atlantic rather than tropical origin. This was backed up with transport measurements of the passages of the Southern Lesser Antilles which showed large inflow of North Atlantic Water. In this case the cores illustrate the spreading of a minor flow component entering from the northeast, while the main component from the southeast is invisible through its lack of anomaly. Interestingly, though, recent measurements by Brooks (1978)

in the St. Lucia Passage give a considerably lower transport (1.7×10^6 m^3/sec) than that obtained by Stalcup and Metcalf for the same passage (6×10^6 m^3/sec).

At intermediate depth, the eastern Caribbean has water in which a substantial fraction is of South Atlantic origin (Wust's Subantarctic Intermediate Water). Worthington (1971) noted relatively low salinity anomaly in this layer in the Florida Straits compared to the eastern Caribbean. A flux of salt through the northern passages is indicated, although the amount and mechanism are still in doubt.

Principal among problems of the deep Caribbean is the question of renewal. Wust (1964) suggested that water spills more or less continuously over the Windward and Jungfern sills into the western and eastern basins of the Caribbean. Worthington (1955) hypothesized that the deep water has not been renewed for some time (order centuries). He presented evidence (Worthington, 1966) of warming in the Cayman basin and hydrographic sections across the sills in which no indicative upturning of isotherms could be seen near the sills. Sturges (1965) showed that θ/S characteristics of deep water in the western basin were continuous with both the eastern basin and with the Atlantic but that the eastern basin and Atlantic were discontinuous. This was taken to indicate renewal via the Windward Passage and then from the western to the eastern basin. Any inflow through Jungfern was assumed to have occurred at an earlier time. Richards (1958) found that Caribbean waters were enriched in silicate with respect to the North Atlantic, a fact which supports slow renewal. Sturges (1970, 1975) and Stalcup et al. (1975) used STD and direct current measurements to document sporadic pulses of cold

($\theta < 3.8^{o}$) water across Jungfern sill. Transports of up to .050 x 10^{6} m^{3}/sec were estimated, possibly sufficient (Sturges, 1970) to maintain steady state heat and oxygen budgets in the deep eastern Caribbean. A rate of this magnitude would be much too small to emerge from the noise in our calculations.

C. Data Selection and Treatment

Essential criteria for choosing hydrographic station data were that it

i) be of known high quality

ii) extend vertically to the ocean bottom

iii) extend horizontally into shallow water

iv) define enclosed areas

In addition, good spatial resolution is desirable and optimally, the data should be nearly simultaneous. These last two conditions had to be compromised. The final choice of data is shown in Table 2.1 with station locations in figure 2.1. All data were taken in winter months except for the Fort Pierce and Northeast Providence sections. The summer Fort Pierce section was used rather than a winter one because it, like the other sections, was done by a Woods Hole ship, and also for purposes of comparison because this is a section used in the calculation of Wunsch (1978). All data were collected either by W. G. Metcalf or L. V. Worthington.

Figure 2.1 shows a total of 103 station pairs defining 5 closed boxes. A valuable addition to the data set would be a section across each of the passages leading into the eastern Caribbean, crossing near sill depths.

After some experimentation, the water column was divided into 7 layers, separated by surfaces of potential density for pressures less than 1000 decibars and potential density referred to the 2000 or 4000 decibar surface for deeper water. The defining surfaces are listed in Table 2.2. A smaller number of layers gave significantly poorer results. A 15-layer system was tried using one area only, and did not seem better than the 7-layer system. The 7-layer system was adopted for computing economy.

D. Results

1. Volume transport

The initial (unbalanced) and final (balanced) transports in the top four layers plus the total water column are shown in Table 2.3. Below σ_θ = 27.4, corresponding to the densest water flowing through the Straits of Florida, there is no significant net mass transport in any of the sections. Singular value decomposition solutions are given for rank 18 and 27 in the case where the initial reference level is 1000 meters. The high stability of the solution is demonstrated by the fact that none of the corresponding transports differ by more than 2×10^6 m ^{3}/sec. Ridge analysis solutions are shown for initial reference levels of 1000 and 4000 meters. The degree to which the transports are well determined is shown by the differences between these solutions, always 1×10^6 m ^{3}/sec or less although the initial fields differ by as much as 20×10^6 c ^{3}/sec.

Initial imbalances are predominately in the lower layers. Because of the small vertical shear below the thermocline, typically a couple of centimeters per second between 1000 meters and 4000 meters, the initial

transports in the upper layers are much the same for the 1000 meter and 4000 meter cases and are nearly in balance. In the solutions, relative small adjustments are made in the net transport of the upper layers while the lower layers are adjusted to satisfy the powerful constrants of no deep net flow.

It was felt that, for purposes of comparison, water masses defined by temperature as in Worthington (1976) would be useful. Therefore, using the solutions obtained from potential density layering, the transports were calculated for temperature layers $17^{o}C$, 12^{o}-$17^{o}C$, and 7^{o}-$12^{o}C$. The coldest water in the Straits of Florida is about $7^{o}C$. Worthington (1976) refers to these layers as the warm water layer, the upper thermocline, and the middle thermocline. Transports for these 3 layers and total transport above $7^{o}C$ are shown in table 2.4 and figure 2.2. In the following, the transport is described by proceeding from the most general, and therefore best determined characteristics, to the more detailed and less well-determined.

The estimate of 31 x 10^{6} m^{3}/sec through the Fort Pierce section is quite reasonable given the finding of Niiler and Richardson (1973) of a mean transport of 29.5 x 10^{6} m^{3}/sec between Miami and Bimini. For comparison, the 2 x 10^{6} m^{3}/sec through Northeast Providence channel should be subtracted from the 31 since this channel is between Niiler and Richardson's Miami to Bimini section and the Fort Pierce to Mantanilla Shoal section. Of the 29 x 10^{6} m^{3}/sec flowing out from the western Caribbean, about 7 x 10^{6} m^{3}/sec enters the Caribbean from the north via Windward Passage and the remaining 22 x 10^{6} m^{3}/sec flows across the eastern Caribbean from the passages in the Lesser Antilles.

Estimates of geostrophic transport by Gordon (1967), based on much the same data as are used here, but with Defant's method (see chapter 1) to fix a level of no motion, gave transports averaging 29 x 10^6 m^3/sec in the eastern Caribbean and 31 x 10^6 m^3/sec in the western Caribbean. Morrison (1977) calculated transports relative to the bottom of 29 x 10^6 m^3/sec for data collected in the eastern Carribean both in the winter of 1972 and fall of 1973. Although Gordon (1967) and Morrison (1977) do not show transport layer by layer, it is likely that the discrepancy between their estimates and those shown here is mainly in the deep water where the net flux of mass should be small. Worthington (1976), in attempting a property balance for the whole North Atlantic, required roughly 10 x 10^6 m^3/sec to enter the Caribbean through Windward Passage and about 20 x 10^6 m^3/sec to enter the eastern Caribbean.

The 17 x 10^6 m^3/sec of warm water shown leaving the Caribbean in table 2.4 is composed of 12 x 10^6 m^3/sec from the eastern Caribbean and 5 x 10^6 m^3/sec from Windward Passage. An additional 2 x 10^6 m^3/sec through Northeast Providence Channel brings the total through the Fort Pierce section to 19 x 10^6 m^3/sec, close to Worthington's estimates of 20 x 10^6 m^3/sec. Table 2.4 shows 6 x 10^6 m^3/sec leaving the Caribbean in each of the thermocline layers, with 5 x 10^6 m^3/sec having come from the eastern Caribbean in each case. Worthington (1976) calls for 5 x 10^6 m^3/sec in the upper thermocline, all entering from the east, and 5 x 10^6 m^3/sec in the middle thermocline, all entering through Windward Passage. His argument is based on conservation of salt, which will be discussed in a later section.

2. Geostrophic Velocity

Contour plots of velocity for each of the principal sections are shown in Figures 2.3a-g. These are based on the K = 27 singular value decomposition solution using an initial reference level of 1000 meters. For comparison, velocities from the ridge analysis solution using an initial reference level of 4000 meters are shown in Figure 2.4 for the Cuba-Panama section. The two solutions are almost identical in the upper 1000 meters and show some differences at the north end of the section in the sluggish deep flow.

A tempting interpretation of the profiles at 64^{o}W, 68^{o}W, and 73^{o}W (Figures 2.3a, b, and c) is that the flow through the multiple passages of the eastern Caribbean is broken into several streams and eddies, giving the rather confused picture shown in the Virgin Island-Venezuela section. Here there are three (or four?) westward flowing streams separated by counterflows. The broadest of these westward flows shows several secondary maxima. In the Haiti-Venezuela section, there are only two westward flows separated by a counterflow. The southern one has a secondary maximum. In the Haiti-Colombia section, there is perhaps only a single broad current with two maxima. Thus, downstream from the passages, the flow has begun to coalesce, and less small scale energy is apparent. However, one must be very cautious about this interpretation since the station spacing is quite irregular. The spacing is finest in the Virgin Island-Venezuela section and it is not unlikely that a finer spacing at the other sections would reveal more small scale features. An alternate view is given by Morrison (1977). He

suggested that the shallow general circulation in the eastern basin consisted of two separate westward streams with counter currents on the north sides of both.

Progressing to the west, the section from Cuba to Columbia shows a broad Caribbean current in the south, over the Columbia basin. The current, which has entered the Windward Passage, can be seen in the north over the Cayman basin. Once again, it is smoother than the section just inside the passage. The Windward Passage section shows a somewhat confused westward flow about 85 kilometers in breadth, spanned by 7 station pairs. The more organized flow some 500 kilometers downstream is about 170 kilometers wide, spanned by only 3 or 4 station pairs. Between the Windward Passage and Caribbean currents in the 79^{o}W section, a region of small scale recirculation is seen. This could be interpreted either as eddying downstream of Jamaica and the Jamaica Ridge, or it could be an artifact of the northward turning of the Caribbean current, parallel to the section, along the coastline of Central America. The flow is smoother in the Cuba to Panama section, although it still shows the two distinct maxima associated with the two currents entering the Caribbean.

In the deep water, the eastern Caribbean shows evidence of a basin scale cyclonic gyre. Each of three eastern sections shows broad deep westward flow in the north and broad eastward flow beneath the westward Caribbean current. Solutions using an initial reference level of 4000 meters alter the breadth and velocity maxima but not the general structure. The maximum recirculation occurs in the center section, i.e. Haiti-Venezuela, and has a magnitude of about 40×10^{6} m^{3}/sec.

Here, since the meridional scale of the feature is at least comparable to the zonal separation of the sections, the inference of continuity of the feature from one section to the next is stronger than in the case of the flows and counterflows of the near-surface current.

3. Salt Conservation

In chapter I, the scheme for conserving mass in a number of density layers was discussed. For layers of infinitesimal thickness (i.e. isopycnal surfaces), mass conservation would be wrtten

$$\int (\bar{u} \cdot \hat{n}) \, ds = 0$$

The coordinate along the boundary of the isopycnal surface is s. In addition to mass, salt and some other chemical tracers are conserved in the ocean, and in some cases information independent of the mass field can be obtained from the distribution of these tracers. First, imagine a set of isopycnal surfaces along which salinity is constant ($S = S(\rho)$). Then, conservation of salt (neglecting time dependence and diffusion) is given by

$$\int S (\bar{u} \cdot \hat{n}) \, ds = S \int (\bar{u} \cdot \hat{n}) \, ds = 0$$

That is, conservation of mass guarantees conservation of salt. Next, suppose that salinity varies with position along the surfaces.

$$S = S(\rho) + \Delta S$$

The quantity ΔS is called the salinity anomaly. Then

$$\int S\,(\bar{u}\cdot\hat{n})\,ds = S\int(\bar{u}\cdot\hat{n})\,ds + \int \Delta S\,(\bar{u}\cdot\hat{n})\,ds = \int \Delta S\,(\bar{u}\cdot\hat{n})\,ds$$

The field of salt anomaly is conserved independently of the mass field. Note, however, that the neglect of diffusion is less justifiable with salt than with density. In both cases, cross isopycnal mixing, which requires work against buoyancy forces, is ignored. With salinity, mixing along isopycnals is also ignored, though by definition this is not necessary with mixing of density.

In the Caribbean, a tight correlation between salinity and potential temperature (implying $S = S(\rho)$) holds except in a couple of layers. Most Caribbean water is indistinguishable in θ/S from water of the northwest Atlantic. The θ/S correlation for this water was given by Worthington and Metcalf (1961). An anomalous layer in the Caribbean is Antarctic Intermediate Water which is distinguished from standard North Atlantic Water by a negative (fresh) anomaly of salt. South of the Caribbean, Fuglister (1960) shows a northward erosion of the salinity minimum that marks the core of this water. Minimum salinity is about 34.34‰ at 32^{o}S, increasing to 34.70‰ at 16^{o}N near the Antillean arc. Inside the Caribbean, the minimum is about 34.73‰ at 64^{o}W, increasing to 34.82‰ at 84^{o}W.

Figure 2.5 is a map of salinity anomaly with respect to the values of Worthington and Metcalf (1961) for the Caribbean in layer 4, corresponding to $27.2 < \sigma_{\theta} < 27.4$. This layer contains the core of

Antarctic Intermediate Water. The contour interval is .03‰ and the values represent vertical averages over the thickness of the layer. The magnitude of the anomaly is in excess of .3‰ in the southeast, diminishing to values of .2‰ and less in waters leaving the Caribbean. The contouring is, of course, somewhat imaginative since the data coverage is sparse.

Advective constraints on conservation of salinity anomaly were imposed in layers 3 and 4. Salinity anomaly is used rather than salinity because the latter, being nearly a function of density, gives equations that differ from mass conservation equations by a very small amount. The results showed that the advective model is insufficient to account for the observed distribution of salt. Small but consistent residuals showed a loss of salt from all 5 areas, indicating that not enough salt was supplied by advection to account for the downstream loss of anomaly.

Inspection of the map of salinity anomaly supports this conclusion. An advective description, as noted by Worthington (1976), requires a large input of North Atlantic Intermediate Water through Windward Passage in order to produce the smaller anomalies seen downstream in the Fort Pierce section. However, the Cuba-Panama section should then show low anomaly in the north, downstream from the Windward Passage input. The large salt gradient, about .1‰ between the Windward Passage and Cuba-Panama sections supports the smaller mass flux through Windward Passage (less than 1×10^6 m^3/sec) determined in the inverse calculation. Indeed not all of the excess salt can possibly enter through Windward Passage since the Fort Pierce section shows water saltier than the Cuba-Panama section. This suggests some addition of salt through Northeast Providence Channel.

The fact that the advective balance cannot account for the downstream loss of anomaly does not mean that there is no information contained in fields of salt and other tracers, but rather that the distribution of salt has not been adequately modelled. A mixing term could easily be included in the conservation statements. However, in the Caribbean it is unlikely that enough extra information would be contributed to compensate for the unknown variable mixing coefficient. In other problems, an improved modelling of tracer conservation can contribute important information and further improve the integration of the dynamic method with water mass analysis.

If one accepts the small net flux of intermediate water through Windward Passage, how then is the salt balance achieved? The highly structured velocity profile (Figure 2.3f), if representative of instantaneous conditions in Windward Passage, shows that water can be rapidly mixed along the passage. Similarly, Metcalf (1976) has found North Atlantic Intermediate Water on the Caribbean side of Jungfern passage. Here the net flow was found to be a small net flux outward at this level (in agreement with the north end of Figure 2.3a, which spans the passage). Property distribution, however, indicated both inflow and outflow. It is suggested that since advection is insufficient to balance the salt budget in intermediate Caribbean depths, that the necessary excess salt is introduced by oscillatory, highly diffusive motion in the Anegada-Jungfern, Windward and Northeast Providence passages.

4. Resolution

In this section, the methods discussed in Chapter 1 on resolution are applied to the Caribbean example. Relevant questions include: to what extent, in terms of distance or number of station pairs, are features in the velocity field smeared out horizontally because of imperfect resolution? What features are real and what ones are likely to be the product of side lobes from circulation in other areas? How well is the transport through individual sections determined? Bear in mind that, for the solutions discussed in the previous section, only the reference level velocity is a product of smoothing by VV^T. The relative velocities are computed from the unsmoothed data via the thermal wind equation, and are in a sense perfectly resolved. When we speak of transport resolution, this refers only to that part of the transport due to the reference level velocities, i.e. the integral

$$\int b \, d x \, d z$$

Relative transport,

$$\int v^r \, d x \, d z$$

is completely determined within the bounds of measurement errors and ageostrophic effects.

To begin the study of resolution, eight columns from the transport resolution matrix, defined by equation 1.25, are plotted in Figure 2.6a. These are based on a K = 27 solution and the columns, each one showing

the resolution at a single station pair, were selected as being representative of other columns from the same sections, except near the edges. The top two, for comparison, are adjacent station pairs in the Virgin Island-Venezuela section and the others are one each from the other main sections. Every plot shows a main peak centered at or near the location of the given station pair with peak widths of from 4 station pairs on the Windward Passage section to about 9 station pairs in the Virgin Island-Venezuela section. For the former, this corresponds to a smoothing window about 40 kilometers wide and about 600 kilometers for the latter. The area under the central peak (whose width we define by adjacent zero crossings) gives the net transport in the set of station pairs which define a resolution group for the given station pair. If the resolution was perfect, the peak would be a delta function, with unit area. The areas of the eight peaks displayed in figure 2.6a are 1.02 $\pm$ .04. Total transport is conserved in these examples and is conserved for nearly all station pairs in the problem with a very few exceptions near section edges where the area is as low as .7.

A smaller number of eigenvalues gives a system in which the constraints are not as well satisfied. Obviously, if no eigenvalues are used the solution would be zero everywhere and the unit area of the perfectly resolved case would map into zero area. The use of more eigenvalues increases the area of the peaks, approaching unity. Figure 2.6b shows the same eight columns for the case K = 18. All central peaks are somewhat broader and lower than in Figure 2.6a, but only the one in the Fort Pierce section shows a substantially lower area of .71.

A measure of transport resolution for the whole system is obtained by summing elements of the transport resolution matrix as follows. First, for a given column of the matrix, row elements are summed over each individual section. A further reduction is made by summing along rows each column element from a given section. Finally, this matrix, of dimension number of sections by number of sections, is normalized by dividing each row by the appropriate number of station pairs in the section. Thus, for example, since the Virgin Island-Venezuela section occupies columns 1-20, the upper left element of the reduced matrix is

$$\sum_{i=1}^{20} \sum_{j=1}^{20} \hat{t}_{ij}$$

Physically, the reduced matrix is interpreted by the following hypothetical problem. Suppose one unit of transport is divided equally between the station pairs of a section. After inversion (smoothing), how much of this transport is found in the correct section and how much in each of the other sections? Table 2.5 shows the result for K = 27. For perfect resolution, this would be the identity matrix. The largest 'spillage' of transport involves the two short sections, Mona and Northeast Providence which are not by themselves well resolved.

Aside from the central peaks in Figures 2.6a and 2.6b, side lobes of varying amplitude are seen. These represent bogus non-local features that arise as the constraints are forced to be more closely satisfied (i.e. as more eigenvalues are used). Comparison of Figures 2.6a and 2.6b shows the gradual increase in number and magnitude of side lobes as the number of eigenvalues is raised from 18 to 27. The fundamental tradeoff

in the problem between resolution and stability is clear. In a problem like the Caribbean, where the resolution is basically compact (see page 24), the amount that can be learned about the real ocean depends on how much resolution can be obtained before noise due to the use of small eigenvalues begins to dominate.

The effect on net transport due to these side lobes is small. This must be the case since they arise with the inclusion of small eigenvalues which represent small adjustments in the constraints. In this problem, they are basically spurious small scale recirculations. This is in contrast to other problems with non-compact resolution (e.g. the first Gulf Stream '60 calculation in chapter 4) where large eigenvalues give rise to large smooth transports in the wrong section.

Some insight into the cause of the side lobes in the Caribbean problem is gained by a close examination of the station pairs involved. The two largest side peaks for the displayed Fort Pierce station pair, and in fact for most of the Fort Pierce station pairs, are two station pairs in the Cuba-Honduras section. These two are remarkable for the depth change (2000 meters and 3000 meters) between adjacent stations crossing the Cayman Ridge. We have seen that large depth changes are likely to cause large errors in the extrapolation to the bottom of temperature and salinity. The main difference in relative layer thicknesses between these and other station pairs of similar average depth is probably due to these errors and to the linearized bottom profile. However, since the solutions assign large values at station pairs of just such anomalous geometry, this is where the large side lobes appear. The relatively poor quality of resolution in the Fort Pierce

section is not due to the sampling in this section at all, but to the coarse spacing of stations in the Cuba-Honduras section. A similar effect is seen in the Cuba-Panama section. Here the largest side lobe for the station pair plotted in 2.6a is at the next to southernmost station pair of the same section, where the depth changes by 1200 meters. This problem could be greatly reduced by using a finer station spacing over rapidly changing topography.

It is pertinent to point out that although both the velocity resolution and transport resolution matrices have these side lobes, the dominant ones are not in general at the same locations. The two Fort Pierce side lobes (in transport) mentioned above are quite small in velocity, about an order of magnitude below the central peak velocity. However, since the stations are widely separated at these pairs, the small velocities cause significant transports. The velocity resolution side lobes also tend to occur where large depth changes are involved, but usually with narrow station spacings, as is often the case right next to the coast. Examples of these will be pointed out in the velocity profiles.

The velocity resolution is most easily seen by comparing the unsmoothed velocity profiles (Figures 2.3a-g) with profiles of smoothed velocity shown in Figures 2.7a-g. As explained in chapter 1, these are obtained by filtering the relative velocities as well as the reference level velocities by premultiplication with the VV^T matrix. The variable smoothing interval can be seen by inspection in these pictures, from a few tens of kilometers in Windward Passage to hundreds of kilometers in the Haiti-Columbia and other sections. The Windward

Passage section is an especially good example of the power of the smoothing operation. The confused, highly structured profile in 2.3f emerges from the smoothing as a single energetic inflow along the Cuban side of the section with a weaker counterflow at the other end.

Recall from chapter 1 that the smoothed velocity profiles are fully determined in the sense of being independent of any choice of initial reference level. The formal underdeterminedness of the problem is relegated to scales smaller than those of the smoothed profiles. Features in the smoothed profiles are real except those arising from noise (side lobes). Examples of noise-generated features are the intense flows at both edges of the Haiti-Columbia section in Figure 2.7c. These show increased amplitude with respect to the unsmoothed Figure 2.3c that can only be the result of a side lobe in the velocity resolution. Similar effects are seen at edges in a few other sections.

The main features described in the discussion of the unsmoothed velocities are also visible in the smoothed profiles. Downstream from the Lesser Antilles, the trend to larger scale in the Caribbean Current is seen. The separate Caribbean Current and Windward Passage inputs are seen at 79°W and as two maxima at 84°W. Finally, the basin scale cyclonic recirculation in the deep eastern Caribbean is seen in Figures 2.7a, b, and c.

E. Conclusions

The circulation of the Caribbean Sea has been described on a variety of spatial scales. Unsmoothed solutions based on initial reference levels of 1000 meters and 4000 meters were computed and compared. Differences in velocities in these two cases were typically 1 or 2 cm/sec

at all depths. The flow on scales of the station spacing is determined to the order of these differences, subject to the assumption that some deep initial reference level is appropriate. This assumption seems more justifiable in the Caribbean than in the open ocean because of the topographic constraint of no deep outflow through the Florida Straits. Qualitatively, the shallow structures were nearly identical for the two initial reference levels, with some differences in the deep flows. Total volume transports in each section differed by no more than 1 or 2 x 10^6 m^3/sec in the two cases. A total transport of 29 x 10^6 m^3/sec was found to exit from the western Caribbean, of which 22 x 10^6 m^3/sec flowed across the eastern basin and 7 x 10^6 m^3/sec entered through Windward Passage.

The smoothed solution has the advantage of being independent of initial reference level, but it describes the flow on coarser scales, ranging from tens of kilometers in the Windward Passage to hundreds of kilometers in the interior of the basin. The smoothed solution is the product of a known filter on the unsmoothed velocities. This filter, in the Caribbean example, acted as a local horizontal averaging operator except in a few station pairs near land, where non-local effects were observed. The estimated variance of the smoothed velocities was generally of order 1 cm^2/sec^2 or less, indicating that wherever the smoothing was local, the observed features were genuine components of the flow field. Some of the characteristics of the flow that were common to smoothed and unsmoothed solutions were the trend to larger scale in the Caribbean Current as it progresses to the west across the Venezuela basin, the presence of a distinct current from the Windward Passage

westward to 84°W, and a large anti-clockwise recirculation in the deep water of the Venezuela basin.

Most of the data in the interior of the Caribbean were collected in February and March of 1958, and the circulation generally represents conditions during that period. Data collected at other times may be inconsistent by virtue of seasonal variability in volume transport, but such inconsistencies are largely compensated by depth independent adjustments in the shallow passages, as described in the last section of Chapter I.

Chapter III

A. Introduction

The Gulf Stream region in the Northwest Atlantic has received relatively intense scrutiny because of its primary role in oceanic energetics and mass transport as well as because of its proximity to the east coast of the U.S. Despite the attention, it is still difficult to give even a qualitative description of the Gulf Stream. The picture of the core of the Stream as a very narrow, continuous, high velocity ribbon of warm water subject to wave-like oscillations is well substantiated by hydrographic and bathythermograph casts, infrared radiometer data from airplanes and satellites, and some direct velocity measurements. The problems occur along the edges and bottom of the high velocity core, where fluctuating velocities are at least as large as the mean, and the distinction between Gulf Stream, countercurrent, and eddy is difficult to make.

Several authors, including Warren and Volkmann (1968) and Fuglister (1963) have discussed the difficulty of defining the Gulf Stream. Upstream, where the Florida Current occupies nearly all of the channel between Florida and the Bahamas, the question of how much water to include in budget calculations is simple. This fact made the measurements of Niiler and Richardson (1973) and Richardson, Schmitz and Niiler (1969), with transport floats in the Straits of Florida, relatively unambiguous. Beyond Cape Hatteras, neither edge of the Gulf Stream is bounded by land. Along the northern edge, the transition in

T/S characteristics to slope water defines a possible boundary although it is still arguable whether entrained slope water should be considered part of the current. To the south, no water mass transition occurs at the Sargasso Sea boundary in a zone of high eddy activity.

Large differences in estimates of the volume transport of the Gulf Stream result from different assumptions of a level of no motion. Worthington (1976) studied a number of hydrographic sections, using the bottom as a level of no motion except where direct measurements were available, and found the transport to increase from 30 x $10^6 m^3$/sec at the Florida Straits to a maximum of 150 x $10^6 m^3$/sec south of Nova Scotia. The vertical shear is of one sign from top to bottom at the location of the Gulf Stream so that the assumption of a deep level of no motion yields eastward velocities from top to bottom. The use of an intermediate level of no motion, such as by Iselin (1936) or Stommel (1965), gives a much smaller eastward transport and implies westward flow at the bottom.

The limited number of direct measurements do not completely resolve the ambiguity, though one can certainly form a consistent interpretation from these data. A time series of three transport float sections were made by Barrett and Schmitz (1971) near $67^{\circ}W$. High temporal variability was observed, with qualitative differences in the flow over a few weeks time. Eastward transport ranged from 129 to 203 x $10^6 m^3$/sec. Warren and Volkmann's (1968) hydrographic section near $68^{\circ}W$, using neutrally buoyant floats to fix a reference level velocity, showed an eastward transport of 101 x $10^6 m^3$/sec. It also showed some bands of westward flow beneath the surface Gulf Stream. Moored current

meter records, described by Schmitz (1979), along 55°W show a mean westward flow at 4000 meters below an instantaneous location of the Stream axis at about 40°N. A mean eastward flow of nearly 10 cm/sec, almost depth independent from 1000 meters to 4000 meters, was seen at 38°N. This pattern of counterflow below the axis, with a narrow eastward flow to the south, was also observed along 70°W (Schmitz, 1977).

The Gulf Stream '60 data set seemed to be an appropriate one for the application of inverse techniques to estimate a snapshot of velocity in part of the Gulf Stream region. The experiment was designed to provide nearly simultaneous hydrography over a large area with good resolution. Most of the 183 hydrographic stations were taken in a three week period by three ships. Coverage runs from Georges' Bank east to the Grand Banks and from 33°N up to the continental shelf. The nine meridional sections are spaced 2° apart in longitude, with stations on whole degrees of latitude in the south and half (or accasionally third) degrees in the vicinity of the Gulf Stream.

This chapter describes two different inverse calculations. The integral type formulation (as in chapters II and IV) is applied to a two-dimensional slice of data, a perimeter of the box. This perimeter was constructed from sections I and VII , the southernmost stations of sections II through VI (see fig. 3.1), and the land boundary on the north. One would anticipate that the fairly coarse resolution inherent to this method will yield a greatly smoothed Gulf Stream. The second calculation assumes a simplified vorticity balance and is applied pointwise in differential form to the entire three dimensional data set.

It allows a higher resolution picture of the flow but with some possible expense in stability.

B. The Integral Inverse

The calculation was done with a single area after some experimentation using multiple areas. Because one would like to resolve groups of physically adjacent stations, it is desirable to use sections that are geometrically dissimilar from each other in the manner discussed in chapter I. Usually, this means that decreasing the size of an area tends to degrade the compactness of resolution. This was the case with the Gulf Stream '60 data. There is, however, a considerable change in the baroclinicity of the Gulf Stream between the first couple of sections, and the last few, after the New England Seamount chain is crossed. On this basis, the first section and one of the last (section VII) were selected as two sides of the box, with the southern edge of the data (33^{o}N) as the third side and the land boundary as the fourth. Except for the Seamount chain, which is poorly resolved by the grid, there are no large alongstream variations in topography. Large topographic variation was thought to be important in the relatively well resolved Caribbean problem of chapter II.

Mass conservation was imposed in 20 density layers plus the total water column. Many of the layers are superfluous, but the large number was used to extract as much information as possible from the single area. The rank of the matrix A was about 7.

Columns 3 to 12 of the transport resolution matrix (1.19) are shown in figure 3.2. Because of the sign convention for velocity (positive is

east or north), a positive transport at section I has the same effect on the mass balance (i.e. mass flowing into the area) as a negative transport at section VII or a positive transport across 33°N. Columns 3 to 5 represent station pairs in the slope water north of the Gulf Stream. It is clear that the slope water in section I is not resolved separately from the slope water of section VII. This is an example of the non-compactness discussed in chapter I. These station pairs also show noisy side lobes in the 33°N section, attributable to the coarse zonal scale of the grid. Station pair 6 is on the northern edge of the Gulf Stream, on the boundary between slope water and standard water. It is almost completely resolved by itself. To illustrate this point, solutions in which the initial reference level was changed from the bottom to the surface show solution reference level velocities in this station pair ranging -9 cm/sec (bottom reference level) to +83 cm/sec (surface reference level). The fact that this difference is nearly as great as the unsmoothed shear from top to bottom implies that the velocity in this station pair is very well determined. Note that station pair 6 includes a band of fairly strong westward flow below the Gulf Stream. Station pair 7 has the greatest shear from top to bottom (186 cm/sec) but it is very poorly resolved. The station pairs in the Sargasso Sea in section I are not well resolved from the 33°N section, also Sargasso Sea water.

On the whole this problem does not exhibit compact resolution and consequently, different initial reference levels will give rather different solutions. Gulf Stream transport and structure will be dependent on the initial reference level. However, unsmoothed solutions

can still be used to explore some possible, consistent states of this interesting region. Knowledge of the degree of indeterminacy resulting from a particular data set is a significant result by itself.

Contour plots of velocity resulting from initial reference levels of 1000 meters and 4000 meters are shown in figures 3.3a and 3.3b for section I. The deep flow appears entirely different in the two plots. Figure 3.3a shows energetic flow near the bottom and a fairly broad band of counterflow beneath the Gulf Stream. Figure 3.3b shows a Gulf Stream that penetrates nearly to the bottom, although the bottom flow is still westward. Only at station pair 6, in the northern part of the Gulf Stream, are the solutions nearly the same. This station pair is easily recognized in figure 3.3b as the point at which the westward bottom flow penetrates up to about 2000 meters.

How much of the eastward flowing water in figure 3.3a should be identified with the Gulf Stream ? Volume transport in the shallow core is about 56×10^6 m^3/sec in this figure. The eastward feature north of the core carries an additional 17×10^6 m^3/sec and the bottom intensified eastward flow just south of the core transports 42×10^6 m^3/sec.

C. The Differential Inverse

1. Vorticity and Density Balance

It is assumed that, except in surface and bottom Ekman layers, the fluid obeys inviscid quasi-geostrophic conservation of potential vorticity

$$\frac{\partial \zeta}{\partial t} + \bar{u} \cdot \nabla \zeta + f \frac{\partial w}{\partial z} - \beta v = 0 \qquad (3.1)$$

The vertical component of relative vorticity is $\zeta = \frac{\partial u}{\partial y} - \frac{\partial v}{\partial x}$. This equation is scaled

$$u = U\,u^* \qquad v = U\,v^* \qquad w = U\,\frac{\Delta h}{L}\,w^*$$

$$x = L\,x^* \qquad y = L\,y^* \qquad z = H\,z^* \qquad t = \frac{L}{U}\,t^*$$

Here, U, H, and L are typical scales of velocity, depth, and length, and Δh is a typical vertical particle excursion. The starred quantities are non-dimensional. Substitution into 3.1 gives the following coefficients for the four terms.

$$\frac{U^2}{L^2} \qquad \frac{U^2}{L^2} \qquad \frac{f\,U\,\Delta h}{H\,L} \qquad \beta\,U$$

Except in the shallow core of the Gulf Stream, values of $L \simeq 50$ kilometers and $U = 10$ centimeters per second are probably reasonable for the eddy field. With $\beta = 2 \times 10^{-13}$ centimeters^{-1} seconds^{-1}, the ratio of the fourth term to the first or second is

$$\frac{\beta L^2}{U} \sim .5$$

This suggest that changes in relative vorticity are of the same order as the advection of planetary vorticity.

Limited observational evidence support this conclusion in the MODE area. McWilliams (1976) estimated the ratio of planetary vorticity to total potential vorticity in the MODE data, with a range from O(.1) at

150 meters to O(1) at 2000 meters. Owens (1979) numerical analysis uses a 6 layer quasi-geostrophic model to simulate the MODE environment in a statistical sense. In time series at a point, his lower layers show a tendency for the time rate of change of relative vorticity to balance advection of relative vorticity ($\zeta_t \approx - u \cdot \nabla \zeta$) over smooth and rough topography. Vortex stretching (shown as time rate of change and advection of vortex stretching) roughly balances advection of planetary vorticity, especially at longer time scales ($\sim$ 30 days). This means that below the thermocline, water columns tend to preserve their relative vorticity while following f/H contours, where H is the thickness of a layer. Above the thermocline, changes in relative vorticity following the fluid are larger. Therefore, in the differential inverse calculation, a balance of vortex stretching and advection of planetary vorticity is assumed to hold only in the deep layers, while all data above 1000 m are excluded.

A further justification is found in the disparity in vertical scales between planetary vorticity advection and relative vorticity advection. In McWilliams' (1976) maps of planetary vorticity advection and total potential vorticity advection over 10 day periods at several depths, the former is visibly correlated over the interval 750 to 2000 meters while the latter is not. In general, the spectra of higher derivative quantities shift to shorter scales, with the amount of shift increasing with spectral breadth. Thus one expects that the spectrum of squared relative vorticity (enstrophy) is shifted toward high wave number relative to the kinetic energy spectrum. The inverse techniques apply an assumed balance at a series of depths. As long as one tries to extract a

small number of pieces of information from a large number of levels, the effect is to depth average the information over some depth range. Small vertical scales are removed as apparent noise while the longer scales are retained.

Another problem is posed by the density equation. The Gulf Stream '60 data contains no information about time rate of change of density. Therefore the steady balance (1.7) is applied. Bryden (1976) used a scale analysis of the temperature equation to estimate the ratio of vertical advection of temperature to time rate of change of temperature. For eddy scales, this ratio was about 1.6. The time rate of change of density is a potential zeroth order term in the density equation, and lacking measurements, a scheme for estimating this term is desirable.

Given data of sufficient spatial resolution, additional terms could be retained in both the density and vorticity equations. For example, relative vorticity might be included in an iterative solution, in which the zeroth order estimate of ζ would be used to correct the vorticity equation, then to form a new estimate of the velocity field and so on until the solutions converged. The time rate of change of density might be used as an additional unknown, with some assumption about vertical structure. It is not believed that these measures are justified in the case of the Gulf Stream '60 data. For stable estimates of derivative quantities, like ζ, the field must be quite densely sampled in order to be slowly varying on the grid scale. a criterion that is not satisfied by the Gulf Stream '60 data. The addition of unknowns also places a heavy demand on the data. While decreasing the residuals, it will tend to make solutions more sensitive to noise by using poorly determined linear combinations of the data.

2. Calcuations

The assumptions discussed in the last section (equations 1.9 and 1.10) together with continuity (1.1) and the thermal wind equation (1.4) lead to 1.11, the beta-spiral equation used by Stommel and Schott (1977). Initial attempts at solutions using 1.11 failed. There was a tendency for the level of no motion ($u_o = -u'$) to migrate to the center of whatever depth range was used. This type of behavior is expected if the data is dominated by noise. The source of the noise could be either a failure of the crude dynamical assumptions or in errors in the estimation of second derivatives of density. Differentiation by finite difference is inherently noisy and it is perhaps optimistic to compute second derivatives of vertically interpolated hydrographic data. An alternative is obtained by vertically integrating the vorticity equation (1.7) and combining with the undifferentiated density equation (1.6) to give

$$u_o h_x + v_o h_y - w_o = - u' h_x - v' h_y + \int_{z_o}^{z} \frac{\beta v'}{f} dz \qquad (3.2)$$

An additional unknown, the integration constant w_o, has been introduced, but the order of the highest derivatives is reduced from two to one. Solutions to this equation were generally stable with respect to the addition or deletion of several standard depths, as long as shallow data were excluded.

The zonal station spacing (about 160 kilometers) is coarser than the meridional spacing (30 to 110 km). In order to have similar scales in the calculation, rectangular boxes were formed with the corners of each

In matrix form, the equations for each box are

$$\begin{pmatrix} h_x(1000) & h_y(1000) & -1 \\ h_x(1000) & h_y(1100) & -1 \\ \cdot & \cdot & \cdot \\ \cdot & \cdot & \cdot \\ \cdot & \cdot & \cdot \\ h_x(4000) & h_y(4000) & -1 \end{pmatrix} \begin{pmatrix} u_o \\ v_o \\ \\ \\ w_o \end{pmatrix} = \begin{pmatrix} (-u'h_x - v'h_y)_{1000} + \int_{z_o}^{1000} \frac{\beta v'}{f}\, dz \\ \cdot \\ \cdot \\ \cdot \\ (-u'h_x - v'h_y)_{4000} + \int_{z_o}^{4000} \frac{\beta v'}{f}\, dz \end{pmatrix}$$

$$\text{or} \qquad A_{16 \times 3}\ b_{3 \times 1} = -\Gamma_{16 \times 1}$$

A row scaling and a column scaling are used (see chapter I), the former to give equal weight to the data at each level and the latter to give equal weight in the solutions to adjustments of each of the variables.

An alternative to solving each box independently would be to impose some conservation constraints on adjacent boxes and then solve the whole coupled system at once. This was not done because of considerations of computer storage (the whole system would have to be done piecewise because of hardware limitations). Also, since the coupling would be an underdetermined problem, it would serve only to smooth the solutions in space. Instead, the coupling-smoothing is performed at a later stage, in a manner described below.

For each box, the solution is obtained by a singular value decomposition of the appropriate matrix A. A formal estimate of errors gives an indication of the severity of the noise. One assumes that the b and Γ matrices are made up of normally distributed random variables. If

box spaced 1 degree apart in latitude (about 110 km) and 2 degrees in longitude (160 km). This provided two overlapping grids, one consisting of 69 boxes with corners on whole degrees of latitude. A second grid of 32 boxes in the Gulf Stream region had corners on half degrees of latitude.

Typical bottom depth was about 5000 meters, but standard depths below 4000 meters were not used because of diminishing vertical gradients (increased interpolation errors) and to stay above the bottom frictional layer. Toward the coast, stations shallower than about 3500 to 4000 meters were not used since the shallow stations contain less data with which to reduce the severe noise. Also, moored array data along $55^{o}W$ (Schmitz, 1978) indicate a reduction in spatial scales north of the Gulf Stream. The Western Boundary Undercurrent, if there was one during the survey, is north of the cutoff.

Interpolation and other numerical techniques are those used in the integral inverse calculations (appendix). Isopycnal slopes are calculated for potential density referred to a local pressure surface at every standard depth from 1000 meters to 4000 meters. There are 16 standard depths in this range, but for statistical purposes the number of independent estimates of the data is taken to be the number of observed depths in this range, usually 12 or 13.

the variance of Γ is

$$\text{Variance } (\Gamma) = \sigma^2$$

then the variance of the b's is

$$\text{Variance } (b) = \sigma^2 C_{jj}$$

$$C = (A^T A)^{-1}$$

Elements of the C matrix are computed from the singular value decomposition (Lawson and Hanson, 1974)

$$C_{jj} = \sum_{i=1}^{N} \frac{v_{ji}^2}{1_{ii}^2}$$

where V_{ij} are elements of the V eigenvector matrix and 1_{ii} are the singular values. An estimate of σ^2 is obtained from the problem residuals

$$R = A\,b - \Gamma$$

$$\sigma^2 = \frac{\sum_{i=1}^{M} r_i^2}{M-N}$$

N is the number of unknowns, 3, and M is the number of independent estimates, about 12. An element of b is significantly different from zero at the 95% confidence level if its magnitude is more than 1.96 times its standard deviation. Using this criterion in the 69 box grid, 42 out of the 69 values of u_o passed the significance test, compared to 31 out of 69 for v_o and 27 out of 69 for w_o.

The zonal velocity was the best determined of the three. Perhaps this was because there was more zonal kinetic energy than meridional

kinetic energy. The standard deviation of u_o varied quite a lot from one box to the next, ranging from a few tenths of a centimeter per second to several centimeters per second in the most energetic regions. With the interpretation of the reference level velocities as an average over the area of the box, the reference level velocities together with the mean vertical shear determine transport. For a box 100 kilometers on a side and 5 kilometers deep a 1 cm s^{-1} error in velocity would cause an error in the estimated transport of $5 \times 10^6 m^3 s^{-1}$. Of this error, approximately $1 \times 10^6 m^3 s^{-1}$ would be above the base of the thermocline (say the 7^oC isotherm) and the rest below.

Although the mean velocities give transport estimates, some of the structure of the velocity field has been sacrificed by using a coarse station grid. The structure can be partially reconstructed by using overlapping or adjacent boxes to form smooth estimates of the pointwise velocities. Given a set of mean velocities and an appropriate assumption about the averaging operator, the pointwise estimates are made by a simple inverse calculation. A graphical analog of this process was discussed by Warren and Volkmann (1968). At each depth, they plotted mean velocity, station pair by station pair, versus distance on a bar graph. A smooth curve was then drawn through the bars such that, in each interval, the area under the bars was preserved.

Here, the averaging operation is taken to be a convolution of the pointwise velocities with a rectangle function of width 110 kilometers (that is, 1^o of latitude, the grid spacing). Depending on whether the

actual station spacing is 1^o or $.5^o$, the forward operator is either

$$\bar{U} = (U_1 + U_2)/2 \quad \text{or} \quad \bar{U} = .25\ U_1 + .5\ U_2 + .25\ U_3$$

Zonal averaging could also be removed, but for reasons of stability and to avoid inverting a very large matrix, this has not been done. The averaging operations are coupled because of common stations and the system of equations for a whole meridional line may be written as

$$A\ u = \bar{u}$$

or, for example

$$\begin{pmatrix} .5 & .5 & 0 & 0 & 0 & 0 & 0 & \cdots \\ 0 & .5 & .5 & 0 & 0 & 0 & 0 & \cdots \\ 0 & 0 & .25 & .5 & .25 & 0 & 0 & \cdots \\ 0 & 0 & 0 & .25 & .5 & .25 & 0 & \\ \cdot & \cdot & \cdot & \cdot & \cdot & \cdot & \cdot & \\ \cdot & \cdot & \cdot & \cdot & \cdot & \cdot & \cdot & \end{pmatrix} \begin{pmatrix} u_1 \\ u_2 \\ u_3 \\ \cdot \\ \cdot \\ \cdot \end{pmatrix} = \begin{pmatrix} \bar{u}_1 \\ \bar{u}_2 \\ \cdot \\ \cdot \\ \cdot \\ \cdot \end{pmatrix}$$

In the longer sections, 14 averages were available to make 16 point estimates, making the A matrix 14 x 16. The problem is slightly underdetermined. A small amount of noise added to the A matrix has the physical significance of a recognition that the velocity is not exactly linear, and that the average values on the right hand side are not precisely correct. Numerically, this stabilizes the problem.

The solution which represents the smoothest possible velocity profile consistent with the data is computed by the tapered cutoff type inverse (see chapter I)

$$u = A^T (AA^T + \bar{\sigma}^2\ I)^{-1}\ \bar{u}$$

$\bar{\sigma}^2$ is the noise stabilization parameter and I is the identity matrix. The

solution contains no structure which is not necessary to describe variations in the average velocities.

This process provides a series of point estimates at a single depth. By applying it at all standard depths, a discretely sampled estimate of the whole field is made. Note that although only the deep data were used to determine reference level velocities, the thermal wind equation can be used to calculate velocities at all depths once the reference level velocity is known. Each of the 8 sections was processed in this manner and used to construct 8 vertical sections of zonal velocity. These are shown in figures 3.4a to h. To avoid confusion with Fuglister's numbering scheme, the first of these sections, constructed using data from Gulf Stream '60 sections I and II, will be called section A, the second (from sections II and III), section B and so on.

In consequence of the error estimates made earlier, structures in the deep water that are associated with significantly non-zero mean velocities are "real" under the statistical and dynamical assumptions. Generally, these are the more energetic features, often found in the Gulf Stream region. The less energetic motion to the south and far north is more often associated with boxes that failed the significance test. Near the surface, errors as great as several centimeters a second are not capable of causing a sign reversal in the velocity simply because of the larger speeds involved. Therefore the shallow structure is held to be "real" (though aliased) nearly everywhere. Quantitative results may be questionable at the edges where numerical stability can be a problem.

3. Results

The net zonal transport of water warmer than 7°C and colder than 7°C for each of the 8 sections, is shown in table 3.1. Because of the large geographical variability in the errors, it is difficult to assign expected errors to the net transports. Rather, these should be based on the consistency of consecutive sections, bearing in mind that the deep transport errors are roughly four times as great as the shallow ones. The estimates above 7°C are quite consistent and show the same trend to a minimum near section V as Fuglister's (1963) calculations of net transport relative to the bottom. These are also shown in table 3.1.

The estimates cover an area from the continental rise almost to the latitude of Bermuda. Bermuda is a somewhat arbitrary boundary, but since hydrographic sections are often made from the U.S. to Bermuda, some comparisons in net transport can be made. The mean value (from table 3.1) of 48 x 10^6 m^3/sec is quite close to the 49 x 10^6 m^3/sec found by Wunsch (1977) in water warmer than 7°C between Cape Henry and Bermuda. Subsequent estimates of Wunsch (1978) using a larger data set gave a range of 30 to 47 x 10^6 m^3/sec. The integral inverse calculation using Gulf Stream '60 data gave transports of 45 x 10^6 m^3/sec at section I and 37 x 10^6 m^3/sec at section VII for water warmer than 7°C and initial reference level of 1000 meters. Worthington's (1976) circulation diagrams are based on geostrophic calculations in the Gulf Stream and water mass continuity in the recirculation region. The diagrams for water warmer than 17°C, 12° to 17°C, and 7° to 12°C show a net flow of about 43 x 10^6 m^3/sec between the U.S. and Bermuda.

The eight estimates in table 3.1 for water colder than $7^{o}C$ are more scattered. The range of -24 to +30 x 10^{6} m^{3}/sec probably indicates some substantial errors, but may also be attributed to meridional flows through the boundary of the region. A single eddy centered on $33^{o}N$ could produce this variation. The mean value of 0 x 10^{6} m^{3}/sec is to be compared to Wunsch's (1977) estimate of -7 x 10^{6} m^{3}/sec and Worthington's (1976) -6 x 10^{6} m^{3}/sec. These net westward flows are associated with the Western Boundary Undercurrent, a feature that Worthington (1976) associates with isopycnal slopes in water of depth 3000 to 4000 meters (Atlantis stations 5422 to 5425) along the 50^{o} West meridian. If the current was present during the Gulf Stream '60 survey, it is at least partly to the north of the 3500 to 4000 meter cutoff used in this study.

If the vertical velocities were sufficiently well determined, then by averaging over the whole area, one could make an estimate of the mean upwelling or downwelling along the sloping isopycnal surfaces. However, with vertical velocities of order 10^{-3} cm/sec, varying rapidly in space and having errors of the same magnitude, there are not enough estimates to extract a mean that may be 10^{-4} cm/sec or less. At best, the vertical velocities can be checked for consistency by a scaling argument. The linear steady vorticity balance implies

$$W = O\left(\frac{\beta UH}{f}\right) \sim \frac{2 \times 10^{-13} \times 10^{1} \times 10^{5}}{10^{-4}} = 2 \times 10^{-3} \text{ cm/sec}$$

The computed vertical velocities at 2000 meters were usually of this order of magnitude, with a range from 10^{-4} to 10^{-2} cm/sec.

Figures 3.4a to h show vertical sections of zonal velocity. Because of the computational method, each figure is a composite of two hydrographic sections. That is, section A (fig. 3.4a) is a composite of the hydrographic sections I and II, section B is from II and III and so on. One might compare figure 3.4a with figure 3.3a (velocity at section I from the integral inverse) bearing in mind that they represent somewhat different data as well as different methods of computation. There are some strong similarities even in the deep water.

The most distinctive deep features in the velocity profiles are the narrow bottom intensified flows near crossings of the Gulf Stream. Interpretation of these flows is subject to the ambiguity of Gulf Stream definition mentioned in the introduction. For example, consider section A (figure 3.4a). If only the eastward flowing water in an area contiguous with the velocity maximum is included, then the Gulf Stream transports at most about 60 x 10^6 m^3/sec through this section and is confined to the upper 1000 meters. However, the deep eastward flow centered at 36.5°N should perhaps be included. The section could be contoured in such a way that this feature was contiguous with the shallow part of the Stream. In this case a total transport near 100 x 10^6 m^3/sec would be estimated, with the Stream extending to the bottom.

No firm conclusion can be made as to whether any of these deep structures extend zonally through several sections or are local eddies with similar zonal and meridional extent. If the recirculation was local then one would perhaps not wish to identify them with the Gulf Stream. Inspection of figures 3.4a, b, and c shows some suggestive similarities at consecutive longitudes. The strong deep westward flow in section A

(fig. 3.4a) has a maximum speed of about 30 cm/sec and is directly below the eastward flowing Stream which is centered at 37.5°N. Just to the south is the eastward flow mentioned above, with a maximum speed of about 20 cm/sec. In section B, the deep westward flow appears just north of the Stream axis. Its maximum speed is about 25 cm/sec and again there is an eastward flow with speeds up to about 20 cm/sec just to the south, now directly below the axis. In section C the deep westward flow again has a maximum speed of about 30 cm/sec and is again just north of the Stream. The corresponding eastward feature has peak currents of 20 cm/sec and is again directly below the axis. Beyond section C there are near surface features that Fuglister (1964) identifies with multiple crossings of a meandering Gulf Stream. It is difficult to reference the deep currents to the position of the shallow Stream. There are, however, deep flows in sections D and E between 38° and 39°N with the westward flowing member of a pair on the northern side of the eastward member. The final three sections appear to have less kinetic energy in the deep water and counterflowing pairs are difficult to identify. The similarity in position and amplitude of the deep pairs at, for example, sections A and C, which are based on completely separate data, suggests that these features have zonal scales of at least several hundred kilometers.

Whether zonally contiguous or not, the narrow bottom intensified bands appear to be a fairly widespread feature of the deep water near the Gulf Stream and might be expected to appear in other sections of velocity made at other times. Three sections were made by Barrett and Schmitz (1971) using transport floats near 67°W. The most striking aspect of this data set is the high temporal variability. Sections taken a few

weeks apart appear very different. The first section shows a big Gulf Stream, with eastward flow from top to bottom in a 150 kilometer crossing of the Stream. The third section, on the other hand, has some obvious similarities to figure 3.4a. It shows a narrow band of westward flow directly below the Stream axis with an eastward band to the south followed by a second, less intense band of deep westward motion. As in figure 3.5a, each of these bands is bottom intensified except for the center one where a scarcity of data causes some ambiguity. The second section of Barrett and Schmitz (1971) also had deep westward flow below the core.

Warren and Volkmann (1968) constructed a velocity section using hydrographic data and neutrally buoyant floats. Near 68^{o}W and 38^{o}N a narrow band of westward flow was found below the Gulf Stream axis. Again, an eastward band and a second westward band were found to the south. The westward currents reached their maxima at the bottom. In both the Warren and Volkmann (1968) and Barrett and Schmitz (1971) profiles, the cross stream scale of the features is somewhat smaller than in figure 3.4a, perhaps due to spatial aliasing in the Gulf Stream '60 data. No attempt is made to suggest that this pattern of deep structures is a steady state, but the reoccurrence of transient features could contribute significantly to the mean flow.

Fuglister (1963) describes the trajectories of several neutrally buoyant floats that were tracked for a period of a few days just a couple of weeks after most of the Gulf Stream '60 density survey was completed. Three floats released near section III at depths of 2550 to 3500 meters were all placed below the velocity core of the Gulf Stream. All three

proceeded to move eastward with speeds of 11 to 17 cm s^{-1}. Fuglister's (1963) figure 10 shows these observed velocities on a contour plot of the geostrophic velocity relative to the bottom in section III. The large eastward speeds have subsequently been used as evidence for a deep Gulf Stream, for example by Worthington (1976). The velocity in section C (figure 3.4c) at the 3000 meter level below the core of the Gulf Stream agrees remarkably well with the float observations. However, the intense westward flow shown just to the north makes the deep Gulf Stream interpretation ambiguous.

The distribution of zonal kinetic energy with latitude is shown in figures 3.5a to c. These estimates are made by taking the sum of the squares of the pointwise zonal velocities and the dividing by two. Recall that the procedure for making the pointwise estimates removed the meridional averaging over a box but made no attempt to remove the zonal averaging. Therefore the kinetic energy may be biased toward a low value by the coarse grid spacing. Figures 3.5a to c show the distribution of zonal kinetic energy with latitude at depths of 200, 1000, and 4000 meters. Since these figures describe a single realization of the velocity field, no conclusions about the time averaged values can be drawn. However, the 4000 meter level can be compared to Schmitz's (1978) graph of low frequency kinetic energy along 55°W taken from current meter data of POLYMODE array II. He shows a peak of about 150 cm^2 s^{-2} near 39°N, tapering off fairly rapidly on both sides. The ratio of the peak kinetic energy to the kinetic energy at 32°N in this plot is roughly 15. The corresponding distribution in figure 3.5c is less smooth since the only averaging is over the eight sections.

However, the same tendency to a peak near the Gulf Stream is seen and the energy levels are comparable. Figure 3.5b, from the 1000 meter level, shows a similar distribution with the same, or slightly more, energy. The energy at 200 meters (figure 3.5a) is up by an order of magnitude compared to the deep values, but the distribution with latitude is quite similar. Ratios of the maximum zonal kinetic energy to the energy at 33°N are 20, 13, and 25 at 200, 1000, and 4000 meters respectively. Changes with respect to longitude of the zonal kinetic energy show a large drop in the deep energy level to the east of the New England Seamount chain.

D. Conclusions

Two different inverse calculations have been described on the same data set. The first uses only a two dimensional slice of data from the boundary of the region. It makes no assumption about vorticity dynamics in the interior of the region. The resulting solution has coarse resolution which does not allow firm estimates of Gulf Stream transport or structure. Its usefulness is in exploring the range of solutions that are consistent with the hydrography.

The second calculation uses the entire three dimensional data set. A fully determined problem was obtained by imposing a vorticity balance. Unfortunately, limitations imposed by the spatial and temporal sampling of the field required that the vorticity and density equations be rather crude approximations. The same sampling limitations yield some ambiguities in interpretation of the solution. However, a fairly highly resolved snapshot of the velocity field was obtained, and it is one that

shows qualitative and a few quantitative similarities to the direct measurements in the same region.

The solution obtained by the second method supports the conclusion that the Gulf Stream does not, in a steady sense, penetrate into the deep ocean although there are large deep eastward flows near the core of the Stream. Strong deep westward flows are also seen, usually fairly small in scale. The deep kinetic energy is strongly peaked in the vicinity of the surface Gulf Stream.

Chapter IV

A. Introduction

The poleward transport of heat by the oceans and atmosphere is a major factor in the maintenance of world climate. A substantial fraction of the incoming radiation in the tropics is exported to higher latitudes to balance the net loss in regions of low solar input.

A number of observational studies of heat flux in the oceans and atmosphere have been made, using ships, moored instruments, radiosondes, and satellite radiometers. Some of these studies are summarized below. A major observational program to monitor oceanic heat flux is under discussion for the 1980's. In advance of such an undertaking, it is important to measure the information content of the existing data. One can hope to learn how and where additional data should be collected.

The studies by Vonder Haar and Oort (1973) and Oort and Vonder Haar (1976) made use of satellite radiometer data to estimate net radiation as a function of latitude for the entire northern hemisphere. Radiosonde measurements gave an estimate of net meridional heat flux in the atmosphere. Meridional heat flux in the oceans was calculated as the residual of total heat flux minus the atmospheric flux. Their mean annual values of oceanic heat transport are shown in figure 4.5. These numbers have been widely quoted although, as the authors stated, the errors in the residual calculation were large. With estimates of oceanic heat transport ranging from 0 to 3 x 10^{15} watts and with a standard error of 1 to 3 x 10^{15} watts, none of the estimates were significantly different from zero at the 95% confidence level. In addition to the

annual mean, Oort and Vonder Haar (1976) also tabulated monthly values of oceanic heat flux as a function of latitude. The variability was as large as the annual mean, but the monthly variations were not very regular and one cannot determine whether a genuine seasonal signal was present, or merely noise.

The other evidence for variability in the Atlantic heat flux was given by Niiler and Richardson (1973). A careful investigation of the temperature and velocity structure in the Florida Straits showed a small temperature increase throughout the water column in the summer, accompanied by a June maximum in transport. Montgomery (1974) pointed out that, with the arbitrary temperature scale, an increase in mass flux does not necessarily imply an increase in heat flux. One needs to know the characteristics of the corresponding southward flow in the interior of the ocean. If the increase in southward transport is confined to the near surface (warm) layers, then the variation in heat flux would be small. Only if more deep water flows southward in the summer could the annual variability be comparable to the mean.

The oceanic heat flux for individual oceans was computed by Hastenrath (1979). Shipboard measurements of air and sea temperature, wind speed and direction, dew point, barometric pressure, and cloudiness are used to compute air-sea exchange of heat in the band from 30°S to 30°N using empirical formulas. Unfortunately, old values of Budyko (1963) were used at higher latitudes. These are less accurate than the more modern values of Bunker (1976). A northern boundary condition was taken from Aagaard and Greisman's (1975) estimates for the Arctic and the meridional heat flux is calculated by integrating the net gain or loss

southward from the northern boundary. When summed over all oceans, Hastenrath's (1979) estimates (see figure 4.5) are rather close to those of Oort and Vonder Haar (1976). Earlier calculations of oceanic heat flux based on heat input and extraction were made by Sverdrup (1957) and Emig (1967). Hastenrath's (1979) results show an interesting asymmetry in the Atlantic and Pacific Oceans. Whereas in the Pacific, the heat flux is directed poleward in both hemispheres, in the Atlantic the heat is found to flow northward all the way from 60°S to 60°N. The Indian Ocean values are all southward.

Bryan (1962) made estimates of oceanic heat flux based on hydrographic data, using zonal sections of the Atlantic and Pacific. At every station pair, he found a reference level that produced zero net transport. Then, away from the western boundary, observed values of the wind stress curl were used to specify a barotropic velocity at each station pair through the Sverdrup relation. The western boundary current was, by continuity, required to balance the Sverdrup flux. Finally, Ekman transport was calculated from observed wind stress. Heat flux was estimated from the resulting field of mass transport. At 36°N in the Atlantic, Bryan found a net heat flux of 77×10^{13} watts. A possible source of large errors in this type of calculation is the neglect of horizontal correlations of velocity and temperature. That is, a barotropic flow in relatively shallow water, if balanced by an opposing flow in deep water, would result in a net flux of heat by virtue of the difference in the vertically averaged temperatures of the two currents.

The difference in latitudinal dependence of the oceanic and atmospheric heat fluxes found by Oort and Vonder Haar (1976) and the

Atlantic-Pacific asymmetry noted by Hastenrath (1979) can be attributed to different physical processes operating in the two fluids. The dominant mechanism for heat transport in the atmosphere is the baroclinic eddy field that is strongest at mid-latitude. Warm eddies moving to the north and cold eddies moving southward are the result of the equatorward gradient in available potential energy generated by differential heating (Holton,1972). Meridional circulations in the vertical plane, driven by convective penetration at the equator, play a relatively minor role.

In discussing oceanic heat flux, it is convenient to consider the three major oceans to be enclosed to the north. The Indian Ocean is enclosed, while the Atlantic and Pacific are connected by the Arctic Ocean. Coachman, Aagaard, and Tripp (1975) summarised transport estimates through the Bering Straits, where about 1.5×10^6 m^3/sec leaves the Pacific toward the Atlantic. In the present calculation this will be considered to be part of the noise, so that the net meridional transport of mass is zero. Evaporation and precipitation are thus also ignored as noise. Along any latitude circle across an ocean, the net time averaged flux of heat is given by

$$\int_0^L \int_{-H}^0 \overline{\rho C_p \theta v}\, dz dx \qquad (4.1)$$

where C_p, θ, ρ, and v are the specific heat capacity (about 4.18 joules/^oC gram), potential temperature, density, and meridional velocity. If ρ' and θ are decomposed into a time average and a fluctuating part (bar denotes the time average and prime denotes the fluctuating part)

$$\rho\ v = \overline{\rho v} + (\rho v)'$$

$$\theta = \overline{\theta} + \theta'$$

then 4.1 can be rewritten

$$\int_0^L \int_{-H}^0 c_p\, \overline{\rho v}\ \overline{\theta}\, dz\, dx + \int_0^L \int_{-H}^0 c_p \overline{(\rho\ v)'\theta'}\, dzdx$$

The time average can be computed over any interval which is long enough to allow transient storage of mass to be ignored. A steady mass flux of 1 x 10^6 m^3/sec into a closed basin 5000 kilometers on a side would cause sea level in the basin to rise by an average of 1 cm in less than 3 days. Because large sea level changes are not observed, transient mass storage must be small over time scales of interest here, a few weeks to years.

Several mechanisms for the transport of heat by the oceans have been discussed, and their relative importance is still a matter of contention. For conceptual purposes, the mechanisms will be subdivided into recirculations in a horizontal plane and recirculations in a vertical plane.

The heat flux due to horizontal recirculation results from surface water flowing poleward, being cooled by the atmosphere, and returning equatorward still near the surface. The currents responsible for this flux may be either large scale, permanent features, like the Gulf Stream, or small scale transient eddies. The large scale currents as well as the eddy field have fluctuations that may result in changes in the amount of heat transported. Because the surface cooling is atmospherically forced, one might expect to

find the large time scales of the atmosphere, seasons and years, mirrored in the oceanic transport of heat.

An estimate of heat flux can be made from the product of the mass transport of a current, the approximate temperature difference between the current and its corresponding counterflow, and the specific heat capacity. Sverdrup et. al (1942) made such an estimate for the Atlantic Ocean at 55^{o}N based on 10×10^{6} m^3/sec of water flowing north near the surface in the eastern part of the ocean and an equal amount flowing south in the Labrador Current at a temperature reduced by 5^{o}C. This gives a net heat flux of about 20×10^{13} watts.

An estimate of the eddy transport of heat was made by Voorhis, Schroeder, and Leetmaa (1976) using data from the Mid-Ocean Dynamics Experiment (MODE). They suggest a pattern of near surface alternating bands of northward moving warm water and southward moving cold water driven by a series of baroclinic eddies. A single eddy was thought to be capable of transporting about $.8 \times 10^{13}$ watts. It is difficult to account for a substantial fraction of the probable total heat flux through this mechanism.

The second subdivision is meridional recirculation in a vertical plane. This includes any meridional flow which is balanced by a counterflow at a different depth. For example, suppose water flows poleward either on the surface or along some submerged isopycnal that eventually intersects the surface. Surface cooling increases the density of the water which eventually returns equatorward on a deeper isopycnal, possibly after convective penetration to great depth. Jung (1952) suggested that meridional circulations in the vertical plane could

produce a very large heat flux in the ocean. On a volume basis, this type of circulation is more efficient than the horizontal recirculation mechanism because of the large temperature difference, especially at low and middle latitudes, between surface and deep water. By adjusting a level of no motion to give zero net mass flux for a pair of hydrographic stations spanning the Atlantic at 27^{o}N, Jung (1952) estimated a net northward flux of about 120×10^{13} watts.

The vertical recirculations need not necessarily result in a poleward heat flux. In the Atlantic, for example, because the primary source of deep water for the whole ocean is in the Norwegian and Labrador Seas, the deep water may have a net southward transport even in the South Atlantic. If balanced by a shallow northward flow, then the net heat flux would be northward everywhere. This can explain Hastenrath's (1979) observed asymmetry in the Atlantic and Pacific. He found a poleward flux of heat in both hemispheres in the Pacific, but a northward heat flux in both the North and South Atlantic. There is no renewal of abyssal water in the North Pacific.

Meridional Ekman transport, driven by zonal wind stress, can also be considered as part of a vertical recirculation if the surface flow is balanced by an opposing flow in the interior. Again the heat flux can be directed either poleward or equatorward depending on the sign of the zonal wind. The Ekman transport is ageostrophic and will be ignored in the present calculation. The size of the neglected heat flux will be discussed later.

On the basis of the earlier work, several questions may be formulated for the present study. First of all, what is the range of heat flux

values that is consistent with the hydrographic data? Can these data support as large a heat flux as that suggested by Oort and Vonder Haar (1976) and Hastenrath (1979)? Second, how much heat is transported by recirculations in the horizontal plane and how much by recirculation in the vertical plane? If the large values are indeed correct, then the vertical recirculations are favored because of the much larger temperature difference in the vertical plane than in the horizontal.

B. The Inverse Calculation

The Atlantic Ocean was chosen first for a heat flux calculation because of the existence of the IGY zonal hydrographic sections at a number of latitudes from 32°S to 59°N. A calculation using the entire data set would be desirable, but limitations on computer storage and time necessitated selection of a subset for this study. Therefore, rather than as a conclusive determination of the heat flux, the problem was regarded as one of investigation of the suitability of the heat flux problem to a solution by inverse calculations, a testing of appropriate constraints, and an exploration of the range of values of heat flux that are compatible with the limited data. The mid-latitude sections at 24°N (along with a Florida Straits section), 36°N, and 48°N (Table 4.1) were selected to include part of the region where the flux is supposed to be large, while excluding areas near the equator where the errors in geostrophic calculations become large.

The areas enclosed by the selected data are very large relative to the problems discussed in chapters II and III. Also, the sections were made in several different years, and in different seasons. There is

therefore some concern about the internal consistency of the system with the assumptions of geostrophy, steadiness, and no flow across isopycnal surfaces. Because of the length of the sections, Ekman transport (a departure from geostrophy) may be on the order of 3×10^6 m^3/sec. This could give rise to significant imbalances in geostrophic upper layer transport between latitudes with opposing zonal wind stress. A scheme for rectifying this problem will be described later. The steadiness assumption encounters problems from several different time scales. One would prefer to have data taken over a short period of time in order to eliminate inconsistencies due to seasonal or interannual variations. One must assume that the transport variations are not too great and will be smoothed out in the inversion. However, even with simultaneous data, one would have only a single realization of a field containing eddies that evolve significantly in a few weeks. Because the eddies are imbedded in the hydrography, they are likely to have some expression in the solutions, but since the eddy field is not well sampled and is also not well resolved by the inverse method, the eddy heat flux cannot be adequately estimated. Finally one should note that even a small net cross-isopycnal flow can cause problems in very large areas. The area of the North Atlantic between 24^oN and 36^oN is about 10^{17} cm^2. A mean cross isopycnal velocity of only 10^{-5} cm/sec would give a mass flux of 10^{12} gm/sec between layers.

Some trial runs were made with different potential density layers and different numbers of potential density layers, using the UU^T matrix (derived from the matrix U of eigenvectors) to determine the information content of individual layers. Layers with large information content were

subsequently subdivided and layers with little information were combined. The final choice of 14 layers is listed in Table 4.2. A larger number of layers is used in this problem than in the Caribbean example (chapter II) because in the Caribbean, less information was contained in the deep water.

The conservation constraints were imposed as follows. The three latitudes define two closed areas. If a layer does not surface inside an area, then mass is assumed to be conserved in that layer. The top three layers surface between 36^{o}N and 48^{o}N and so no conservation requirement is used in these layers in the northern area. This gave a total of 25 mass conservation equations for individual density layers, and these equations were given equal weight. Two temperature layers (3^{o} - 4^{o}, and $< 3^{o}$C) were also defined and used for four additional mass conservation equations. Total mass is constrained to be conserved in each area, and since the ocean basin is closed to the north except for the small input from the Arctic, total mass flux is required to be zero at each latitude. The total flux of salt (not salinity) is also constrained to be zero at each latitude. This is because the atmosphere does not transport a significant amount of salt, and the input of salt through river runoff is negligible. Total flux constraints were given a higher weight than layer constraints. At 24^{o}N, the flow through the Florida Straits is required to be 30×10^{6} m^{3}/sec toward the north in order to agree with the results of chapter II and with direct measurements. This constraint would be superfluous if the Caribbean data (chapter II) were included in the present problem, but with the sparse data being used, it constitutes additional information. The IGY 24^{o}N

section is then required to carry the corresponding $30 \times 10^6 m^3/sec$ southward. The total number of equations in the system was 39. A second problem was constructed to investigate the compatibility of the hydrographic data (and the model) with the large meteorologically determined values. In accord with Hastenrath (1979), the oceanic heat flux was required to be 155×10^{13} watts at 36^oN and 63×10^{13} watts at 48^oN, thus giving 41 total equations in the second problem. The heat flux constraints were given large weights.

The choice of constraints outlined above is not the only one possible in the problem. Rather than coupling the sections through conservation equations for individual layers, Wunsch (private communication) made a calculation using single sections and conserving mass in each layer at a low weight relative to the conservation of total mass. This can be interpreted as minimizing the amount of northward flowing surface water which is converted to southward flowing deep water. It could be expected to give a fairly small heat flux, dependent on the relative weight of the layer equations to the total mass equation.

C. Results and conclusions

1. Transport

In order to investigate a range of consistent solutions, five test cases were run. A mid-depth initial reference level (1000 meters, case 1a) and a deep initial reference level (4000 meters, case 1b) were used to sample the range of unsmoothed solutions resulting from different initial conditions. For each initial reference level, solutions were computed with and without a heat flux specified at 36^oN and 48^oN. The conditions for each case

are listed in Table 4.3. Sharp cut-off type solutions (see chapter I) were computed using 15 eigenvalues (K = 15) when heat flux was specified and 13 eigenvalues when heat flux was not specified. Because the heat flux constraints constitute independent equations with respect to the conservation equations, they increased the rank of the matrix A by 2. That is, the 15th eigenvalue in the solutions with heat flux specified is about equal to the 13th in the other case (with the first eigenvalues also being about equal).

The initial (unbalanced) transport in each layer for the 1000 m and 4000 m initial reference levels are listed in Table 4.4 along with the final (balanced) transports for each of the four cases. For easier reference, and to disclose any systematic imbalances in mass, Table 4.5 shows the final transports summed over the top layer ($\sigma_\theta < 26.8$), layers 2 to 5 ($\sigma_\theta > 26.8$ and $\sigma_2 < 36.5$), layers 6 to 10 ($36.85 < \sigma_2 < 37.09$), and layers 11 to 14 ($37.09 < \sigma_2$). Because of T/S variations, the temperatures of the layer interfaces are variable, but in mid-ocean in the 36°N section, the interfaces are at roughly 14°C for the bottom of layer 1, 4.7°C for the bottom of layer 5, and 2.8°C for the bottom of layer 10.

First, consider the results of cases 1a and 1b, in which no heat flux was specified. The top five layers show generally northward flow, with most of the northward transport in the top layer. Layers 1, 2, and 3 intersect the surface south of 48°N. There is no layer 1 water in the 48°N section, but a large increase in the northward flow of layers 2 and 3 reflects the cooling of layer 1 through contact with the atmosphere

and its conversion to layer 2 and layer 3 type water. The lower nine layers have generally southward flow, fairly evely distributed in depth. The final transports in both case 1a and case 1b resemble the initial field with reference level 1000 (1a) meters more strongly than they do the one with a deep reference level (1b). This reflects the fact that the latter initial field is farther out of balance than the former. With a deep initial reference level, relative flow is generally northward at all levels (except mid-depth at 36^{o}N). Consequently, a lower value of $b^{T}b$ (the squared length of the solution vector) results in case 1a, and the solution shows slightly better mass balances.

At 24^{o}N and 36^{o}N the amount of northward flowing warm water is $8.5 \times 10^{6} m^{3}$/sec in case 1a. Case 1b shows an inconsistency in this layer, with $8.4 \times 10^{6} m^{3}$/sec at 24^{o}N becoming $15 \times 10^{6} m^{3}$/sec at 36^{o}N. One might favor the lower value because of the better consistency of case 1, but most of the difference could be made up by the northward Ekman transport at 24^{o}N and southward Ekman transport at 36^{o}N. The total amount of warm water flowing northward which must be converted to colder water ranges from 12 to $17 \times 10^{6} m^{3}$/sec at 24^{o}N and 36^{o}N. The 48^{o}N section shows the largest difference, with the two solutions giving about 9 and $22 \times 10^{6} m^{3}$/sec for the northward flux.

Next, look at the transports resulting from cases 2a and 2b, in which a large heat flux is used as a constraint at 36^{o}N and 48^{o}N. Again, the upper five layers flow north and the bottom nine flow south, but the amplitude of this cell is increased. Furthermore, the amplitude of the meridional cell is much less dependent on initial reference level, being

$23 \pm 2 \times 10^6$ m^3/sec at both 36°N and 48°N. At 24°N, apparently the mass constraints in individual layers are not sufficiently strong to drive an equally large cell in the vertical plane. It is interesting that the northward flow of warm water at 24°N (i.e. the top layer) is virtually the same in each of cases 1a and b and 2a and b. It will later be seen that the net flow in this layer determines the heat flux to a first approximation. It was concluded that the smaller amplitude cell at 24°N indicated one of two things. Either the large heat flux, which is consistent with the hydrography at 36°N, is inconsistent at 24°N or the mass conservation constraints were simply not weighted heavily enough to drive a larger cell at 24°N. Case 3 was run to test this alternative.

The net heat flux given by Hastenrath (1979) at 24°N is 155×10^{13} watts. In order to apply this as a constraint, estimates of the flux integral 4.1 were made for the Florida Straits. Here the transport is assumed to be well determined layer by layer from chapter II, and the result is 233×10^{13} watts for the flux integral. This is not yet a heat flux because of the arbitrary zero in the temperature scale. However, if the 24°N section carries 30×10^6 m^3/sec southward with a value of the integral 4.1 of -78×10^{13} watts, then the net northward heat flux is the requisite 155×10^{13} watts. Case 3 is identical to case 2a except with the addition of the heat constraints in the Fort Pierce and 24°N sections. The results of this run showed that the last constraint is incompatible with the rest of the system. The large weight given to the heat flux equation caused it to dominate over the mass constraint, thus driving a large net flow northward to increase the value

of the flux integral 4.1. The size of this net flow, 12.4 x 10^6 m^3/sec, for the combined Fort Pierce and 24°N sections is indicative of the magnitude of the incompatibility. Again, even with the large mass imbalance, the flow of warm water at 24°N was increased only to 9.6 x 10^6 m^3/sec, barely more than in the other four solutions.

In summary, it was found that, layer by layer, the net transports were much better determined by the constraints at 24°N than at 36°N or 48°N. At 24°N, these transports are relatively insensitive to the choice of initial reference level. Further, an attempt at driving a large heat flux at 24°N gave an incompatible system. Large heat fluxes at 36°N and 48°N were compatible and served to fix the amplitude of the vertical meridional recirculation. The incompatibility of the 24°N section resulted from a different amplitude having independently been determined by the other constraints. These differences between 24°N and the other sections are due to differences in the topography, hydrography, and the imposed mass conservation constraints. This will be explained in the next section.

2. Resolution

On the whole, the problem resolution was compact, though not surprisingly, the spatial scales which were resolved tended to be much broader than in the Caribbean example (chapter II). This is simply because the number of effective constraints, relative to the areal coverage of the data, was much smaller. A considerable spatial variability in both the quality and scale of the resolution was observed.

Figure 4.2 shows 8 columns of the transport resolution matrix (equation 1.16) resulting from the second problem (in which heat flux was used as a constraint at 36^{o}N and 48^{o}N) and two of the corresponding columns from the first problem (no imposed heat flux). The eight chosen columns cannot fully represent all 136 columns of VV^{T} but in each case, they are very similar to several adjacent columns. The resolution matrix changes rather gradually over groups of five or ten columns. The bottom most two plots (4.2a and 4.2b) show the resolution at station pair 4 in the Florida Straits. In each case, the central peak is about the same, but the side lobes are greatly different. This can be understood as follows. The demand for a large heat flux at 36^{o}N in problem 2 forces strong small scale correlations of velocity and temperature. The side lobes on the 36^{o}N section are strongest over the abrupt topography of the Mid-Atlantic Ridge, and the familiar problem of poor resolution due to poorly resolved topography has been aggravated by the large heat flux constraint. Quite a number of station pairs show side lobes in resolution over the Mid-Atlantic Ridge, particularly in the 36^{o}N section which has the roughest topography. They are always more serious in problem 2. Figure 4.2e shows the resolution of a station pair located in the Gulf Stream along 36^{o}N. Again, it looks very noisy. One would conclude that very little of the structure of the Gulf Stream will be revealed in the smoothed velocity. At 48^{o}N, the topography is less severe, so the resolution vectors are not as noisy, but figures 4.2i and j show that the resolution is of very large scale. Again, one should not expect, for example, to resolve the North American Current in the smoothed velocity. The 48^{o}N section is the least highly resolved because it has the fewest effective constraints.

The Fort Pierce and 24°N sections are the best resolved. The shallowness of the Florida Straits together with the separate transport constraints on the two sections effectively serve to resolve them from each other. The 24°N section shows compact resolution (4.2c and d) with sharper peaks in the western station pairs.

An overview of the resolution for a section is provided by a comparison of unsmoothed (reference level dependent) and smoothed (unique) sea level. In either case, the sea level slope is proportional to the surface geostrophic velocity. Figures 4.3a and b show plots of unsmoothed and smoothed sea level at 24°N and 36°N. One can judge the scale of the resolution in the tendency for small features to be removed. Severe side lobes are revealed if the smoothed plot looks quite different from the unsmoothed. The large side lobes at 36°N are quite apparent. Much of the sea level change across the Gulf Stream at this latitude has been spread right across the section. The 24°N plots look considerably better.

Contour plots of velocity at 24°N are shown in figures 4.4a, b, and c for case 1a and case 1b unsmoothed velocities and the unique smoothed velocity which results from any initial reference level. The smoothed velocity shows two bands of southward moving surface water, the stronger one west of the Mid-Atlantic Ridge and the second just above and to the east of the ridge. The deep southward flow is shown as being very broad and sluggish. No evidence of westward intensification in the deep flow is seen. In the unsmoothed velocities of figure 4.4b (case 1b), there is no clearly defined western boundary undercurrent in this section, although it does appear in figure 4.4a (case 1a).

A strong Antilles Current appears in smoothed and unsmoothed solutions. The total northward flow of this current, for water warmer than $7^{o}C$, corresponding to the velocities shown in figures 4.4a to c, is 24 x 10^{6} m^{3}/sec (unsmoothed, initial reference level 1000 meters), 27 x 10^{6} m^{3}/sec (unsmoothed, initial reference level 4000m) and 11 x 10^{6} m^{3}/sec (smoothed). There is not sufficient data in this problem to identify this water with the transport increase in the Florida Current north of the Straits of Florida, but the amount is certainly consistent. The transport float measurements by Richardson, Schmitz, and Niiler (1972) indicated that between the Florida Straits and Cape Fear about 23 x 10^{6} m^{3}/sec was added to the Florida Current. A feature similar to this is seen in the inverse solution of Wunsch (1978) in the Bermuda to Mona Passage and Antilles to Bermuda sections. The fact that the feature in figure 4.4c has remained after smoothing is further evidence that it is not purely a locally recirculating eddy. Finally, it is consistent with the Caribbean solution of chapter II, which showed about 7 x 10^{6} m^{3}/sec of this water to be drawn into the Caribbean via Windward Passage and another 1-2 x 10^{6} m^{3}/sec to enter the Florida Straits by Northeast Providence Channel.

3. Heat Flux

The flux integral 4.1 was evaluated at each latitude for solutions 1a and b and 2a and b with the results shown in table 4.6. The units are 10^{13} watts. Numbers in parentheses are the total mass imbalance at each latitude in 10^{12} gm/sec. Since the heat flux calculation is based on zero mass flux, the numbers in this table should be adjusted slightly

to compensate for the imbalances. The magnitude of the corrections is small but an ambiguity exists in determining which layer or layers should be adjusted.

The values given in table 4.6 represent heat flux due to the geostrophically balanced velocity. Ageostrophic corrections to the mass flux are small (they are treated here as part of the error), but heat flux corrections due to Ekman transport may be significant because this ageostrophic correction affects the warmest water in a section. For example, at 24^{o}N the zonal wind stress charts of Leetmaa and Bunker (1978) show a moderate (about .5 dynes cm^{-2}) westward wind stress across most of the Atlantic. If the resulting Ekman transport was 3 x 10^{6} m^{3}/sec to the north and was balanced by an interior return flow averaging 15^{o}C cooler than the surface water, then the correction to the geostrophic heat flux would amount to about 20 x 10^{13} watts. The simplest way of incorporating this type of correction in the inverse calculation would be to constrain the geostrophic transport to have a net value equal and opposite to that of the best estimate of Ekman transport. Then, the flux integral could be corrected by adding the product of the Ekman transport with the average temperature of the frictional layer.

The heat flux at both 24^{o}N and 36^{o}N is relatively insensitive to the variation in initial reference level. The primary difference is that the 36^{o}N section can be forced to carry a much larger flux (albeit with some indication of intensified noise), as the results of cases 2a and 2b demonstrate, but case 3 showed that the larger flux at 24^{o}N is implausible. The transport constraints at 24^{o}N together with the

resolution afforded by a shallow Florida Straits and a deep interior are sufficient to prevent large variations in the horizontal correlation of temperature and velocity.

A large difference in heat flux is observed at 48^{o}N in cases 1a and 1b. The cause is a southward movement of the warmest water in the section (about 14^{o}C) in the solution with a 4000 meter reference level. This warm flow nearly cancels the effect of the meridional cell below. Such a flow is impossible since there is no heat source for the water (and indeed the smoothed solution as well as the case 1a unsmoothed solution do not show it). The flow is a residue of the initial field relative to 4000 meters. It is therefore likely that case 1a gives a better estimate of the heat flux at 48^{o}N, though it is by no means well determined at this latitude.

In each of the solutions and at every latitude, the heat flux is dominated by meridional recirculation in the vertical plane. Horizontal recirculations, because of the small horizontal temperature differences, contribute very little. For example, at 24^{o}N about 19 x 10^{6} m^{3}/sec of water warmer than 17^{o}C flows northward in the Florida Straits. About 12 x 10^{6} m^{3}/sec is returned southward in the interior at an average temperature only about 1^{o}C cooler than the northward flow, giving a heat flux of 5 x 10^{13} watts. The remaining 7 x 10^{6} m^{3}/sec, plus an additional 6 to 8 x 10^{6} m^{3}/sec that flows northward mainly between 7^{o} and 12^{o}C is balanced by 13 to 15 x 10^{6} m^{3}/sec of southward flow colder than 4^{o}C. The temperature differences for the surface and mid-depth northward flows contrasted to the deep southward flow are about 18.5^{o} and 6.5^{o}C respectively. The corresponding heat flux values are

about 54×10^{13} and 19×10^{13} watts. Most of the transport uncertainty at 24^{o}N is in the mid-depth and deep flows. Since the temperature difference between these layers is not large, the resulting uncertainty in heat flux is not great. The magnitude of the heat flux is determined to a large extent by the net flow of warm water to the north. An important corollary is that if seasonal variability in the oceanic heat flux is as great as the annual mean, as suggested by Oort and Vonder Haar, then there must be a strong seasonal signal in the net northward transport of surface water.

A comment on the strength of the meridional cells is in order. In cases 1a and 1b, the total vertical recirculation ranges from 12 to 16 x 10^{6} m^{3}/sec at 24^{o}N and from 15 to 22 x 10^{6} m^{3}/sec at 36^{o}N. These are considerably higher than Worthington's (1976) box model, which shows about 7 x 10^{6} m^{3}/sec at both latitudes. The heat flux implied by his model is fairly small, about 40 x 10^{13} watts at 24^{o}N. Although no solution was obtained in the inverse calculations using a low heat flux as a constraint, it is unlikely to be any more compatible than the high value in case 3 unless the flow through Florida Straits was considerably reduced.

In retrospect, how should the calculation be done? The lesson from cases 2a and 2b is that a meteorologically determined heat flux is an important constraint that helps to fix the strength of the vertical recirculation. However, the weight given this flux should mirror the uncertainty in the measurements. Hastenrath's (1979) use of Budyko's (1963) values for oceanic heat flux divergence probably led to a significant overestimate of the oceanic flux at 30^{o}N. Using more

recent values of ocean-atmosphere heat exchange by Bunker (1976), Bryden and Hall (1979) obtained a value of 100 x 10^{13} watts for the northward heat flux at 24°N. This gave good agreement with their estimate of 110 x 10^{13} watts using hydrographic data analyzed by a method similar to that of Bryan (1962). It also agrees well with the inverse calculation result of 90 x 10^{13} watts (which does not include northward Ekman transport). This suggests that Hastenrath's (1979) value at 30°N, based on integration of the old Budyko numbers north of 30°, is high by roughly 50%. However, even lowering his values by this amount does not alter his conclusion of northward heat flux in both hemispheres of the Atlantic.

The problem of seasonal variability in heat flux is almost certainly one that can be answered at 24°N. A repetition of the IGY 24°N section, say in June (the time of maximum transport in the Florida Straits), could be combined in an inverse problem with a Florida Straits section given a summer transport constraint (about 33.5 x 10^{6} m^3/sec. Seasonal variability as large as that suggested by Oort and Vonder Haar (1976) should show up easily. Alternately, the problem might also be a feasible application for satellite altimetry. Suppose the summer transport increase in the Florida Straits is compensated by shallow baroclinic flow in the interior. This would be the case if the seasonal change in heat flux is small. Then a seasonal change in the sea level difference, between say the Bahamas and Northwest Africa, on the order of 10 cm is implied by geostrophy. A barotropic return flow in the interior (large seasonal charge in heat flux) would produce a much smaller change in zonal sea level slope. A 10 cm time varying signal should be detectable.

Acknowledgements

I am grateful to my thesis advisor, Carl Wunsch, who gave useful advice throughout the course of this work. Nan Bray was subjected to all of my ideas in their earliest forms and helped bring them to greater maturity. Barbara Grant assisted frequently with computing problems. I would also like to thank Bill Schmitz, Val Worthington, Henry Stommel, and many other members of the W.H.O.I. Physical Oceanography Department for their helpful comments and encouragement. This work was supported by National Science Foundation grants OCE 76-80210 and OCE 78-19833.

Appendix

This section outlines the sequence of data manipulation leading to the solution and smoothing. It is intended for the reader who is curious about the computing details or as an introduction for someone who is interested in using the programs for his own problems. The programs are not complete or finished. They have grown out of an original set of programs written by Barbara Grant and they represent the most recent in a long series of revisions by Ms. Grant and me.

1. Data Manipulation

We begin with magnetic tapes of hydrographic data supplied by the National Oceanographic Data Center. Program PHEAD reads the tapes and prints out header information. This allows location of desired stations on the tapes. Program NODC3 then reads a tape and transfers header information and observed values of temperature, salinity, and depth for selected stations to direct access disk files.

Interpolation of observed values of temperature and salinity to standard depths is done by Program FILL. The standard depths are somewhat different from NODC standard depths, principally in having increments of 250 meters instead of 500 meters in the deep ocean, however the interpolation scheme to obtain standard depth values is the same as that used by NODC.The method is normally a 3 point Lagrangian interpolation although a linear interpolation is used if the Lagrangian interpolated value does not lie between the observed values directly above and below. Any values marked questionable on the tape are not

used. No interpolation is made if adjacent observed values differ in depth by more than 200 meters for shallow bottles (less than 400 meters depth) or 400 meters at mid-depth (400 to 1200 meters).

After this first sequence of interpolations, gaps in the standard depth data are filled according to the following hierarchy. First, if the gap is at the deepest standard depth of the station, and the deepest observed value is deeper than the second deepest standard depth, then the missing datum is filled by a vertical linear extrapolation of from the two deepest observed values. If the gap is in a station which is between two stations that have good values at the given standard depth, then it is filled by a horizontal linear interpolation of the standard depth data. If the gap is in an end station, with good values at the given standard depth in the two adjacent stations, then it is filled by a horizontal linear extrapolation of the standard depth data. At this time, any remaining gaps are brought to the attention of the operator, who may specify values for the missing data or may direct how the missing data is to be estimated. Every station must have values of temperature and salinity at all standard depths. These values are written in a direct access disk file.

Program COMPGV computes geostrophic velocity relative to the surface for each pair of hydrographic stations. Standard oceanographic subroutines are used for the dynamic depth calculation. Geostrophic velocities are printed out along with certain other quantities. These are temperature, salinity, salinity anomaly with respect to the Worthington an Metcalf (1961) curve for the North Atlantic, and potential density. The values are averaged between members of a station pair at

each standard depth. Potential density is computed using the surface as reference pressure for depths of 0 to 1000 meters, using 2000 decibars as the reference pressure for depths of 1100 to 3000 meters and 4000 decibars for depths greater than 3000 meters. The salinity anomaly calculation uses a subroutine written by L. Armi and modified by C. Maillard. It approximates the Worthington and Metcalf (1961) θ/S curve by a cubic spline fit.

The ocean bottom is treated as a series of line segments connecting the positions of the recorded bottom depths at each station pair. In the geostrophic calculation, there is a problem of how to estimate dynamic height along the sloping bottom. The following technique is used, although as discussed in Chapter I, it is not held to be especially accurate. Using data from the two deepest standard depths which are common to a station pair, the slopes of local isothermal and isohaline surfaces are estimated. Temperature and salinity at standard depths along the sloping bottom are estimated by assuming that the slopes of the isothermal and isohaline surfaces are constant with depth and using the data from the deep member of the station pair. Thus, vertical shear is assumed to decrease with depth approximately in proportion to the vertical stratification. This method produces stable estimates unless the shallow member of the station pair is above the thermocline. In this case, unreasonably large estimates of velocity may occasionally result.

The computed geostrophic velocities and the averaged values of temperature and salinity are stored in direct access disk files along with appropriate header information. This completes the preliminary data handling.

2. Solution

The problem is defined and the singular value decomposition is computed in Program SNGLR. User input includes quantities to be conserved (i.e. potential density, temperature, etc.), weights for each conserved quantity, number and weights of layers, definition of later interfaces, number of enclosed areas, hydrographic station pairs to be used, and initial reference level. The A matrix of areas of layers at each station pair, and the weighted Gamma matrix of relative transport of conserved quantities are filled by Subroutine COMPAG, using the stored values of relative geostrophic velocity and average temperature and salinity. Interpolations to locate depths of layer interfaces and to assign values to variables at the interfaces are made by a 3 point Lagrangian interpolation scheme. Numerical integrations are made with the trapezoidal rule. Program SNGLR and its associated subroutines use double precision arithmetic.

The singular value decomposition solution is computed as follows. Define

$$C = (A A^{T})$$

Solve the eigenvalue problem

$$C u = l^{2} u$$

for the eigenvectors, u, and the singular values, l. This is done by a standard subroutine from the International Mathematics Subroutine Library.

Next, compute

$$V^T = L^{-1} U^T A$$

Finally

$$b' = - V L^{-1} U^T S^{1/2} \Gamma$$

and

$$b = W^{1/2} b'$$

(See Chapter I section D) The solution is built iteratively, using one additional singular value and its corresponding eigenvectors for each iteration. Solution information is printed after each iteration and the user may specify a maximum number of iterations. The eigenvector matrices, U and V, the singular values, weights, and the Gamma matrix are all stored on a disk file.

Program LSTSQS operates like Program SNGLR except that it computes a tapered cutoff solution (1.15) to problem 1.14 rather than the sharp cutoff type solution. The user specifies a value of $\bar{\sigma}^2$.

Program SMOOTH reads the station pair relative velocities and the results of the singular value decomposition into memory. The rank, K, of the matrix A is input, and the deweighted velocity resolution matrix is computed (1.24). At each standard depth, the geostrophic velocities relative to the initial reference level form a 1xN vector. There are 37 such vectors, or less if a smaller number of standard depths are required. The transposed vectors are each premultiplied by the deweighted velocity resolution matrix to form the smoothed relative

velocities. The total smoothed solution (1.21) is obtained by computing the reference level velocity vector and adding this to each of the smmothed velocity vectors. As indicated in Chapter I, the result is to have multiplied the total unsmoothed velocity by the resolution matrix to obtain the unique smoothed solution.

Printed output from Program SMOOTH includes the deweighted velocity resolution matrix, the transport resolution matrix, the UU^T matrix, and the total smoothed and unsmoothed velocities. The user also has the option of generating contour plots of smoothed and unsmoothed velocity and smoothed and unsmoothed sea level.

References

Aagaard, K., P. Greisman, 1975. Toward new mass and heat budgets for the Arctic Basin, J. Geophys. Res., 80, 3821-3827.

Barrett, J., W. Schmitz, 1971. Transport float measurements and hydrographic station data from 3 sections across the Gulf Stream near 67°W, R. V. Crawford Cruise 168, June-July, 1968. WHOI Reference No. 71-66.

Brooks,I., 1978. Transport and velocity measurements in the St. Lucia Passage of the Lesser Antilles, Abstract in Trans. Amer. Geophys. Union, 59, 1102.

Bryan, K., 1962. Measurements of meridional heat transport by ocean currents, J. Geophys. Res., 67, 3403-3413.

Bryden, H., 1976. Horizontal advection of temperature for low frequency motions, Deep-Sea Res., 23, 1165-1174.

Bryden, H., M. Hall, 1979. Heat transport by ocean currents across 25°N latitude in the Atlantic, in preparation.

Budyko, M., 1963. Atlas of the heat balance of the Eart, (in Russian), Kartfabrika Gosgeoltehizdata, Leningrad.

Bunker, A., 1976. Computations of surface energy flux and annual air-sea interaction cycles of the North Atlantic Ocean, Monthly Weather Rev, 104, 1122-1140.

Coachman, L., K. Aargaard, R. Tripp, 1975. Bering Strait: The regional physical oceanography, University of Washington Press, 172 pp..

Davis, R., 1978. On estimating velocity from hydrographic data, J. Geophys. Res., 83, 5507-5509.

Defant, A., 1941. Die absolute topographie des physikalischen meeresniveaus und der druckflachen sowie die wasserbewegungen im Raum des Atlantischen Ozeans, Wiss. Ergebn. Dtsch. Atlant. Exped. 'Meteor', 6, 191-260.

Defant, A., 1961. Physical Oceanography, Vol. 1, London: Pergamon Press, 728 pp.

Emig, M., 1967. Heat transport by ocean currents, J. Geophys. Res., 72, 2519-2529.

Fuglister, F., 1960. Atlantic Ocean Atlas of temperature and salinity Profiles and data from the International Geophysical Year of 1957-1958, Woods Hole Oceanographic Institution Atlas Series, 1, 209 pp.

Fuglister, F., 1963. Gulf Stream '60, Progr. Oceanogr., 1, 265-385.

Gordon, A., 1967. Circulation of the Caribbean Sea, J. Geophys. Res., 72, 6207-6223.

Hastenrath, S., 1979. Heat budget of tropical ocean and atmosphere, in preparation.

Helland-Hansen, B., 1934. The Sognefjord section, In Johnstone Memorial Volume, Liverpool, Univ. Press, 348 pp.

Hidaka, K., 1940. Absolute evaluation of ocean currents in dynamical calculations, Proc. Imp. Acad. Tokyo, 16, 391-397.

Hoerl, A., R. Kennard, 1970a. Ridge regression: Biased estimation for non-orthogonal problems, Technometrics, 12, 55-68.

Hoerl, A., R. Kennard, 1970b. Ridge regression: Applications to non-orthogonal problems, Technometrics, 12, 69-82.

Holton, J., 1972. An Introduction to Dynamic Meteorology, New York, Academic Press, 319 pp.

Iselin, C., 1936. A study of the circulation of the western North Atlantic, Pap. Phys. Oceanogr., 4, 101 pp.

Jacobsen, J., A. Jensen, 1926. Examination of hydrographical measurements from the research vessels Explorer and Dana during the summer of 1924, Conseil Perm. Internat. p. l'Explor. de la Mer, Rapp. et Proc.-Verb., 39, 31-84.

Jordan, T., J. Franklin, 1971. Optimal solutions to a linear inverse problem in geophysics, Proc. Nat. Acad. Sci., 68, 291-293.

Jung, G., 1952. Note on the meridional transport of energy by the oceans, J. Mar. Res., 11, 2.

Lanczos, C., 1961. Linear Differential Operators, New York, van Nostrand, Reinhold, 564 pp.

Lawson, C., R. Hanson, 1974. Solving Least Squares Problems, New Jersey, Prentice-Hall, 340 pp.

Leetmaa, A., A. Bunker, 1978. Updated charts of the mean annual wind-stress, convergences in Ekman layers, and Sverdrup transports in the North Atlantic, J. Mar. Res., 36, 311-322.

Leetmaa, A., P. Niiler, H. Stommel, 1977. Does the Sverdrup relation account for the Mid-Atlantic circulation?, J. Mar. Res., 35, 1-9.

McWilliams, J., 1976. Maps from the Mid-Ocean Dynamics Experiment II. Potential vorticity and its conservation, J. Phys. Oceanogr., 6, 828-846.

Metcalf, W., 1959. Oceanographic data from the Caribbean Sea, Crawford Cruise 17, February-March 1958, for the International Geophysical Year of 1957-1958, Ref. 59-9, Woods Hole Oceanographic Institution, 90 pp.

Metcalf, W., 1976. Caribbean-Atlantic water exchange through the Anegada-Jungfern passage, J. Geophys. Res., 81, 6401-6409.

Montgomery, R., 1938. Circulation in upper layers of southern North Atlantic deduced with use of isentropic analysis, Pap. Phys. Oceanogr. and Meteor. 6, 55 pp.

Montgomery, R., 1974. Comments on 'Seasonal Variability of the Florida Current', by Niiler and Richardson, J. Mar. Res., 32, 533-534.

Morrison, J., 1977. Water mass properties used as flow indicators within the Eastern Caribbean Sea during the winter of 1972 and fall of 1973, Ph.D. thesis, Texas A&M University, 85pp.

Niiler, P., W. Richardson, 1973. Seasonal variability of the Florida Current, J. Mar. Res., 31, 144-167.

Oort, A., T. Vonder Haar, 1976. On the observed annual cycle in the ocean - atmosphere heat balance over the northern hemisphere, J. Phys. Oceanogr., 6, 781-800.

Owens, W., 1978. Simulated dynamic balances from mid-ocean mesoscale eddies, J. Phys. Oceanogr., 9, 337-359.

Parr, A., 1937. A contribution to the hydrography of the Caribbean and Cayman Seas based upon the observations made by the research ship Atlantis, 1933-1934, Bingham Oceanogr. Collection, Bull., V.5, art. 4, 110 pp.

Pillsbury, J., 1890. The Gulf Stream, methods of the investigation and results of the research, U.S. Coast and Geod. Surv. Rep. 1890, Append. 10.

Richards, F., 1958. Dissolved silicate and related properties of some western North Atlantic and Caribbean waters, J. Mar. Res., 17, 444-465.

Richardson, W., W. Schmitz, 1965. A technique for the direct measurement of transport with application to the Straits of Florida, J. Mar. Res., 23, 172-185.

Richardson, W., W. Schmitz, P. Niiler, 1969. The velocity structure of the Florida Current from the Straits of Florida to Cape Fear, Deep-Sea Res., 16 Suppl., 225-231.

Schmitz, W., 1977. On the deep general circulation of the western North Atlantic, J. Mar. Res., 35, 21-28

Schmitz, W., 1978. Observations of the vertical distribution of low frequency kinetic energy in the western North Atlantic, J. Mar. Res., 36, 295-310.

Schmitz, W., 1979. Weakly depth dependent segments of the North Atlantic circulation, in preparation.

Schmitz, W., W. Richardson, 1968. On the transport of the Florida Current, Deep-Sea Res., 15, 679-693.

Schott, F., H. Stommel, 1978. Beta spirals and absolute velocities in different oceans, Deep-Sea Res., 25, 961-1010.

Stalcup, M., W. Metcalf, R. Johnson, 1975. Deep Caribbean inflow through the Anegada-Jungfern Passage, J. Mar. Res., 33 Suppl., 15-35.

Stalcup, M., W. Metcalf, 1972. Current measurements in the passages of the Lesser Antilles, J. Geophys. Res., 77, 1032-1049.

Stommel, H., 1956. On the determination of the depth of no meridional motion, Deep-Sea Res., 3, 273-278.

Stommel, H., 1965. The Gulf Stream, A Physical and Dynamical Description, London, Cambridge Univ. Press, 202 pp.

Stommel, H., P. Niiler, D. Anati, 1978. Dynamic topography and recirculation of the North Atlantic, J. Mar. Res., 36, 449-468.

Stommel, H., F. Schott, 1977. The beta spiral and the determination of the absolute velocity field from hydrographic station data, Deep-Sea Res., 24, 325-329.

Sturges, W., 1965. Water charcteristics of the Caribbean Sea, J. Mar. Res., 23, 147-162.

Sturges, W., 1970. Observations of deep water renewal in the Caribbean Sea, J. Geophys. Res., 75, 7602-7610.

Sturges, W., 1975. Mixing of renewal water flowing into the Caribbean Sea, J. Mar. Res., 33 Suppl., 117-130.

Sudo, H., 1965. An analysis of the deep current of the ocean; with its application to the circulation of the Atlantic Ocean, Jap. J. of Geophys., 4, 1-70.

Sverdrup, H., 19 . Oceanography, in Handbuch der Physik, Berlin, Springer-Verlag.

Sverdrup, H., M. Johnson, R. Fleming, 1942. The Oceans, Their Physics, Chemistry, and General Biology, New Jersey, Prentice-Hall, 1087 pp.

Thompson, R. G. Veronis, 1979. Transport observations in the Tasman and Coral Seas, in preparation.

Vonder Haar, T., A. Oort, 1973. New estimate of annual poleward energy transport by Northern Hemisphere oceans, J. Phys. Oceanogr., 2, 169-172.

Voorhis, A., E. Schreoder, A. Leetmaa, 1976. The influence of deep mesoscale eddies on sea surface temperature in the North Atlantic subtropical convergence, J. Phys. Oceanogr., 6, 953-961.

Warren, B., G. Volkmann, 1968. Measurement of volume transport of the Gulf Stream south of New England, J. Mar. Res., 26, 110-126.

Wiggins, R., 1972. The general linear inverse problem: implication of surface waves and free oscillations for Earth structure, Rev. of Geophys. and Space Phys., 10, 251-285.

Worthington, L., 1955. A new theory of Caribbean bottom water formation, Deep-Sea Res., 13, 731-739.

Worthington, L., 1966. Recent oceanographic measurements in the Caribbean Sea, Deep-Sea Res., 13, 731-739.

Worthington, L., 1968. Water circulation in the Caribbean and its relationship to the North Atlantic circulation, in Sykmposium on Investigations and Resources of the Caribbean Sea and Adjacent Regions, Curacao, 1968, 181-191.

Worthington, L., 1976. On the North Atlantic Circulation, Baltimore, Johns Hopkins Press, 120 pp.

Worthington, L., W. Metcalf, 1961. The relationship between potential temperature and salinity in deep Atlantic Water, Rapp. Cons. Explor. Mer., 149, 122-128.

Wunsch, C., 1977. Determining the general circulation of the oceans: A preliminary discussion, Science, 196, 871-875.

Wunsch, C., 1978. The North Atlantic Circulation west of 50°W determined by inverse methods, Rev. of Geophys. and Space Phys., 16, 583-620.

Wust, G., 1935. Schichtung und Zirkulation des Atlantischen Ozeans: Die Stratosphare des Atlantischen Ozeans, Wiss. Ergeb. Deut. Atl. Exped. Meteor., 6, 109-228.

Wust, G., 1964. Stratification and Circulation in the Antillean - Caribbean Basins, 1, Spreading and Mixing of the Water Types with an Oceanographic Atlas, New York, Columbia Univ. Press, 201 pp.

TABLE 1.1

Errors in potential density ($\varepsilon_{\sigma_\theta(T)}$, $\varepsilon_{\sigma_\theta(S)}$) and equivalent errors in estimated isopycnal depth ($\varepsilon_{D(T)}$, $\varepsilon_{D(S)}$) resulting from a temperature error of magnitude .02°C or a salinity error of magnitude .005‰ at selected depths of Crawford 889.

Depth (m)	Temperature	Salinity	σ_θ	$\varepsilon_{\sigma_\theta(T)}$	$\varepsilon_{\sigma_\theta(S)}$	$\varepsilon_{D(T)}$	$\varepsilon_{D(S)}$
40.	20.46	36.551	25.841	.0054	.0038	.30	.21
250.	18.04	36.529	26.461	.0050	.0038	9.7	7.5
510.	17.92	36.521	26.495	.0049	.0038	44.	34.
1070.	7.48	35.064	27.437	.0029	.0039	1.4	1.9
2065.	3.77	34.979	27.832	.0020	.0040	20.	39.
2880.	3.16	34.961	27.883	.0018	.0040	27.	59.
4100.	2.305	34.911	27.926	.0016	.0040	87.	219.

TABLE 2.1

List of Hydrographic Stations

Location	Ship	Cruise	Date
64°W Virgin Is. - Venezuela	Crawford	17	February 1958
68°W Mona Passage - Venezuela	Atlantis	212	December 1954
73°W Haiti - Colombia	Crawford	17	Feb-March 1958
79°W Cuba - Panama	Crawford	17	March 1958
84°W Cuba - Honduras	Crawford	17	March 1958
Mona Passage	Knorr	37	March 1974
Windward Passage	Knorr	37	Feb-March 1974
Northeast Providence Channel	Atlantis	215	June 1955
Fort Pierce - Mantanila Shoal	Atlantis	215	June 1955

TABLE 2.2

Density Layers

Layer Number	Upper Surface	Lower Surface
1	ocean surface	$\sigma_\theta = 26.0$
2	$\sigma_\theta = 26.0$	$\sigma_\theta = 27.0$
3	$\sigma_\theta = 27.0$	$\sigma_\theta = 27.2$
4	$\sigma_\theta = 27.2$	$\sigma_\theta = 27.4$
5	$\sigma_\theta = 27.4$	$\sigma_2 = 36.85$
6	$\sigma_2 = 36.85$	$\sigma_2 = 36.92$
7	$\sigma_2 = 36.92$	ocean bottom

TABLE 2.3

Initial and final transports in upper 4 layers (units are $10^6 m^3/sec$)

Section	Level	Initial Relative to 1000 m	SVD K=18	SUD K=27	Tapered Cutoff σ^2=.003	Initial Relative to 4000 m	Tapered Cutoff σ^2=.003
64°W	1	-10.9	-11.0	-10.6	-10.8	-11.2	-10.7
	2	-7.7	-8.0	-10.0	-9.0	-7.5	-8.7
	3	-3.0	-3.0	-2.0	-2.6	-3.5	-2.7
	4	-1.9	-2.0	-1.2	-1.7	-2.5	-1.9
	Total	-14.9	-24.0	-23.2	-22.8	-26.3	-22.6
68°W	1	-9.5	-9.5	-9.6	-9.5	-10.8	-9.3
	2	-9.6	-9.7	-9.7	-9.7	-12.4	-9.4
	3	-2.4	-2.6	-2.2	-2.4	-4.2	-2.1
	4	-2.9	-3.1	-2.4	-2.7	-6.7	-3.7
	Total	-22.6	-22.3	-22.8	-21.9	-47.8	-22.4
Mona	1	-.5	.3	1.0	.7	-1.0	.7
	2	-1.9	-.8	.3	-.2	-2.7	-.2
	3	-1.0	-.5	-.3	-.4	-1.3	-.4
	4	-.6	.7	.0	.4	-1.1	-.2
	Total	-3.1	1.5	.4	.7	-6.4	.1
73°W	1	-11.5	-11.5	-11.8	-11.5	-11.2	-11.1
	2	-7.4	-7.4	-7.5	-7.3	-7.3	-7.1
	3	-2.7	-2.6	-2.7	-2.6	-2.8	-2.6
	4	-2.2	-2.1	-2.1	-2.1	-2.6	-2.3
	Total	-23.8	-22.5	-22.9	-22.0	-29.1	-22.3
Windward	1	-3.6	-3.7	-3.4	-3.6	-3.7	-3.5
	2	-2.7	-2.7	-2.1	-2.5	-3.0	-2.4
	3	-.7	-.8	-.5	-.7	-.9	-.7
	4	-.4	-.5	-.1	-.4	-.5	-.3
	Total	-3.6	-7.4	-5.9	-6.9	-3.4	-6.3
79°W	1	-15.5	-14.5	-14.4	-14.4	-15.8	-14.3
	2	-11.6	-10.3	-10.1	-10.2	-12.0	-9.3
	3	-4.1	-3.5	-3.2	-3.4	-4.6	-3.3
	4	-3.2	-2.7	-2.3	-2.5	-4.2	-2.6
	Total	-25.4	-29.6	-28.8	-28.7	-45.5	-28.5
84°W	1	-12.1	-12.3	-12.3	-12.3	-12.8	-12.1
	2	-11.1	-11.2	-11.3	-11.1	-12.0	-11.0
	3	-2.9	-3.0	-3.0	-2.9	-3.3	-2.8
	4	-2.9	-2.9	-2.7	-2.8	-3.5	-2.8
	Total	-22.5	-29.5	-28.8	-28.6	-40.9	-28.3
Fort Pierce	1	11.3	13.5	14.0	13.0	11.3	13.0
	2	9.0	11.7	12.2	11.5	9.0	11.4
	3	2.1	3.4	3.6	3.4	2.1	3.3
	4	1.4	2.3	2.5	2.4	1.4	2.4
	Total	23.9	31.0	32.4	30.4	23.9	30.1
N.E.P.	1	.1	.2	-.2	.0	.1	.0
	2	-1.9	-1.6	-2.3	-1.9	-1.9	-1.9
	3	.0	.1	-.1	.0	.0	.0
	4	.0	.0	-.2	.0	.0	.0
	Total	.2	-1.4	-3.3	-1.8	.2	-1.8

TABLE 2.4

Transports in various temperature layers in the Caribbean. Positive is eastward or northward. Units are $10^6 m^3/sec$.

	Eastern Caribbean	Windward Passage	Western Caribbean
> 17°C	-12	-5	-17
12°C - 17°C	-5	-1	-6
7° - 12°C	-5	-1	-6
> 7°C	0	0	0
Total	-22	-7	-29

TABLE 2.5

	64°W	MONA	68°W	73°W	WINDWARD	79°W	84°W	N.E.P.	FORT PIERCE
64°W	.96	.20	-.02	-.01	.01	.0	.0	.01	.0
MONA	.04	1.0	.0	.0	.0	.0	.0	.0	.0
68°W	-.02	.0	.88	.05	.02	.0	.0	.01	.0
73°W	-.02	.0	-.01	.97	.02	.0	-.01	.01	.0
WINDWARD	.03	.0	.08	.06	.88	.05	-.01	.0	.01
79°W	.0	.0	.01	.0	.06	1.0	-.01	.0	.01
84°W	.0	.0	.0	.0	.0	.0	.92	.51	.01
N.E.P.	.0	.0	.01	.01	.0	.0	.21	.98	.0
FORT PIERCE	.01	.0	.02	.02	.04	.02	-.02	.02	.93

TABLE 3.1

Section	I	II	III	IV	V	VI	VII	VIII	IX	Mean
Warmer than 7°C	53	52	54	42	38	50	50	45		48
Colder than 7°C	5	-24	-21	-6	-3	26	30	-5		0
Total Relative to Bottom (Fuglister)	69	70	70	69	48	62	62	60	60	64
Gulf Stream Relative To Bottom (Fuglister)	137	106	88	76	50	80	77	52	82	81

TABLE 4.1

List of Hydrographic Sections

Location	Ship	Cruise	Date
Fort Pierce-Mantanila Shoal	Atlantis	215	June 1955
24°N Bahamas - Spanish Sahara	Discovery II	2	October 1957
36°N North Carolina - Spain	Chain	7	April-May 1959
48°N Grand Banks - English Channel	Discovery II	1	April 1957

TABLE 4.2

Density Layers

Layer Number	Upper Surface	Lower Surface
1	ocean surface	$\sigma_\theta = 26.8$
2	$\sigma_\theta = 26.8$	$\sigma_\theta = 27.2$
3	$\sigma_\theta = 27.2$	$\sigma_\theta = 27.5$
4	$\sigma_\theta = 27.5$	$\sigma_\theta = 27.7$
5	$\sigma_\theta = 27.7$	$\sigma_2 = 36.85$
6	$\sigma_2 = 36.85$	$\sigma_2 = 36.90$
7	$\sigma_2 = 36.90$	$\sigma_2 = 36.96$
8	$\sigma_2 = 36.96$	$\sigma_2 = 37.00$
9	$\sigma_2 = 37.00$	$\sigma_2 = 37.05$
10	$\sigma_2 = 37.05$	$\sigma_2 = 37.09$
11	$\sigma_2 = 37.09$	$\sigma_4 = 45.91$
12	$\sigma_4 = 45.91$	$\sigma_4 = 45.93$
13	$\sigma_4 = 45.93$	$\sigma_4 = 45.95$
14	$\sigma_4 = 45.95$	ocean bottom

TABLE 4.3

Case	Initial Reverence Level	Heat Flux as a Constraint		
		Fort Pierce, 24°N	36°N	48°N
1a	1000 meters	no	no	no
1b	4000 meters	no	no	no
2a	1000 meters	no	yes	yes
2b	4000 meters	no	yes	yes
3	1000 meters	yes	yes	yes

TABLE 4.4

Initial and Final Transports in Each Layer (units are $10^6 m^3/sec$)

	Layer	Initial		Final			
		Relative to 1000 m	Relative to 4000 m	Case 1a	Case 1b	Case 2a	Case 2b
Fort Pierce plus 24°N	1	1.8	6.5	8.2	8.4	8.2	9.3
	2	1.4	3.9	3.8	3.0	4.7	3.5
	3	1.8	5.0	3.4	2.1	4.9	2.6
	4	-.2	2.6	.5	-.3	1.3	.6
	5	-1.2	.7	-.4	-1.1	.3	-.7
	6	-1.2	.2	-.6	-.5	-.5	-.3
	7	-3.1	.7	-1.2	-.2	-.9	.1
	8	-2.9	.2	-1.4	-.7	-1.0	-.4
	9	-5.8	.7	-2.1	-.6	-1.5	-.2
	10	-4.5	-.1	-3.4	-3.2	-3.3	-1.9
	11	-6.4	.4	-4.8	-2.8	-6.3	-1.2
	12	-2.6	.8	.4	-1.2	-.7	-4.6
	13	-10.1	-.8	-5.1	-.4	-5.6	-2.4
	14	7.7	3.9	.3	-1.8	-.4	-4.2
	Total	-25.2	24.8	-2.3	.7	-.8	.2
36°N	1	11.1	16.1	8.9	15.0	12.5	14.6
	2	-2.6	-10.2	-.1	-.6	1.9	1.8
	3	.9	-4.0	2.4	1.5	3.4	2.9
	4	.9	-2.9	1.7	.4	2.6	1.2
	5	.2	-5.8	2.3	.8	3.3	2.5
	6	-.8	1.0	-1.2	-.4	-1.3	-.5
	7	-1.8	3.0	-3.8	-1.6	-4.0	-2.1
	8	1.1	-.5	1.1	-.4	1.3	-.2
	9	.3	1.9	-2.0	-1.1	-2.3	-.7
	10	-2.5	1.5	-2.4	-2.6	-2.5	-3.5
	11	-1.3	.9	-.1	-3.6	-1.9	-4.4
	12	-.6	1.1	-3.3	-1.2	-4.4	-3.3
	13	4.3	.0	-1.9	-2.2	-2.8	-3.1
	14	-9.0	.6	-2.2	-2.0	-3.2	-3.5
	Total	.2	2.7	-.6	2.0	2.6	1.7
48°N	2-3	14.1	20.1	18.6	7.2	19.7	20.1
	4	2.3	5.5	2.9	1.7	3.5	3.8
	5	-.2	2.7	.6	-.1	1.2	1.5
	6	-.9	2.0	-.6	.2	-.5	-.2
	7	-2.9	4.2	-2.1	-.7	-2.2	-2.3
	8	-4.0	3.8	-3.5	-.8	-3.5	-2.2
	9	-5.1	3.3	-4.1	-1.1	-4.2	-2.5
	10	-3.4	1.3	-2.4	-2.0	-2.5	-2.8
	11	-6.8	1.1	-1.1	-1.3	-1.8	-6.0
	12	-2.7	.2	-2.7	-.9	-3.3	-2.3
	13	-1.8	.1	-2.0	-1.4	-2.7	-3.3
	14	-2.2	.2	-2.6	-1.6	-3.4	-3.1
	Total	-12.6	44.7	.0	-.8	.3	.7

TABLE 4.5

Final Transports Summed Over Groups of Layers

(units are $10^6 m^3/sec$)

Case	Layers	24°N plus Fort Pierce	36°N	48°N
1a	1	8.2	8.9	.0
	2-5	7.3	6.3	22.1
	6-10	-8.7	-8.3	-12.7
	11-14	-9.2	-7.5	-9.4
1b	1	8.4	15.0	.0
	2-5	3.7	2.1	8.8
	6-10	-5.2	-6.1	-4.4
	11-14	-6.2	-9.0	-5.2
2a	1	8.2	12.5	.0
	2-5	11.2	11.2	24.4
	6-10	-7.2	-8.8	-12.9
	11-14	-13.0	-12.3	-11.2
2b	1	9.3	14.6	.0
	2-5	6.0	8.4	25.4
	6-10	-2.7	-7.0	-10.0
	11-14	-12.4	-14.3	-14.7

TABLE 4.6

Heat Flux (in units of 10^{13} watts)

Numbers in Parentheses are the Net Imbalance in Transport
(refer to text for explanation)

	Case 1a	Case 1b	Case 2a	Case 2b
24°N plus Fort Pierce	86 (-2.3)	82 (.7)	98 (-.8)	95 (.2)
36°N	81 (-.6)	102 (2.0)	128 (2.6)	128 (1.7)
48°N	49 (.0)	2 (-.8)	60 (.3)	60 (.7)

Figure Captions

1.1 Geometry of Hidaka's (1940) system for determining absolute velocity

1.2 Schematic of example problem 1.16

1.3 Simple illustrations of compact and non-compact resolution

a. location of identical station pairs

b. non-compact resolution, determined part of flow

c. compact resolution, determined part of flow

d. non-compact resolution, undetermined part of flow

e. compact resolution, undetermined part of flow

1.4 Solution variance, $\langle b_j^2 \rangle$, for the 41 station pair Gulf Stream '60 example

2.1 Location of stations used for the Caribbean calculation

2.2 Transport of water warmer than $7^{\circ}C$ in the Caribbean Sea. Contour interval is $3 \times 10^6 \, m^3/sec$

2.3 a. Unsmoothed geostrophic velocity solution for the Virgin Is-Venezuela section. The initial reference level was 1000 meters. K = RANK (A) = 27

b. Same as 2.3a but for Mona Passage-Venezuela

c. Same as 2.3a but for Haiti-Colombia

d. Same as 2.3a but for Cuba-Panama

e. Same as 2.3a but for Cuba-Honduras

f. Same as 2.3a but for Windward Passage

g. Same as 2.3a but for Fort Pierce-Mantanila Shoal

2.4 Same as 2.3e but with initial reference level of 4000 meters

2.5 Salinity anomaly with respect to the Worthington and Metcalf (1961) curve, average over the layer $27.2 < \sigma_\theta < 27.4$.

2.6 a. Representative columns of the matrix T (transport resolution). The horizontal axis is station pair number and the vertical is the value of t_{ij}. The arrow shows the location of the station pair whose resolution is illustrated. K = RANK (A) = 27

b. Same as 2.6a but for K = 18

2.7 a. Smoothed geostrophic velocity solution for the Virgin Is-Venezuela section. The initial reference level was 1000 meters. K = 27

b. Same as 2.7a but for Mona Passage-Venezuela

c. Same as 2.7a but for Haiti-Colombia

d. Same as 2.7a but for Cuba-Panama

e. Same as 2.7a but for Cuba-Honduras

f. Same as 2.7a but for Windward Passage

g. Same as 2.7a but for Fort Pierce-Mantanila Shoal

3.1 Location of stations in Gulf Stream '60 hydrographic survey

3.2 Columns 3 through 12 of the transport resolution matrix. Axes as in 2.6. K = 6

3.3 a. Unsmoothed geostrophic velocity solution for section I. Initial reference level was 1000 meters. K = 6

b. Same as 3.3a but initial reference level was 4000 meters

3.4 Geostrophic velocities from the high resolution, differential inverse calculation

a. Section A (from Gulf Stream '60 Sections I and II)

b. Section B (from Sections II and III)

c. Section C (from Sections III and IV)

d. Section D (from Sections IV and V)

e. Section E (from Sections V and VI)

f. Section F (from Sections VI and VII)

g. Section G (from Sections VII and VIII)

h. Section H (from Sections VIII and IX)

3.5 a. Zonally averaged 200 meter kinetic energy as a function of latitude for the high resolution, differential inverse

b. Same as 3.5a but for 1000 meters

c. Same as 3.5a but for 4000 meters

4.1 Location of hydrographic stations used in North Atlantic heat flux calculation

4.2 Representative columns of the transport resolution matrix for case 1 (4.2b and h) and case 2 (4.2a, c-g, i-j). K = 13 in case 1 and K = 15 in case 2

4.3 a. Smoothed and unsmoothed sea level at 24^{o}N from case 1. K = 13

b. Same as 4.3a but at 36^{o}N

4.4 a. Unsmoothed geostrophic velocity solution at 24^{o}N. Initial reference level was 1000 meters. K = 13, case 1

b. Same as 4.4a but initial reference level was 4000 meters

c. Smoothed geostrophic velocity solution at 24^{o}N. K = 13, case 1

4.5 Estimates of heat transport by the atmosphere (from Oort and Vonder Haar, 1976) and oceans (from Oort and Vonder Haar, 1976, and Hastenrath, 1979).

Figure 1.1

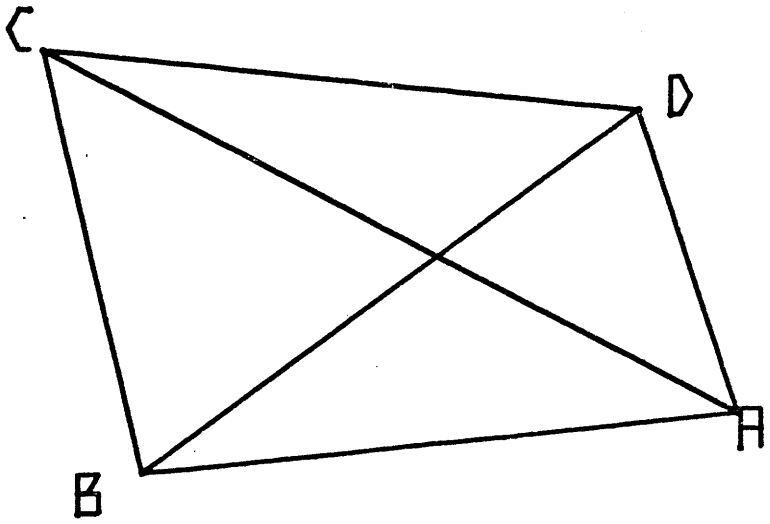

HIDAKA'S SYSTEM: MASS AND SALT CONSERVED IN AREAS ABC, CDA, AND ABD

Figure 1.2

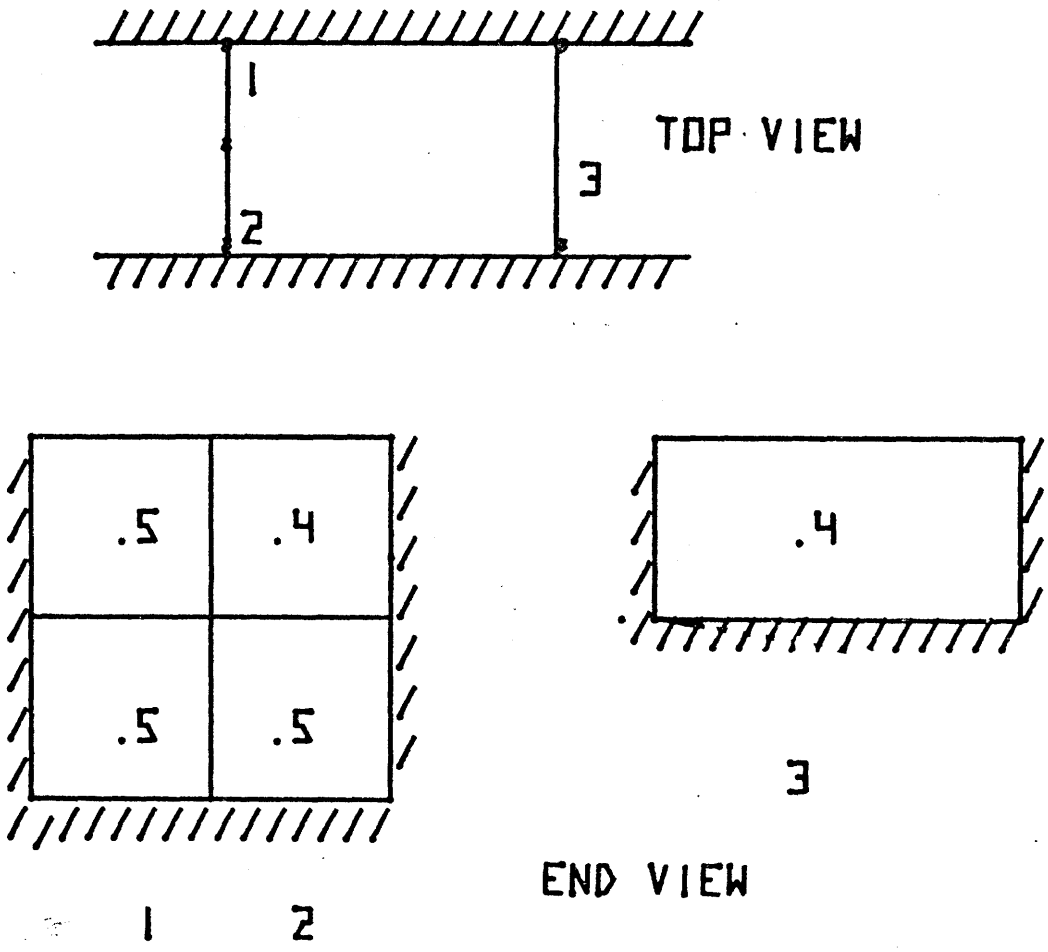

Figure 1.3

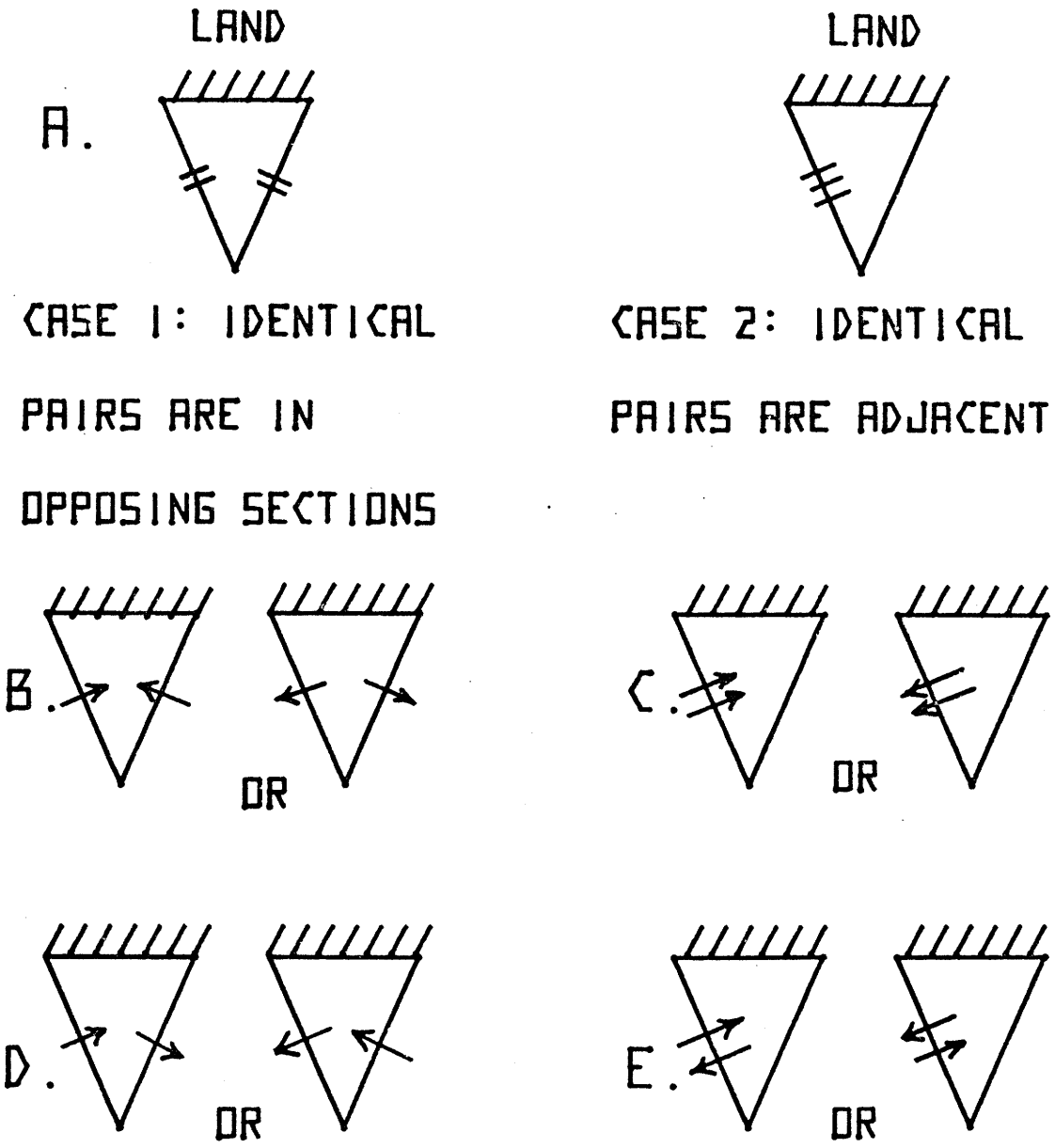
LAND
A.
LAND
CASE 1: IDENTICAL PAIRS ARE IN OPPOSING SECTIONS
CASE 2: IDENTICAL PAIRS ARE ADJACENT
B.
OR
C.
OR
D.
OR
E.
OR

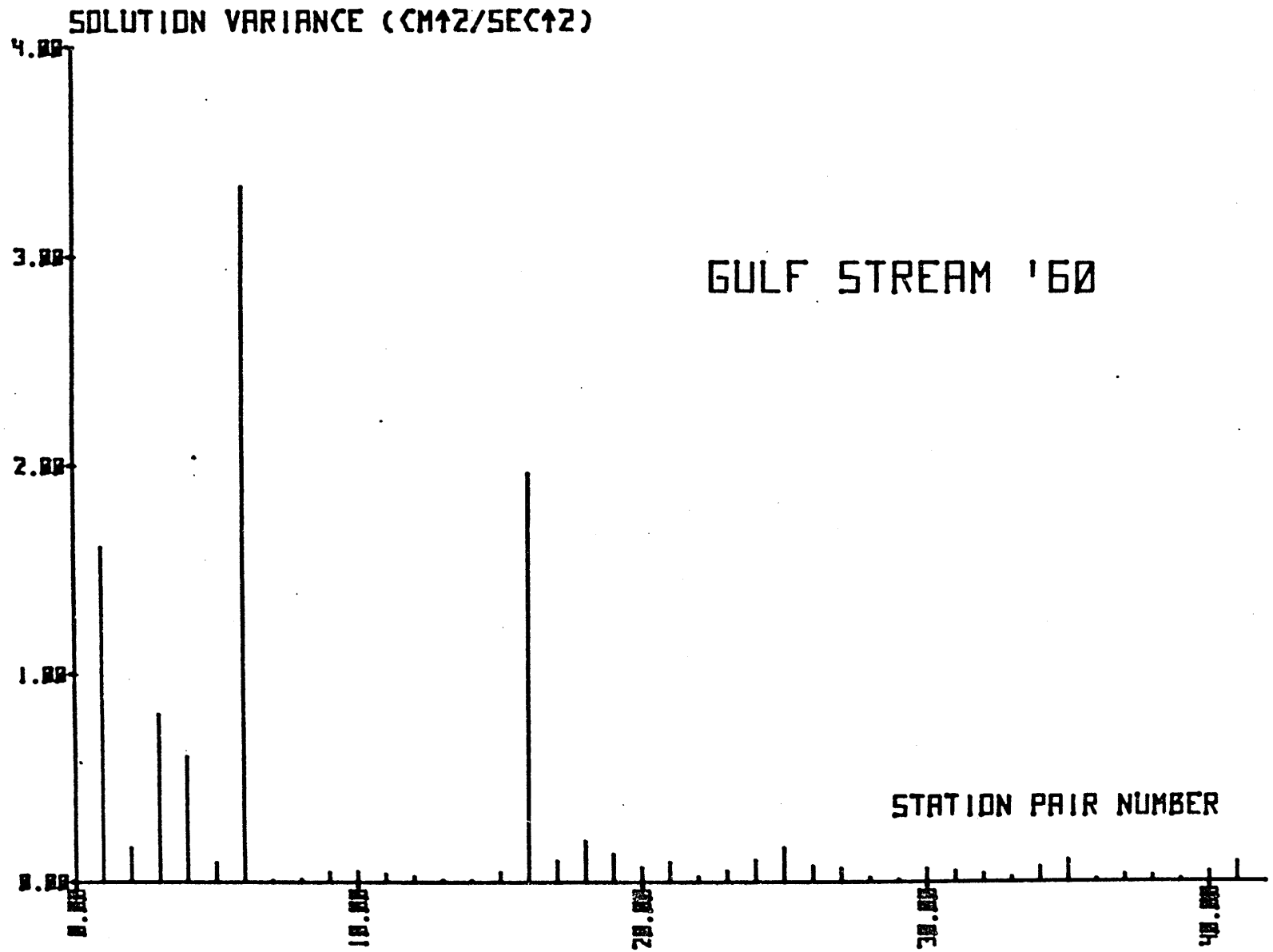
SOLUTION VARIANCE (CM↑2/SEC↑2)
4.00
3.00
2.00
1.00
0.00
0.000
10.000
20.000
30.000
40.000
GULF STREAM '60
STATION PAIR NUMBER

Figure 1.4

Figure 2.1

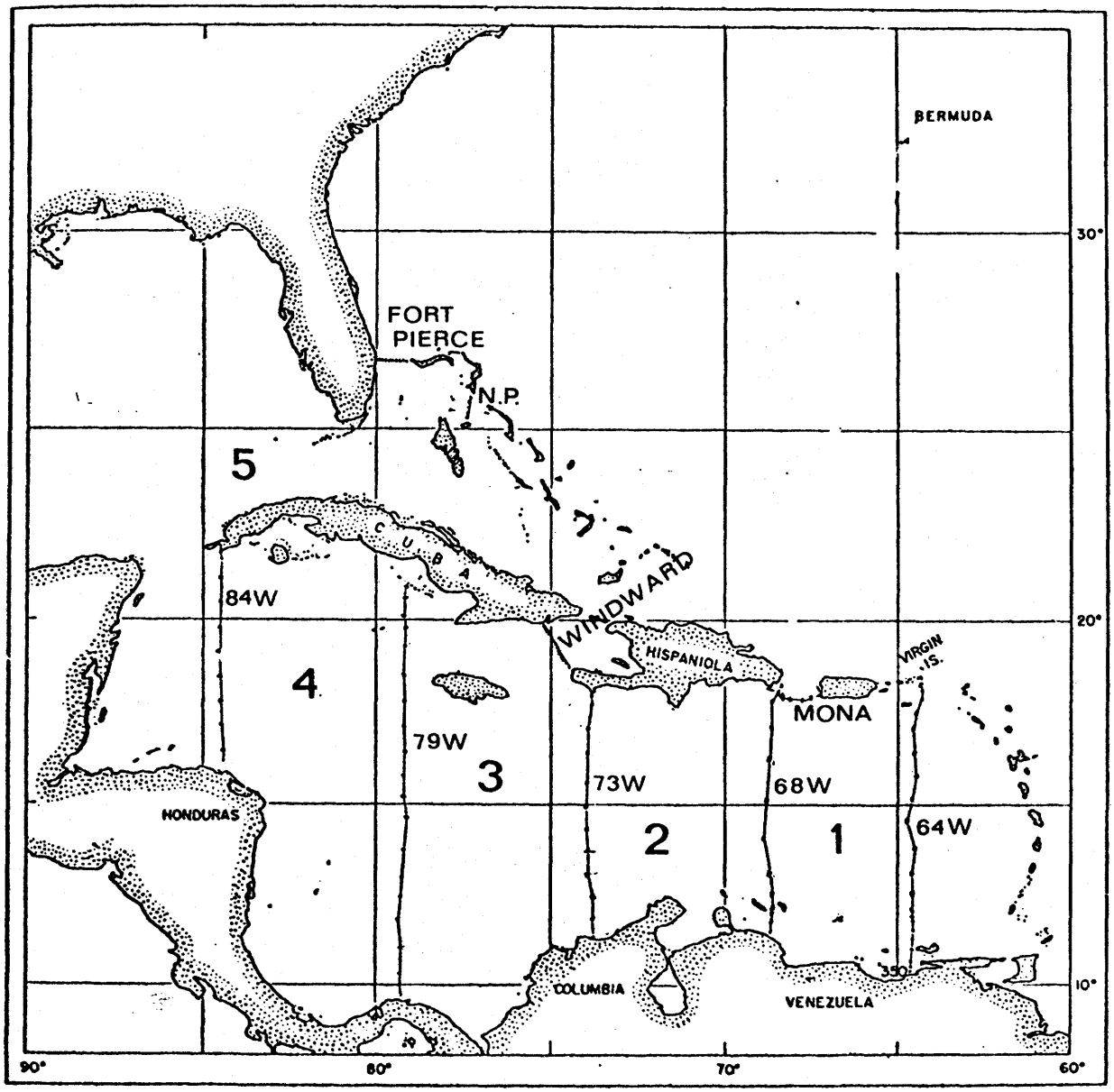
BERMUDA
30°
FORT
PIERCE
N.P.
5
CUBA
84W
WINDWARD
HISPANIOLA
VIRGIN
IS.
20°
4
MONA
79W
3
73W
68W
HONDURAS
2
1
64W
COLUMBIA
VENEZUELA
10°
90°
80°
70°
60°

Figure 2.2

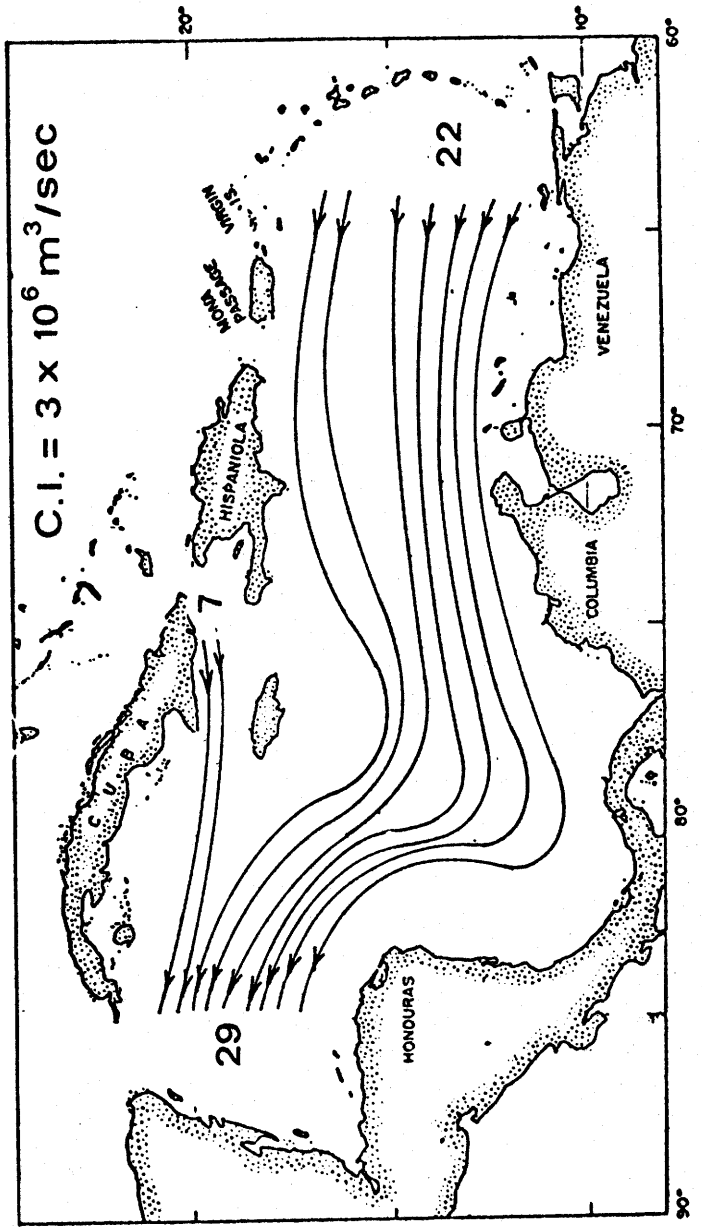
C.I. = 3 x 10⁶ m³/sec
22
7
29
CUBA
HISPANIOLA
MONA PASSAGE
VIRGIN IS.
VENEZUELA
COLUMBIA
HONDURAS
20°
10°
60°
70°
80°
90°

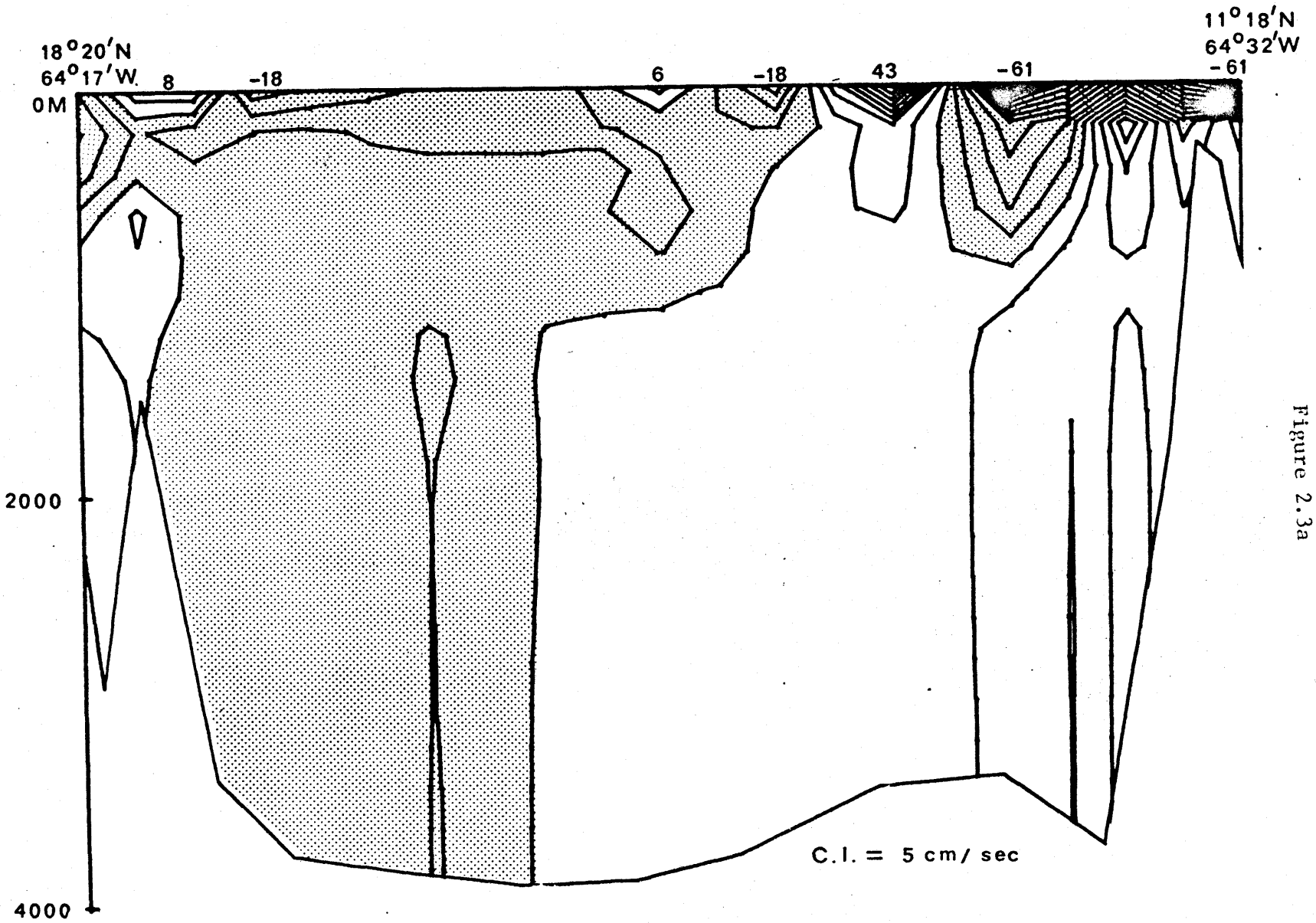
18°20′N
64°17′W
11°18′N
64°32′W
8
-18
6
-18
43
-61
-61
0M
2000
4000
C.I. = 5 cm/ sec

Figure 2.3a

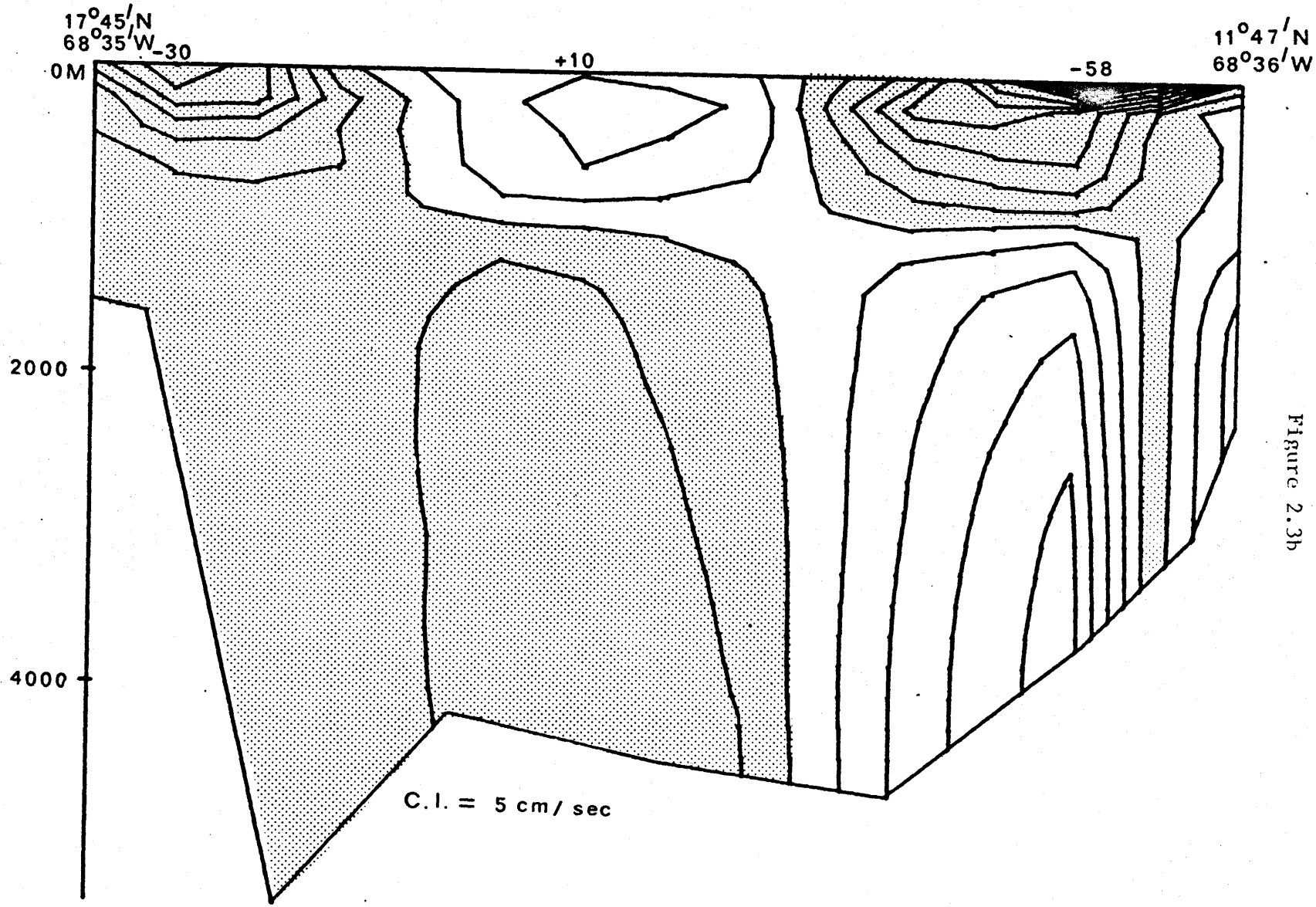

Figure 2.3b

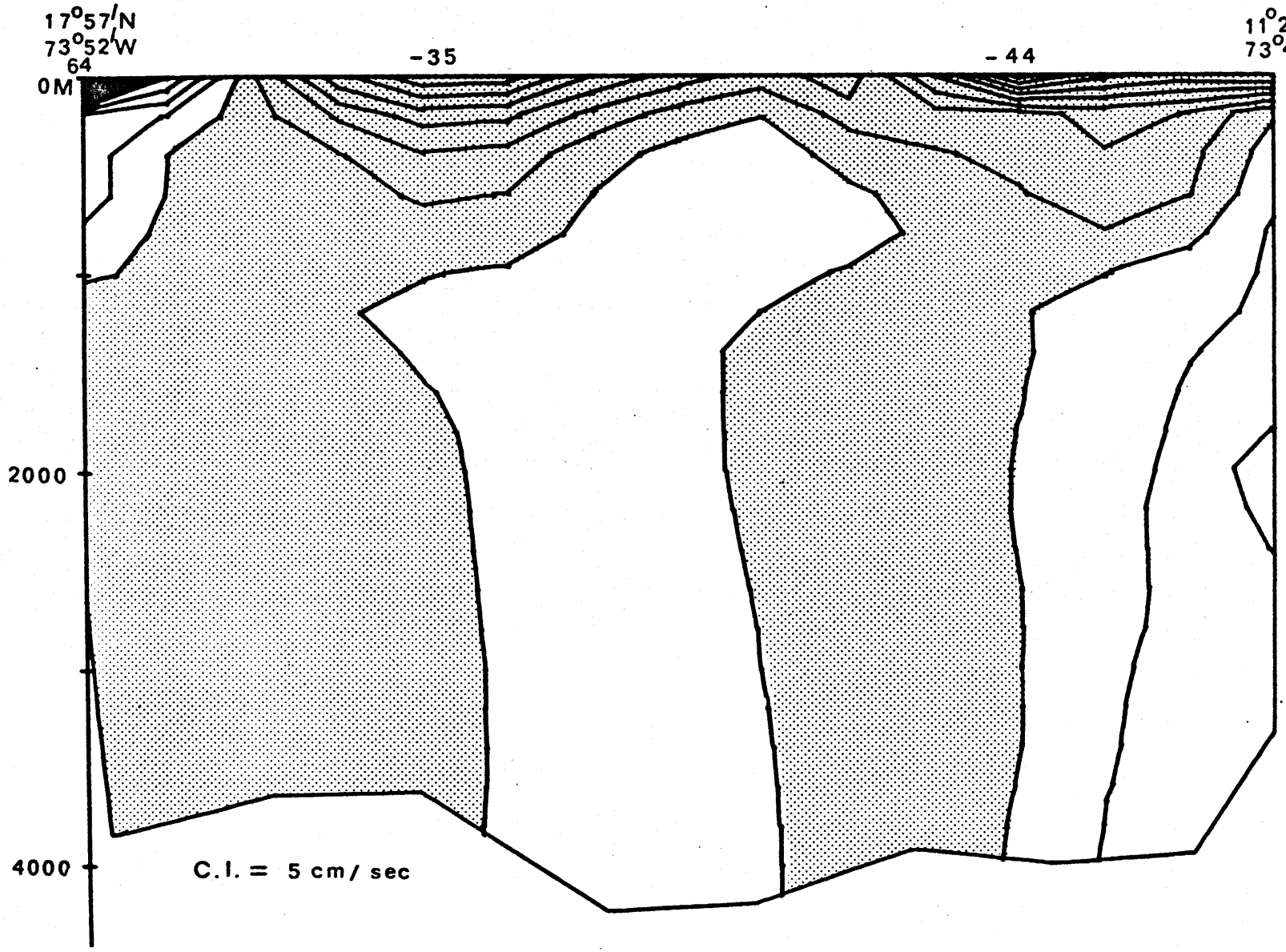

Figure 2.3c

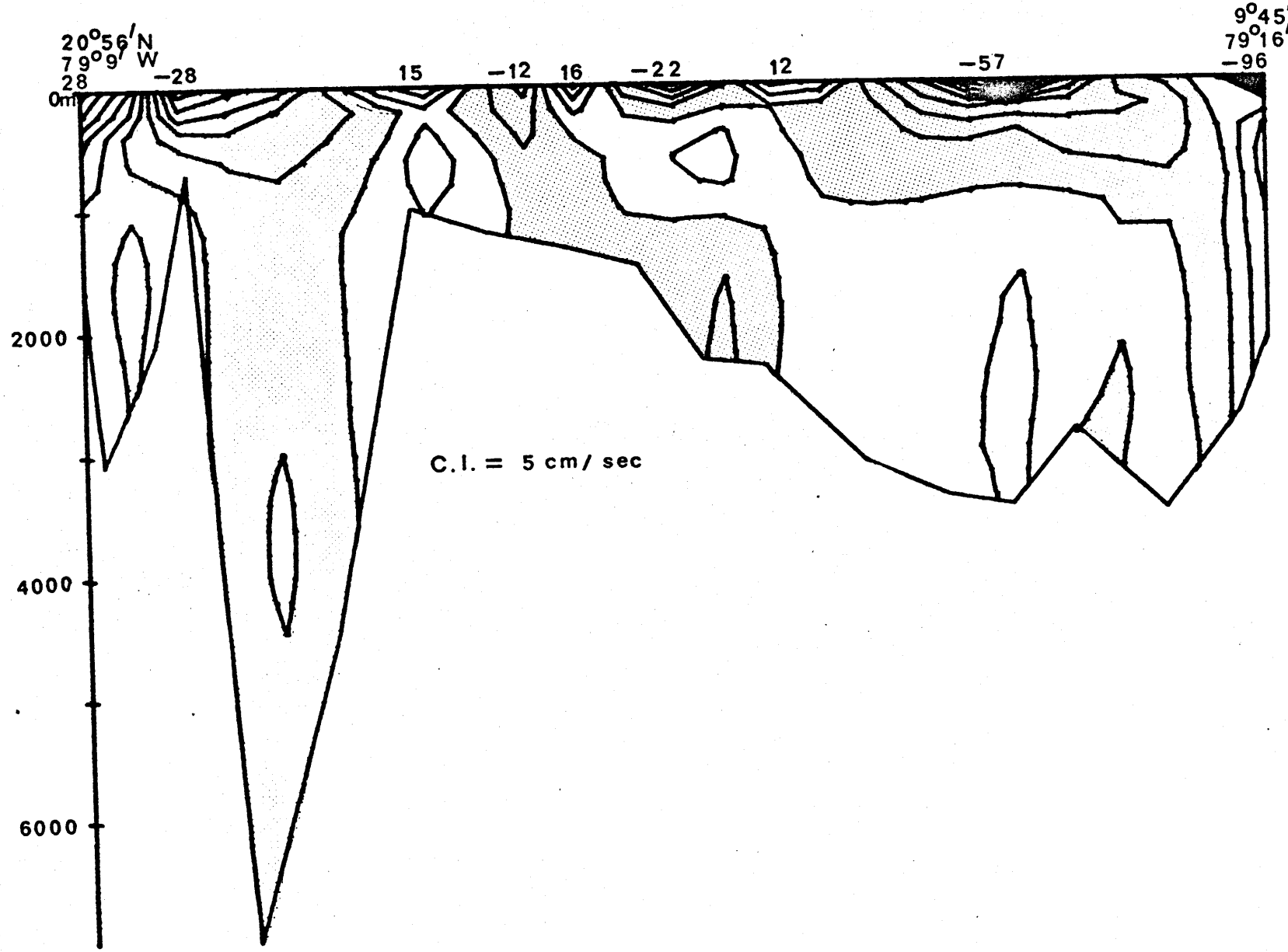
20°56′N
79°9′W
28
0m
-28
15
-12
16
-22
12
-57
-96
9°45′N
79°16′W
2000
4000
6000
C.I. = 5 cm/ sec

Figure 2.3d

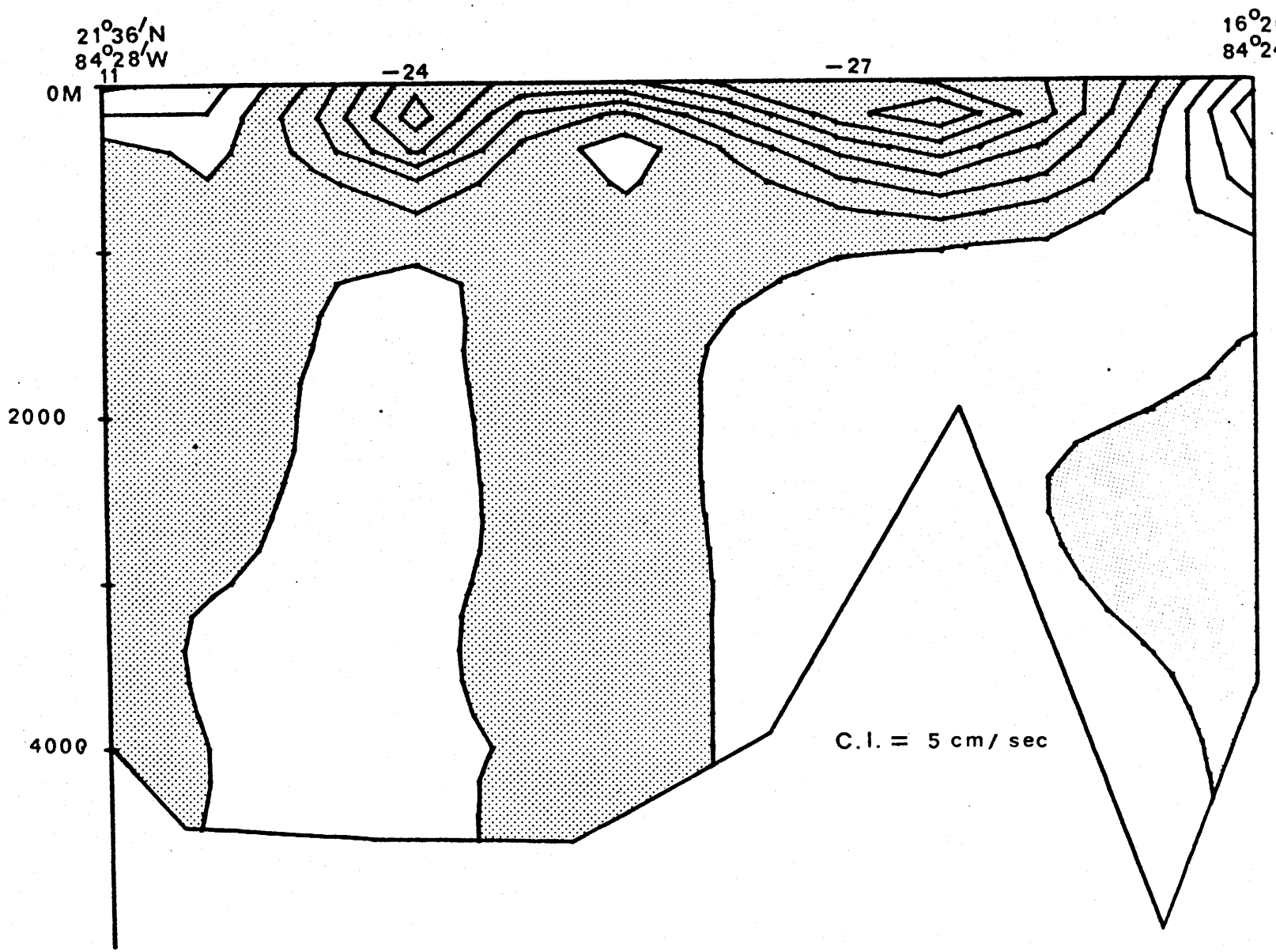

Figure 2.3c

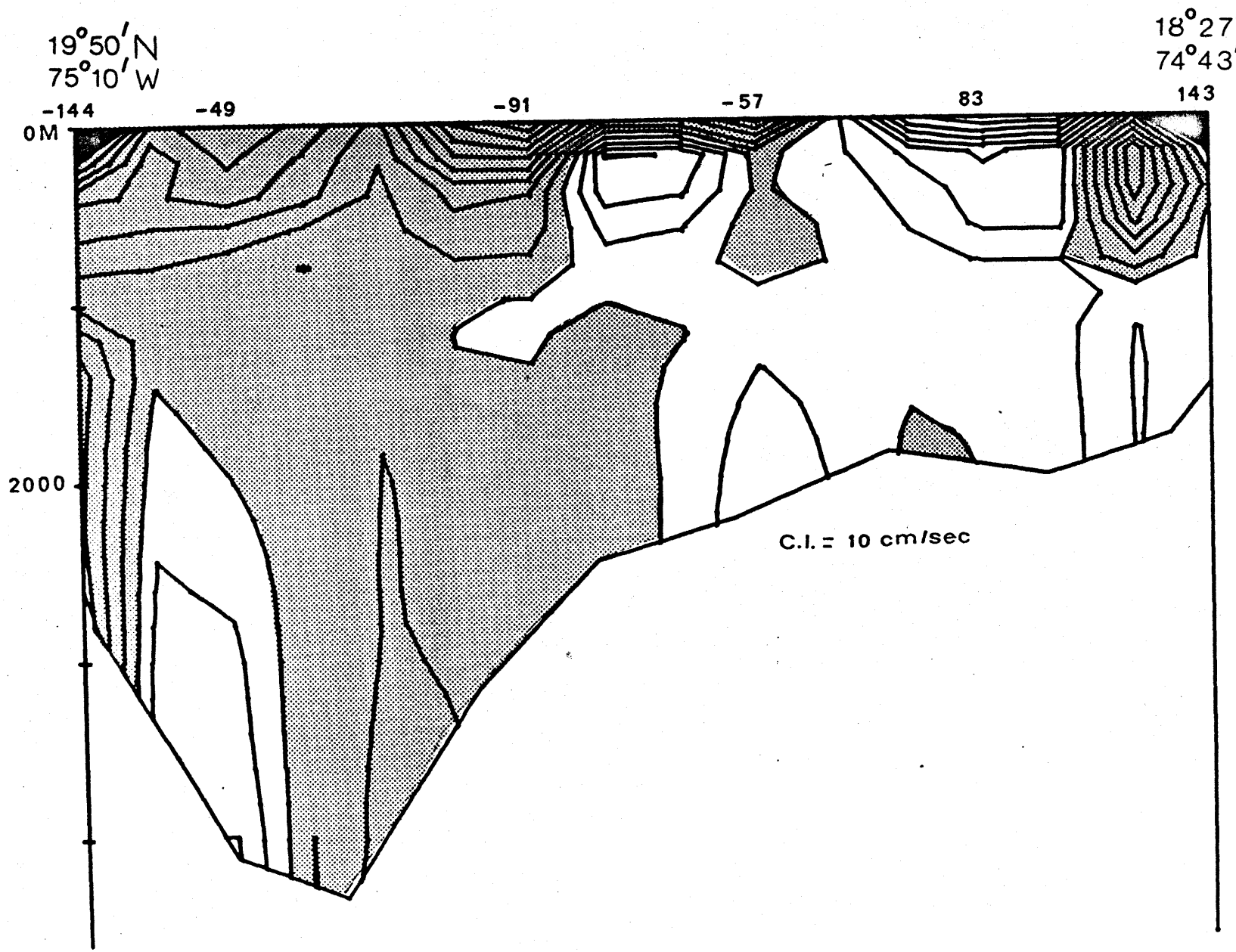

Figure 2.3f

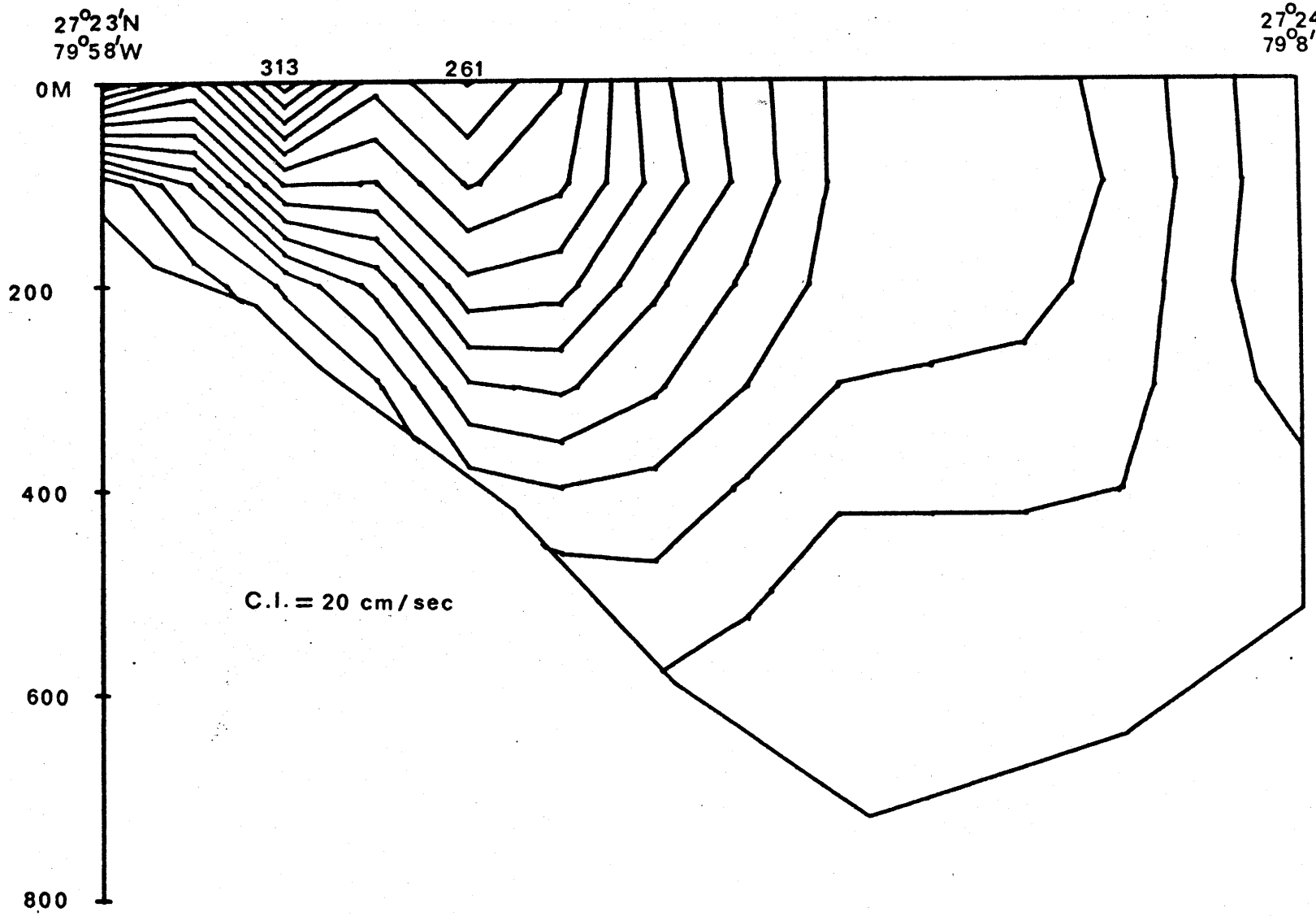

Figure 2.3g

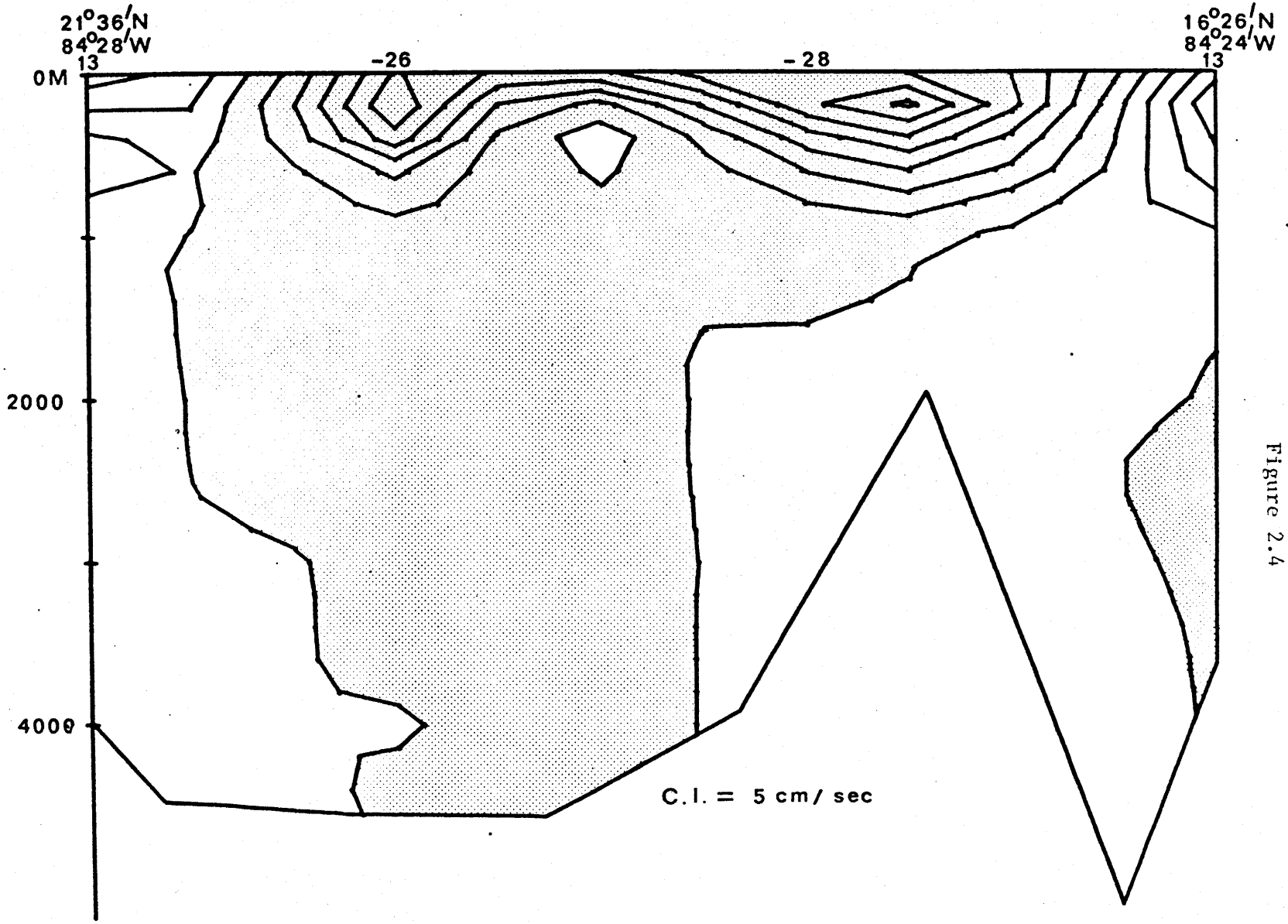

Figure 2.4

Figure 2.5

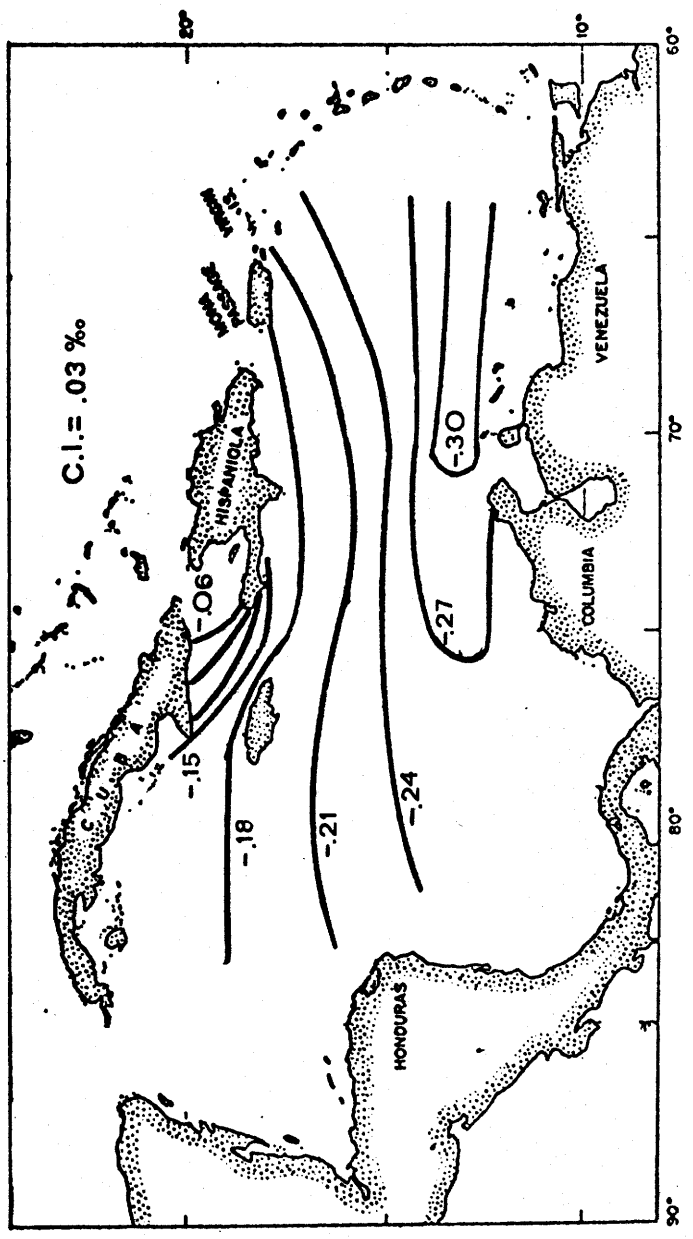
C.I.= .03 ‰
-.06
-.15
-.18
-.21
-.24
-.27
-.30
HISPANIOLA
VENEZUELA
COLUMBIA
HONDURAS
80°
70°
60°
10°
9°
1°

Figure 2.6a

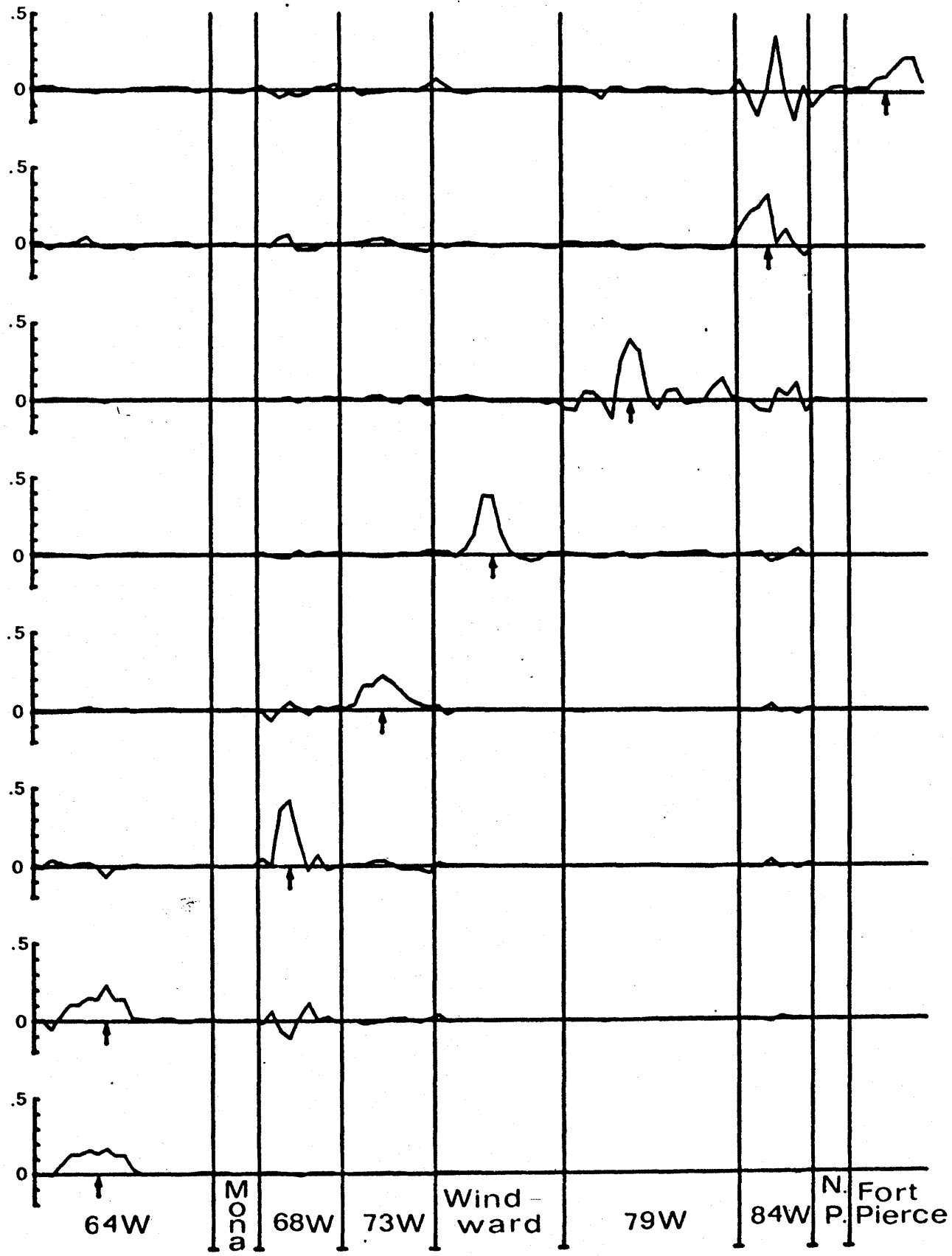

Figure 2.6b

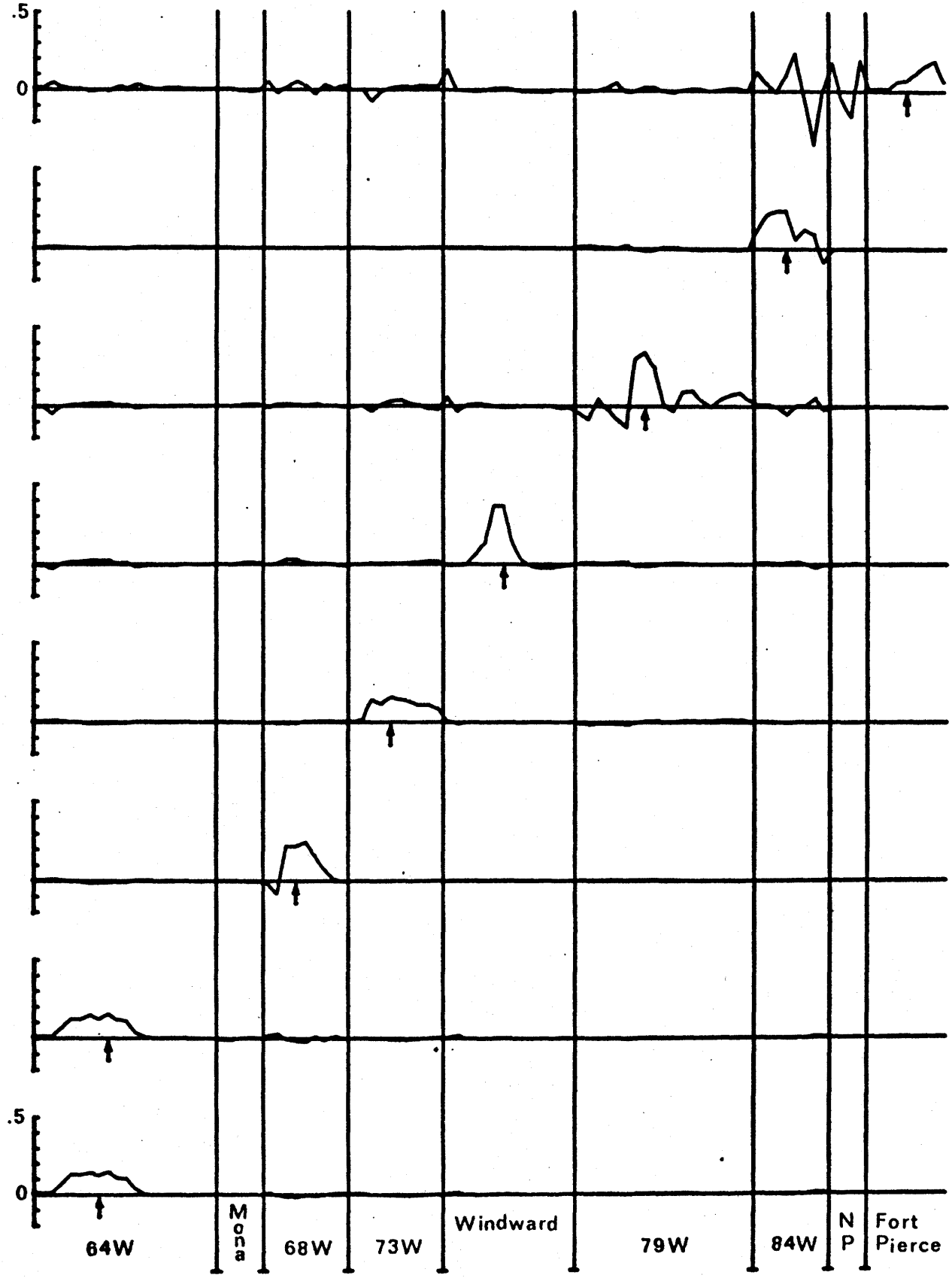

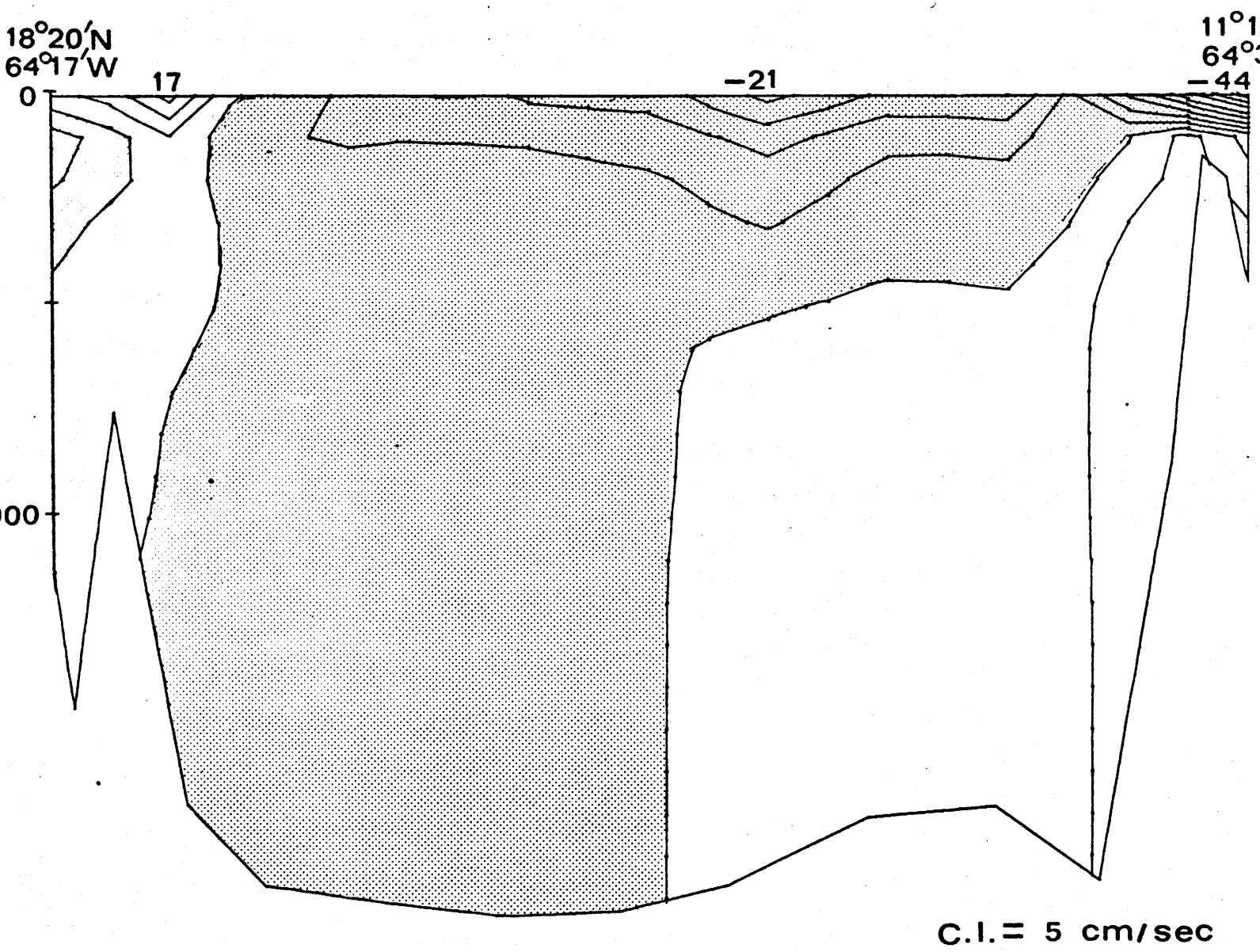

Figure 2.7a

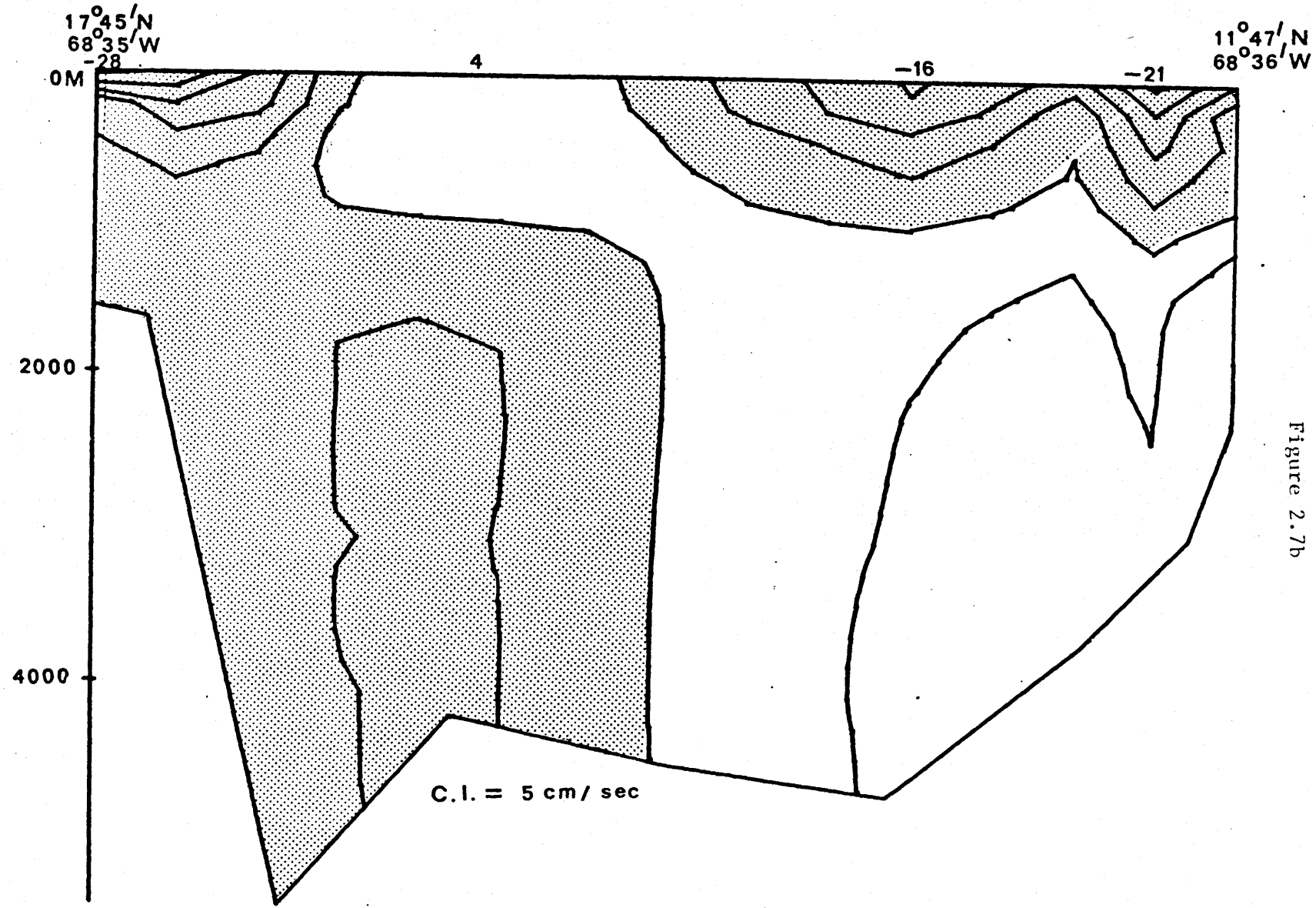

Figure 2.7b

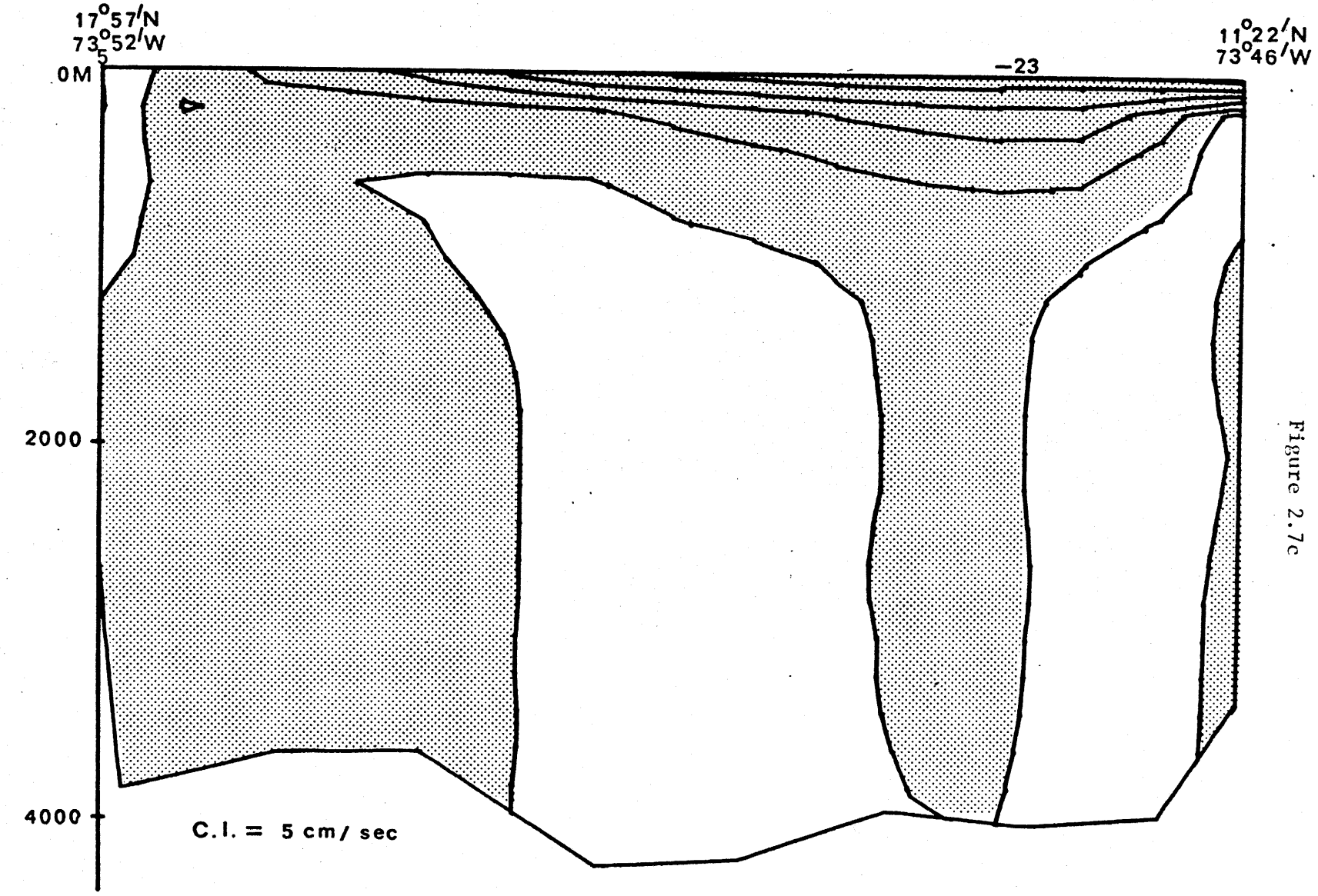

Figure 2.7c

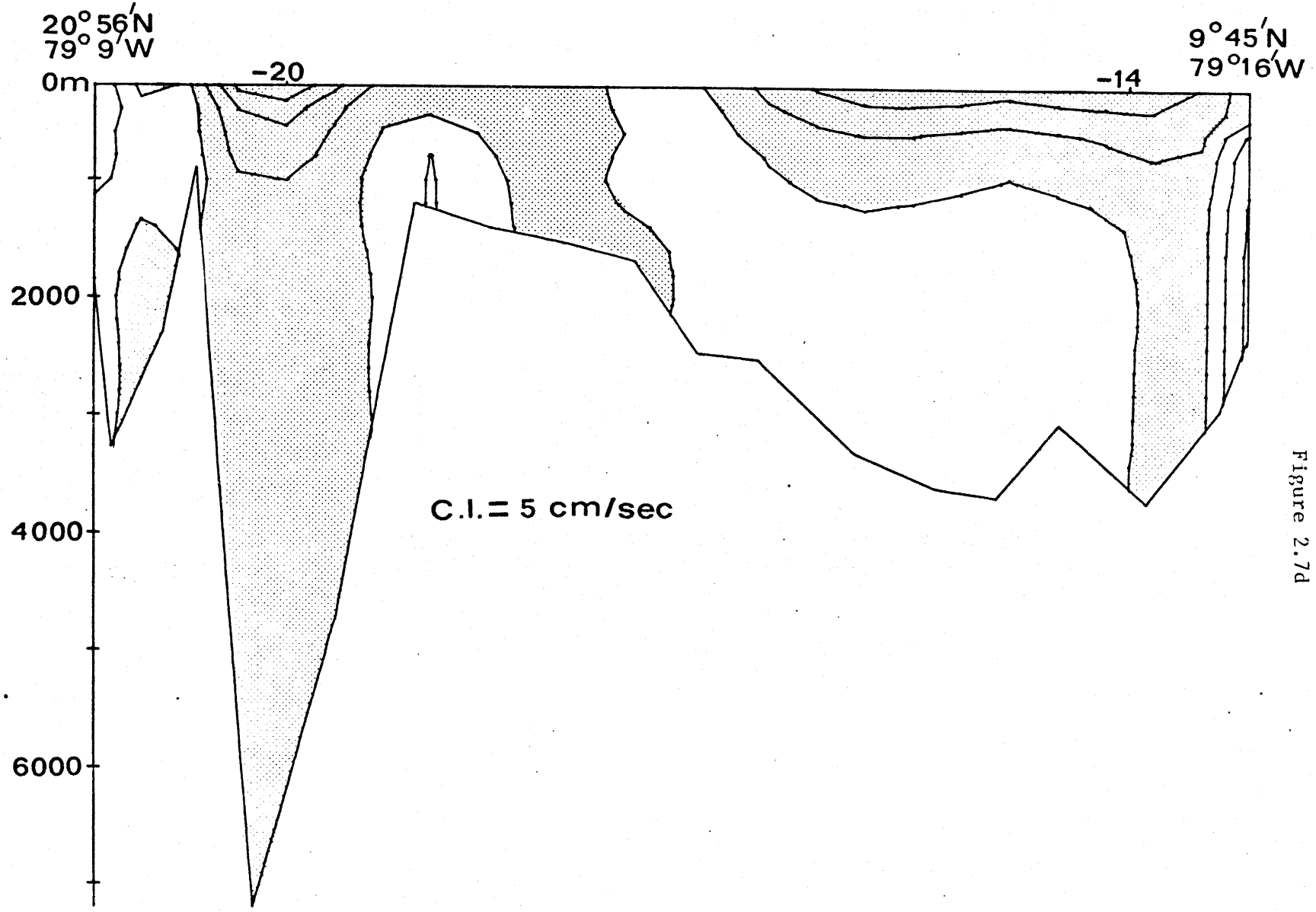

Figure 2.7d

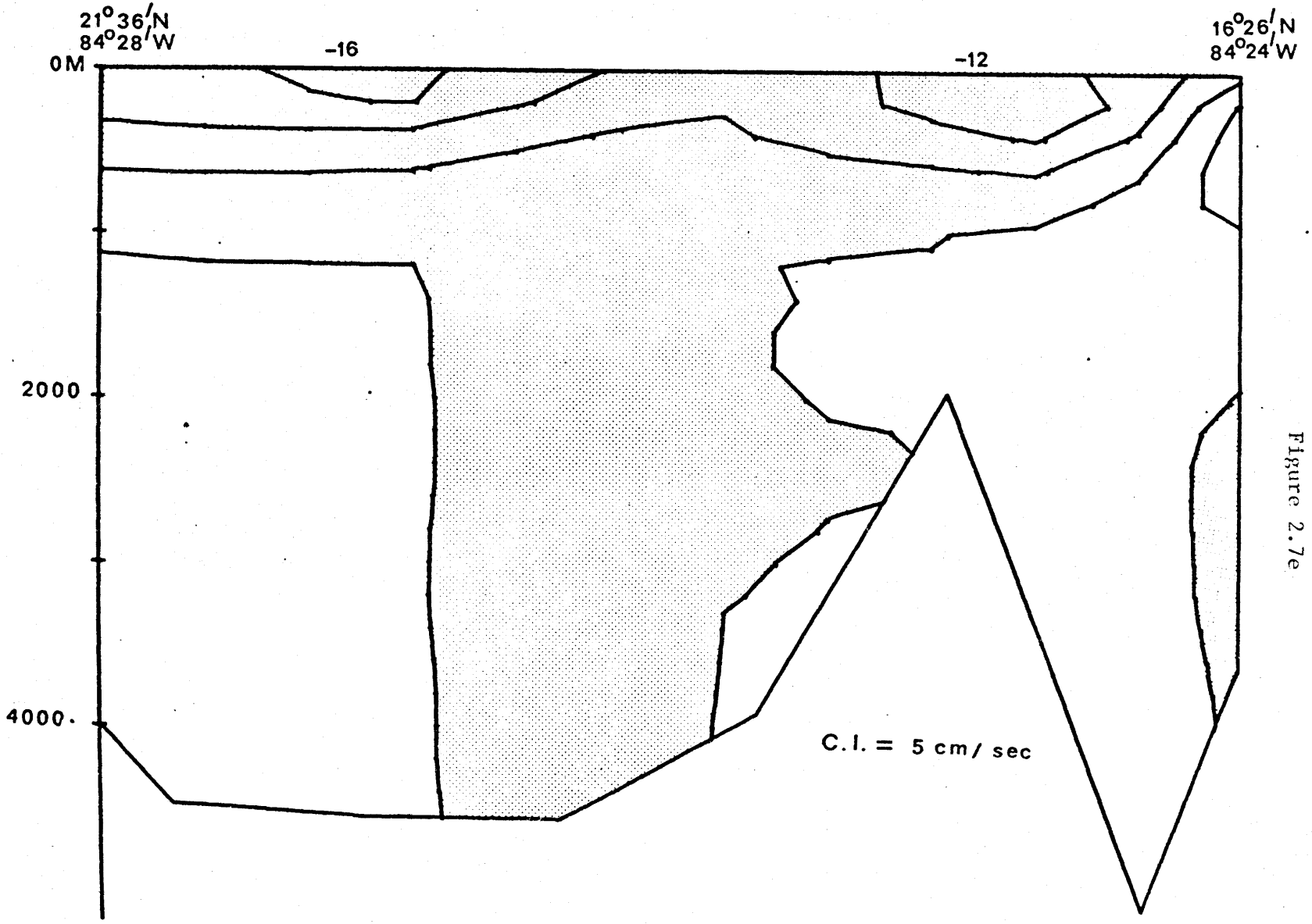

Figure 2.7e

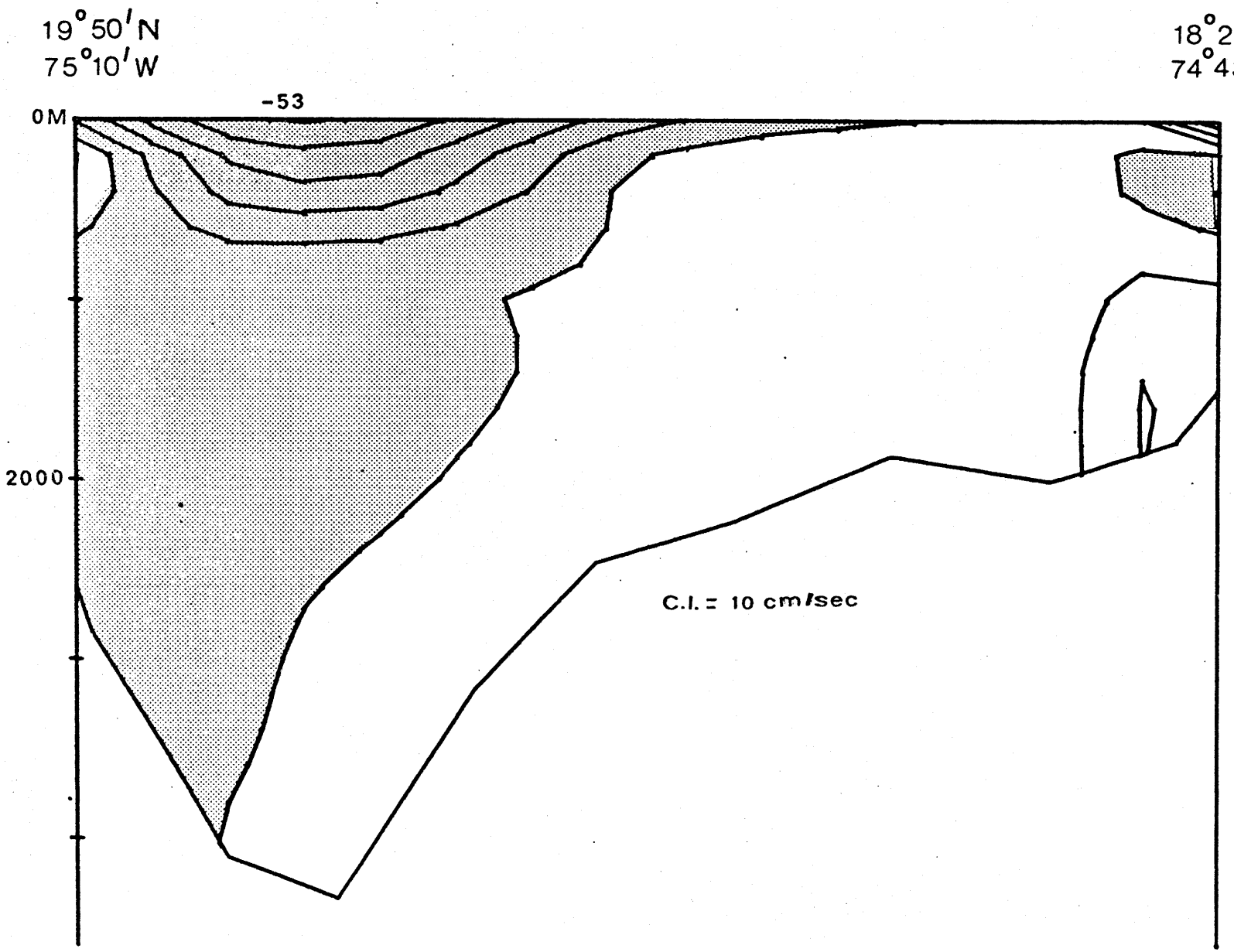

Figure 2.7f

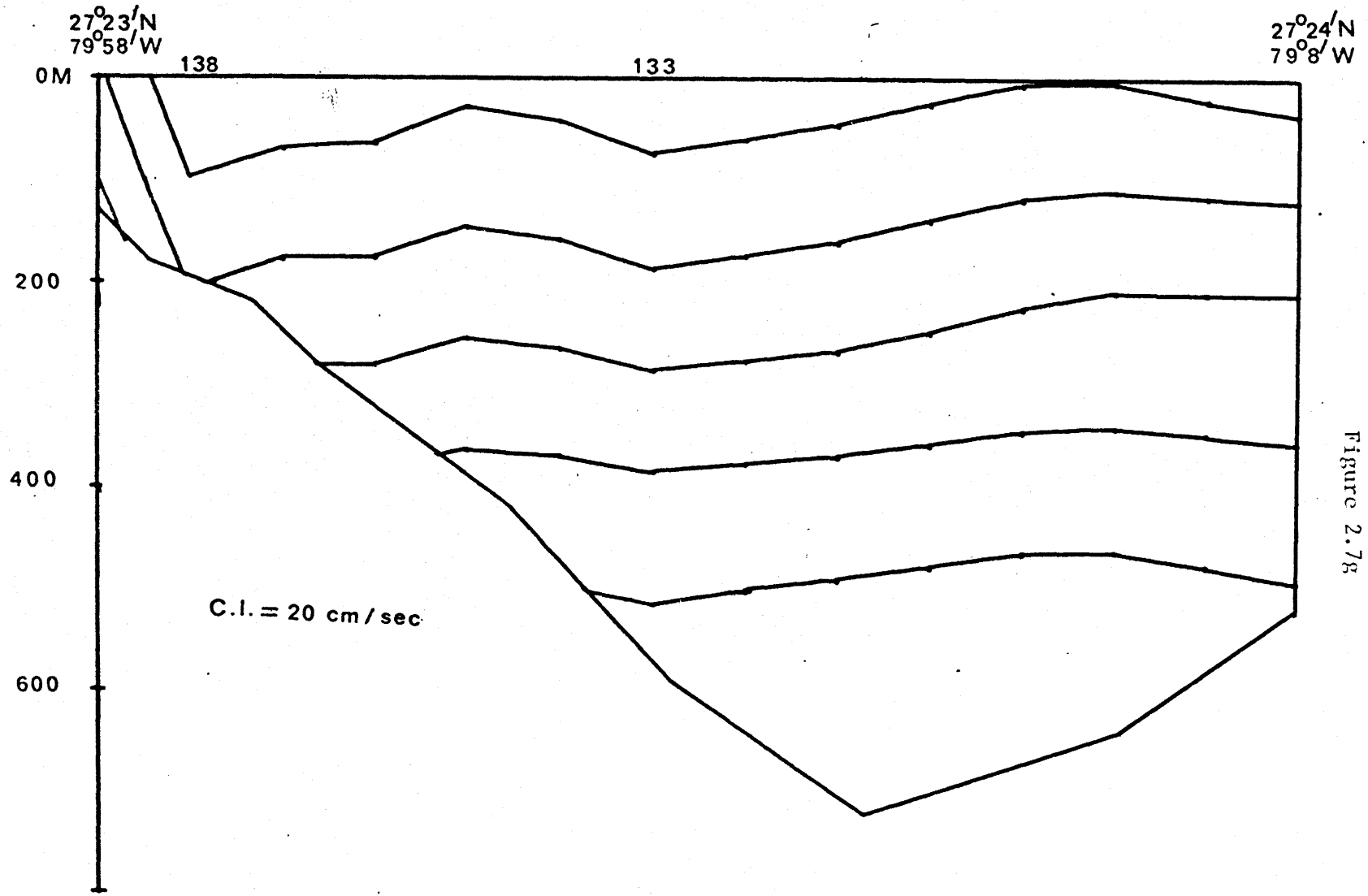

169

Figure 2.7g

Figure 3.1

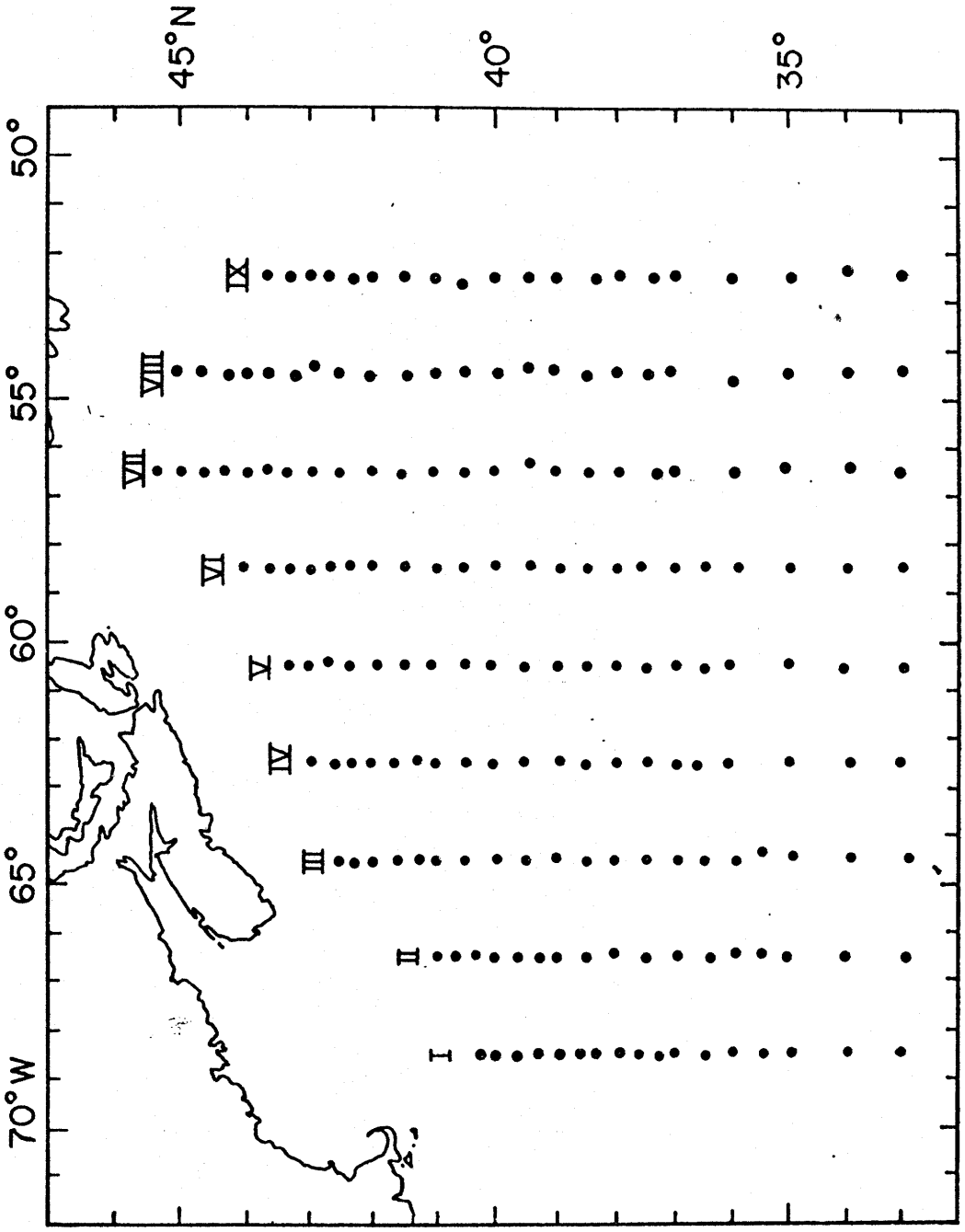

Figure 3.2

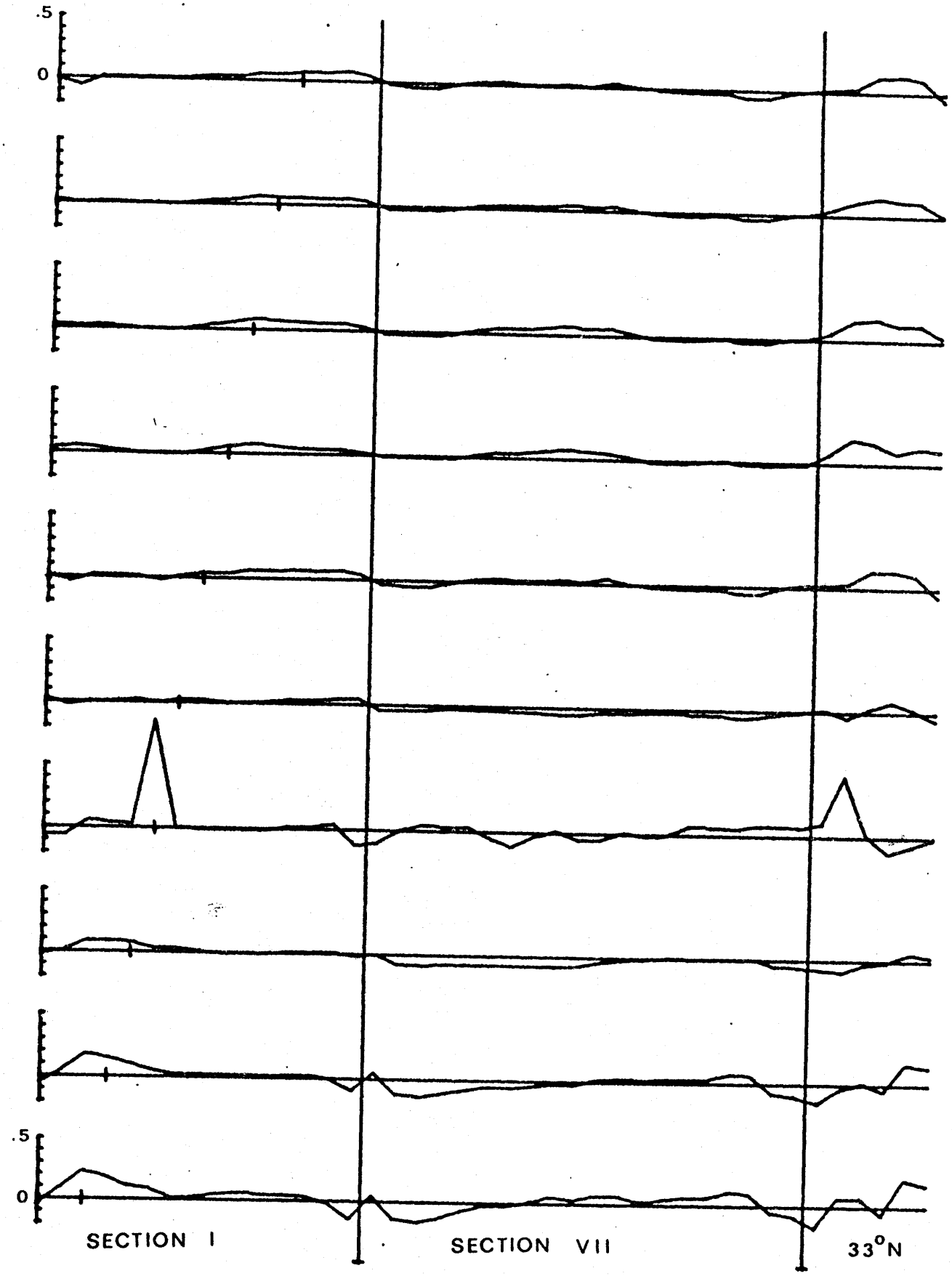

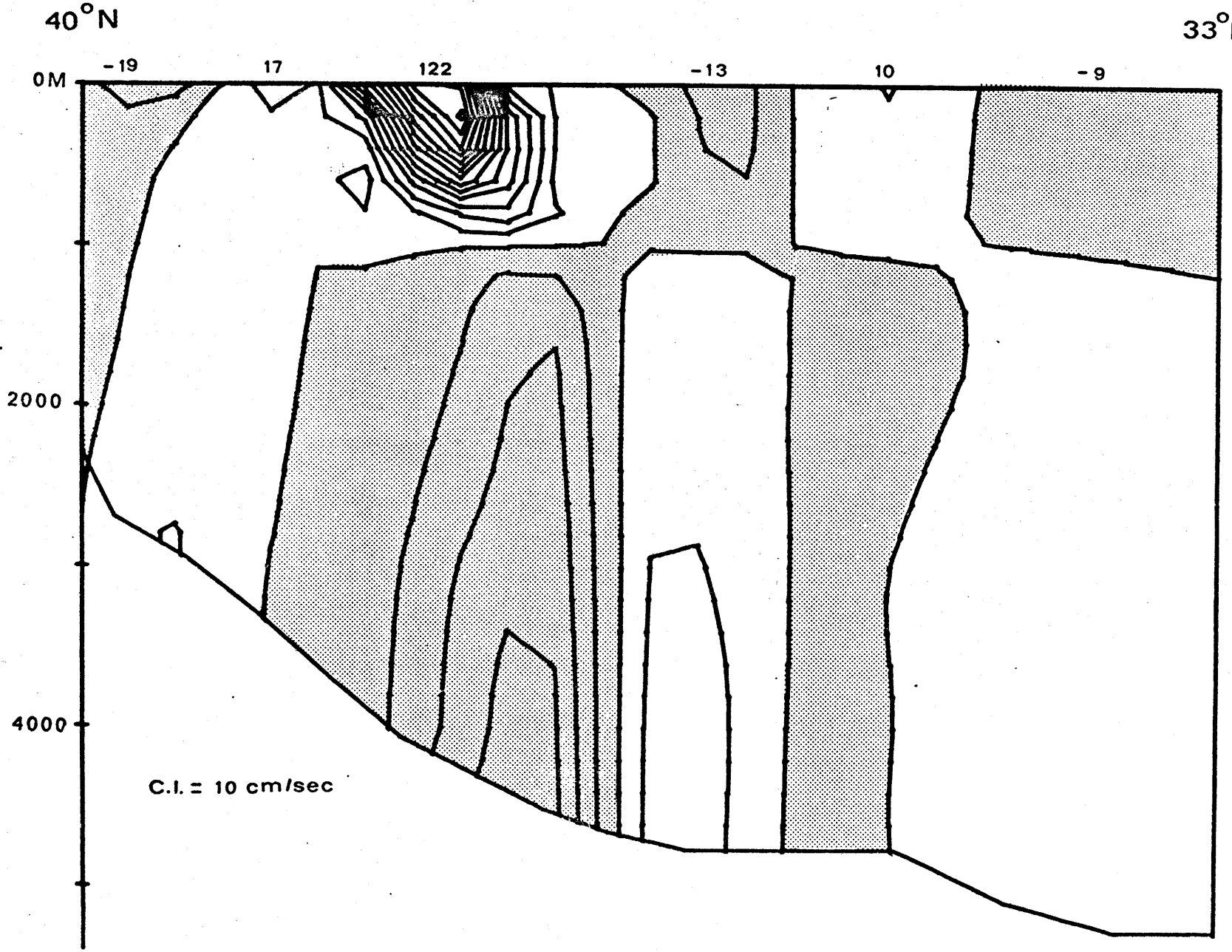

Figure 3.3a

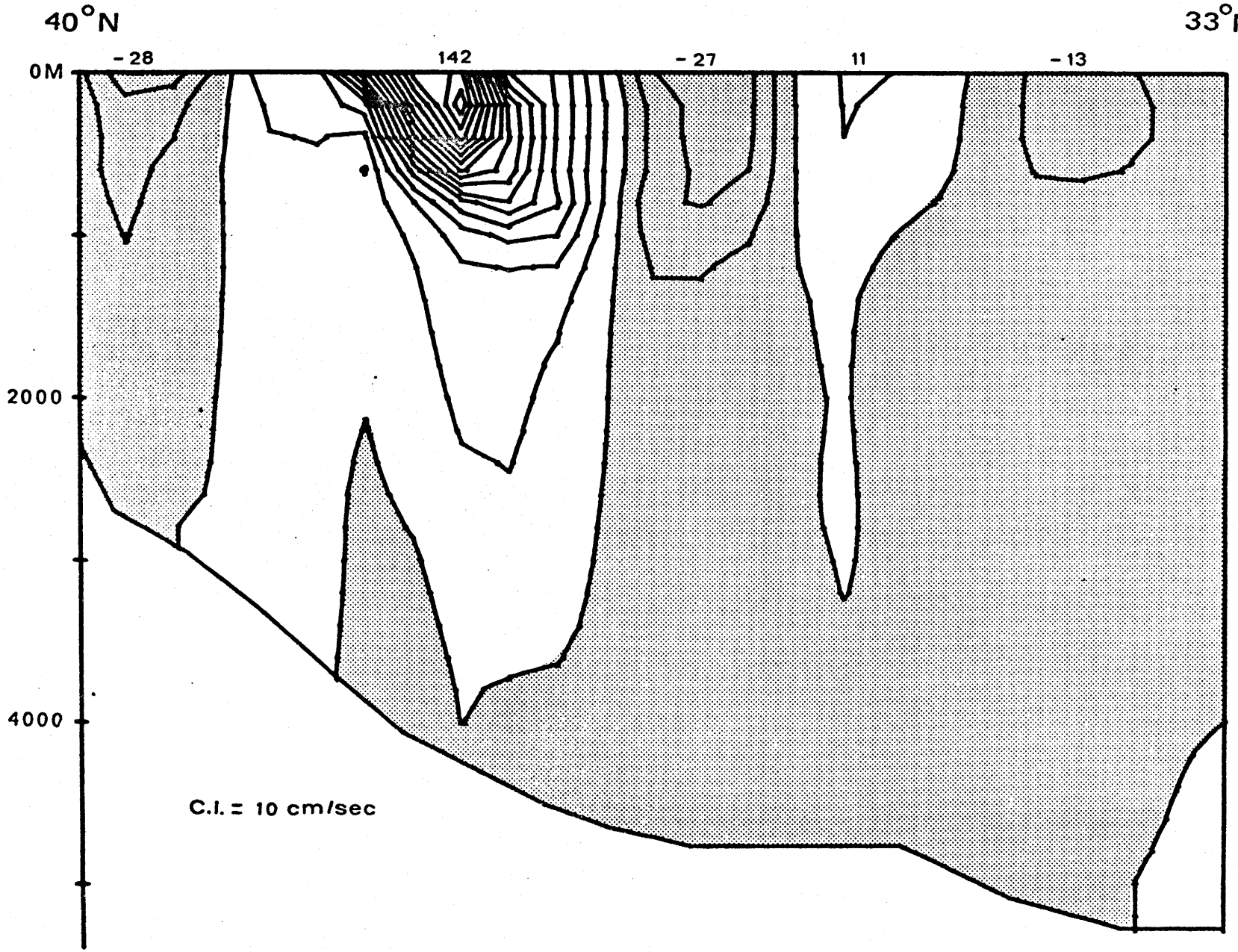

Figure 3.3b

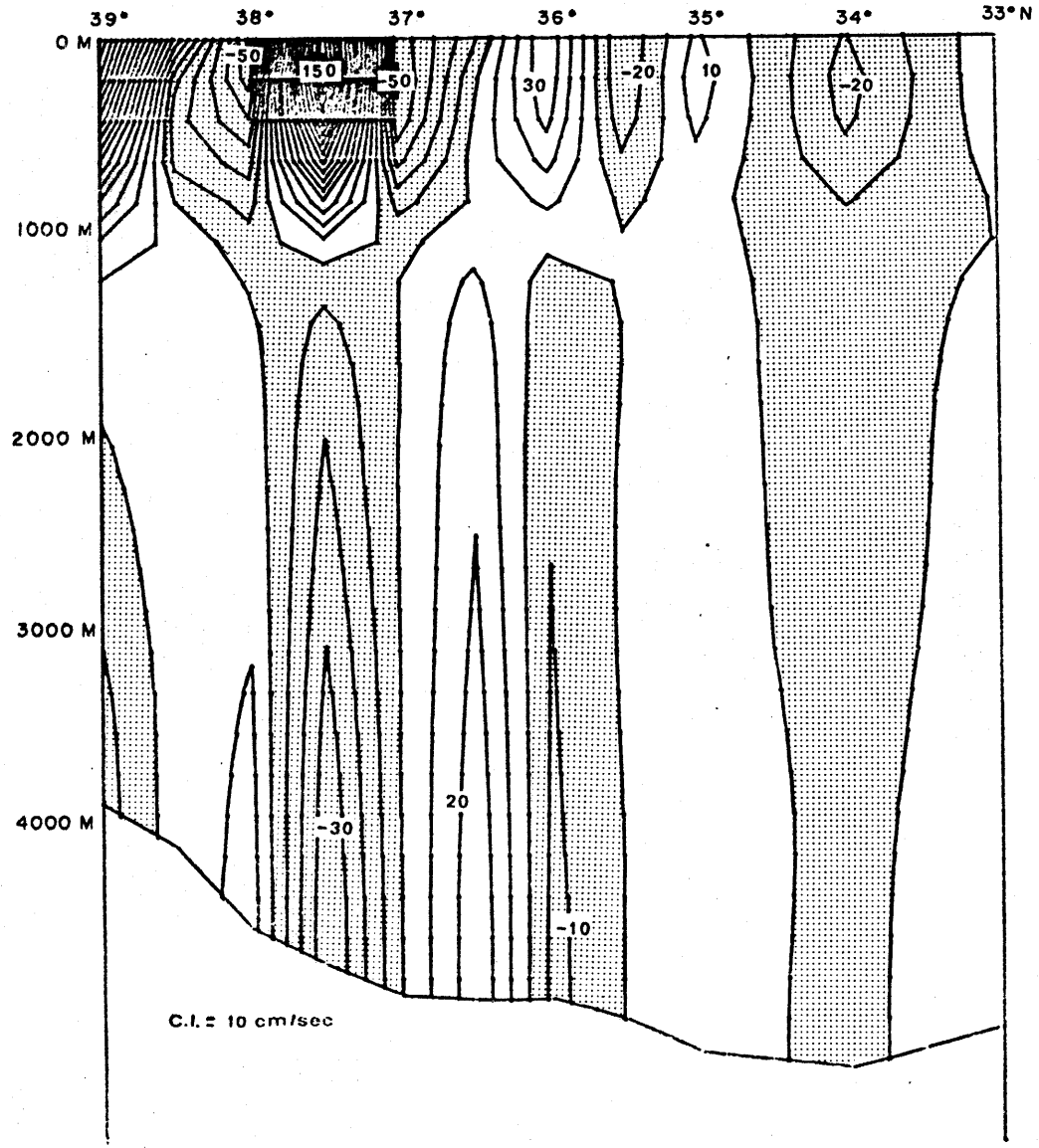
39°
38°
37°
36°
35°
34°
33°N
0 M
1000 M
2000 M
3000 M
4000 M
-50
150
-50
30
-20
10
-20
-30
20
-10
C.I. = 10 cm/sec

Figure 3.4a

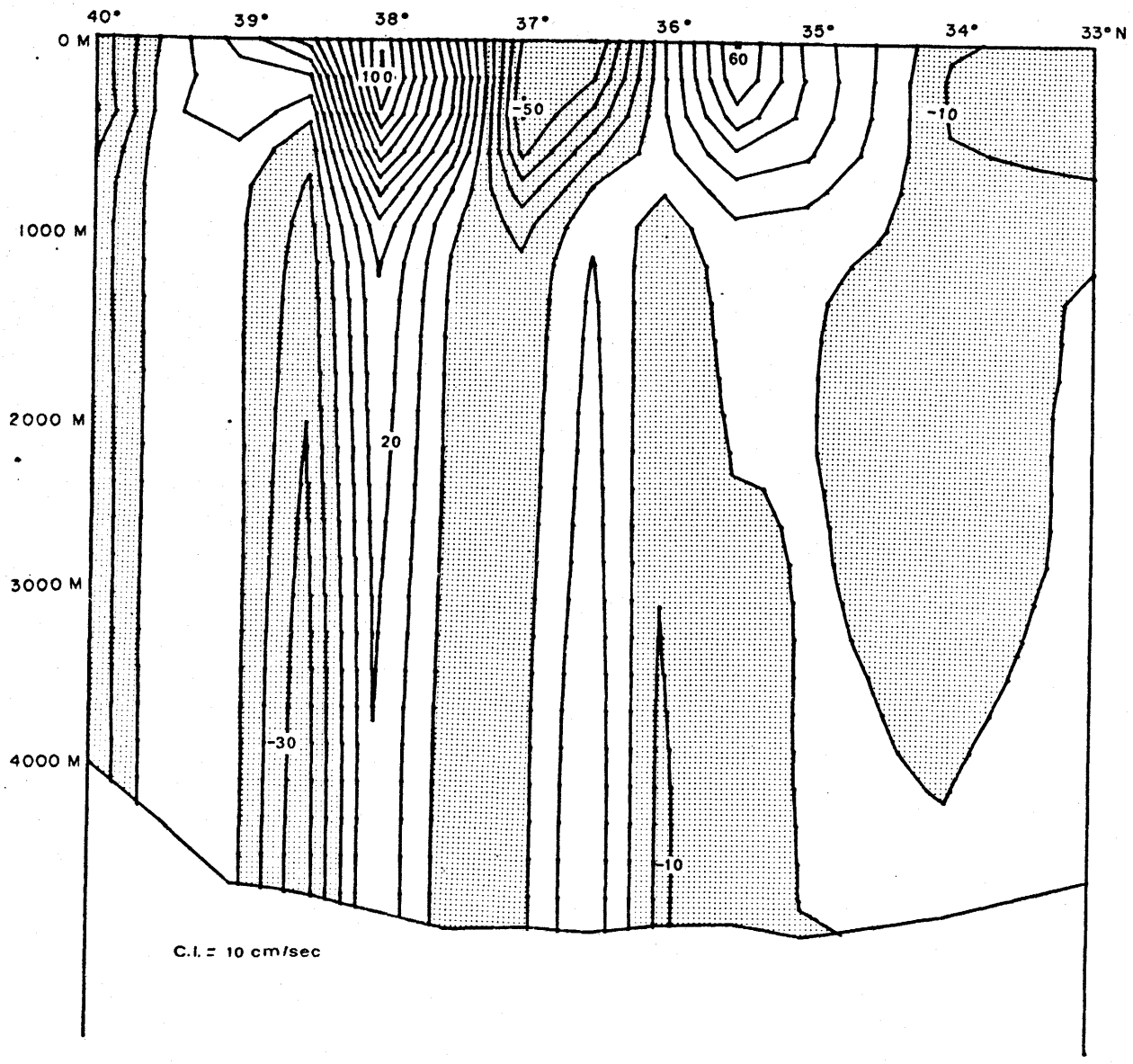
40°
39°
38°
37°
36°
35°
34°
33°N
0 M
1000 M
2000 M
3000 M
4000 M
100
-50
60
-10
20
-30
-10
C.I. = 10 cm/sec

Figure 3.4b

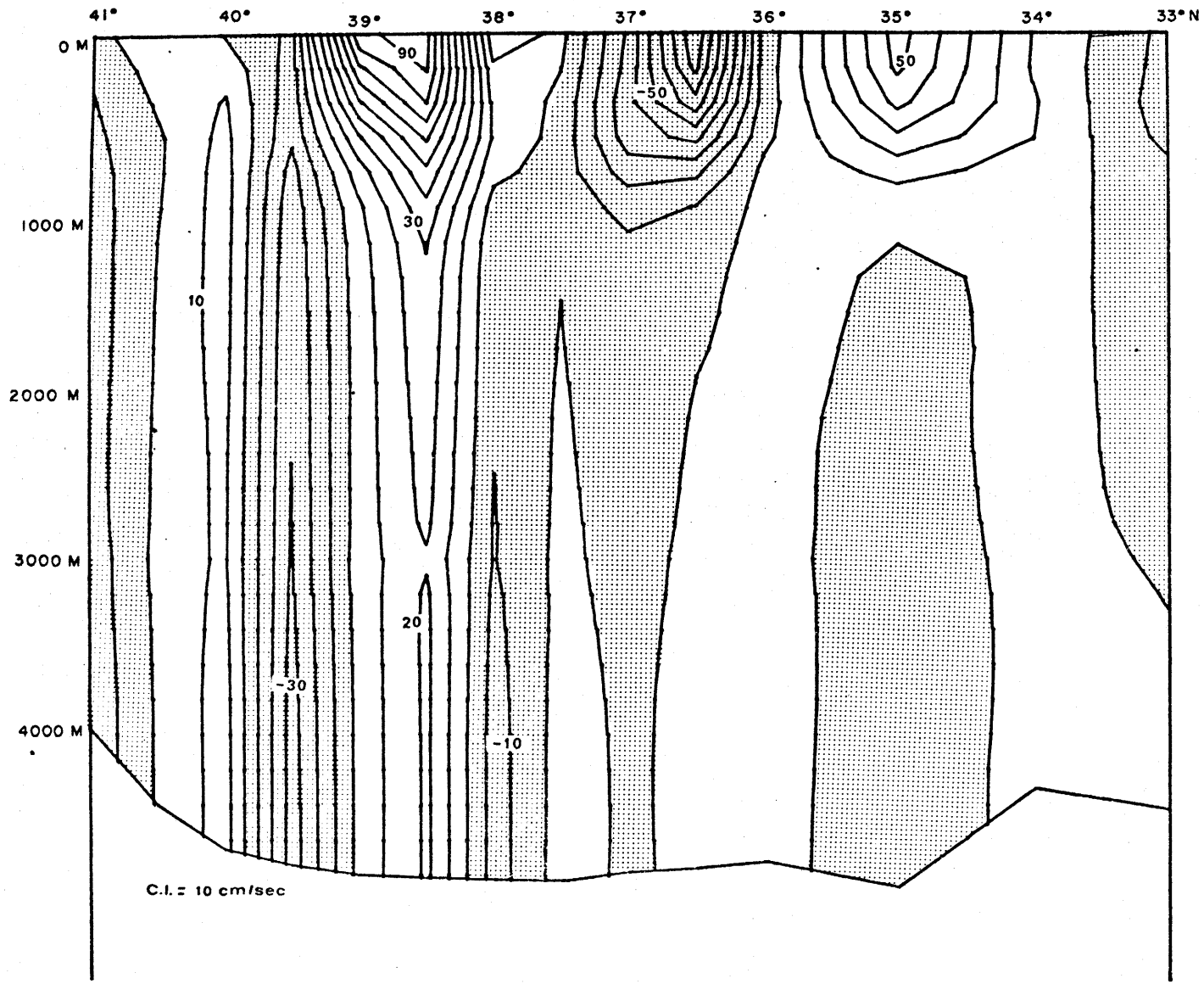
41°
40°
39°
38°
37°
36°
35°
34°
33°N
0 M
1000 M
2000 M
3000 M
4000 M
90
50
-50
30
10
20
-30
-10
C.I. = 10 cm/sec

Figure 3.4c

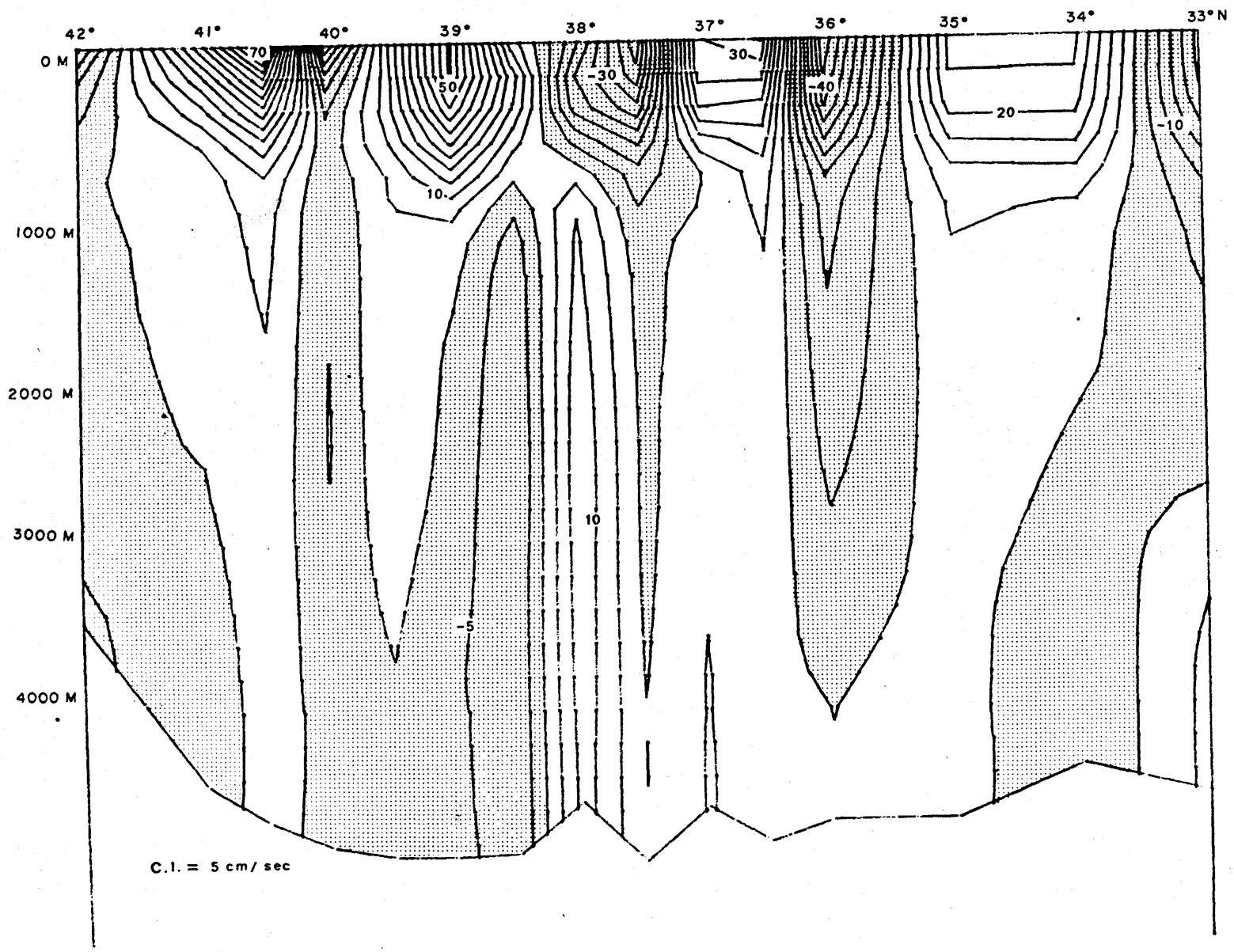
42°
41°
40°
39°
38°
37°
36°
35°
34°
33°N
0 M
1000 M
2000 M
3000 M
4000 M
70
50
10
-30
30
-40
20
-10
10
-5
C.I. = 5 cm/ sec

Figure 3.4d

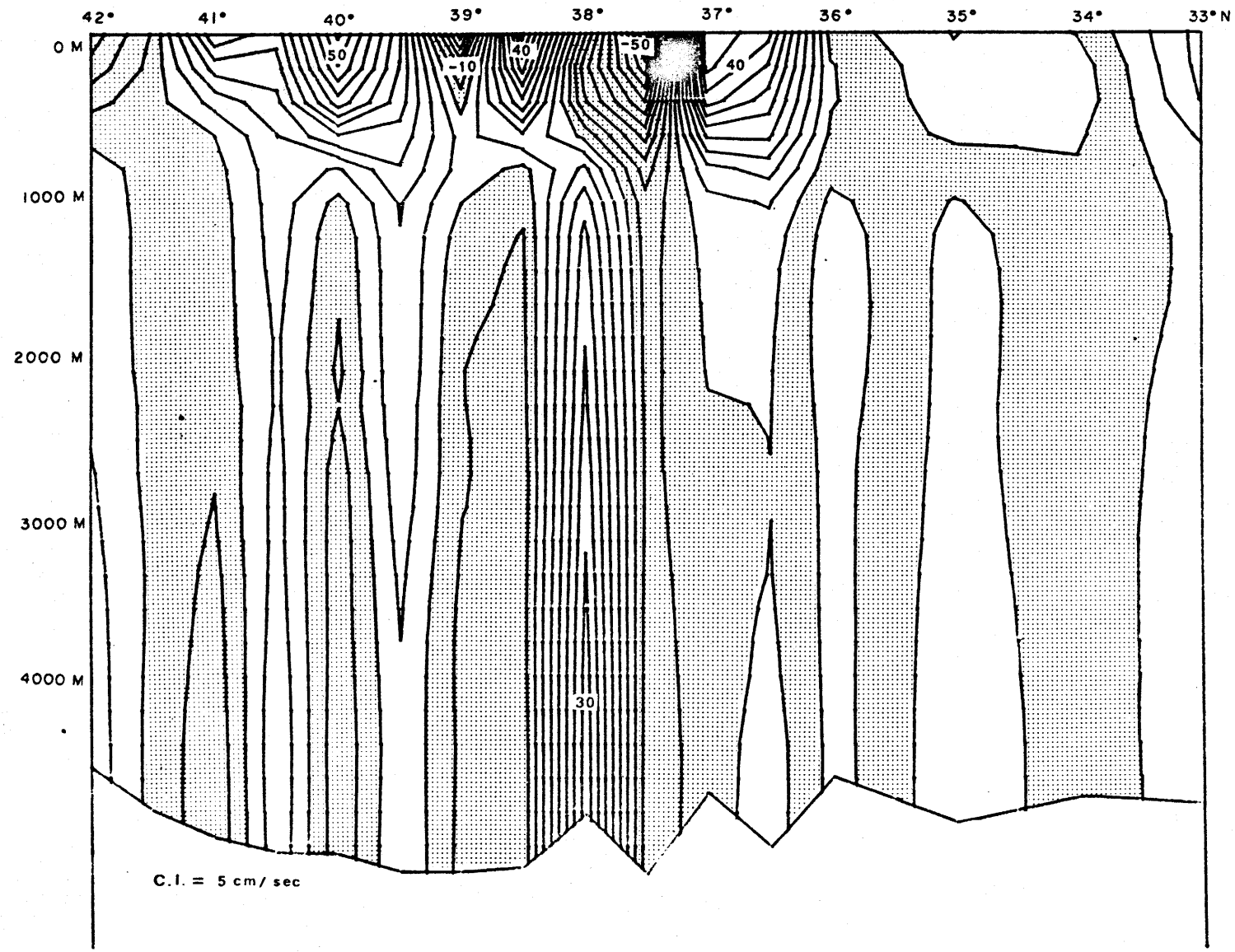
42°
41°
40°
39°
38°
37°
36°
35°
34°
33°N
0 M
1000 M
2000 M
3000 M
4000 M
50
-10
40
-50
40
30
C.I. = 5 cm/ sec

Figure 3.4e

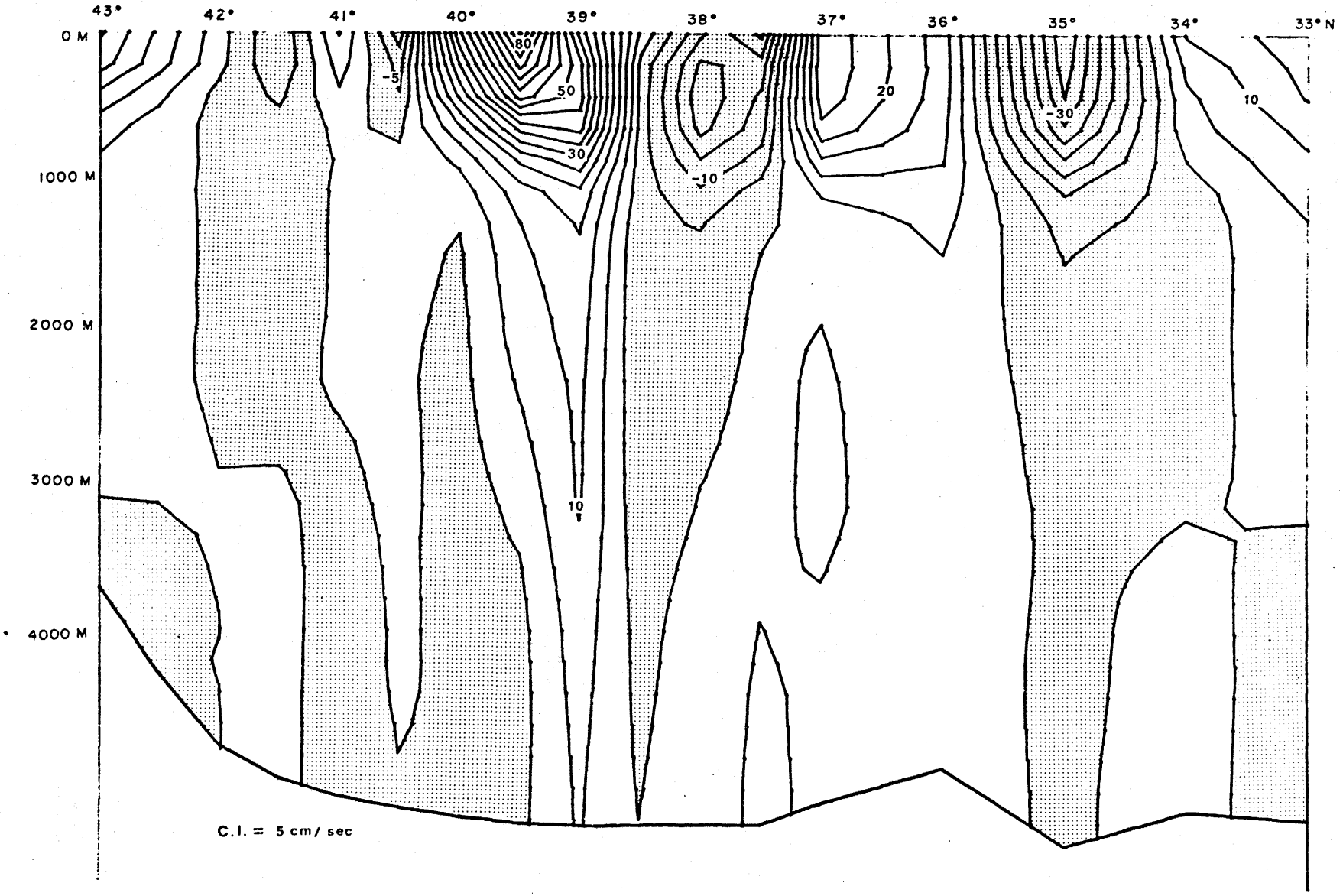
43°
42°
41°
40°
39°
38°
37°
36°
35°
34°
33° N
0 M
1000 M
2000 M
3000 M
4000 M
-5
80
50
30
10
-10
20
-30
10
C.I. = 5 cm/ sec

Figure 3.4f

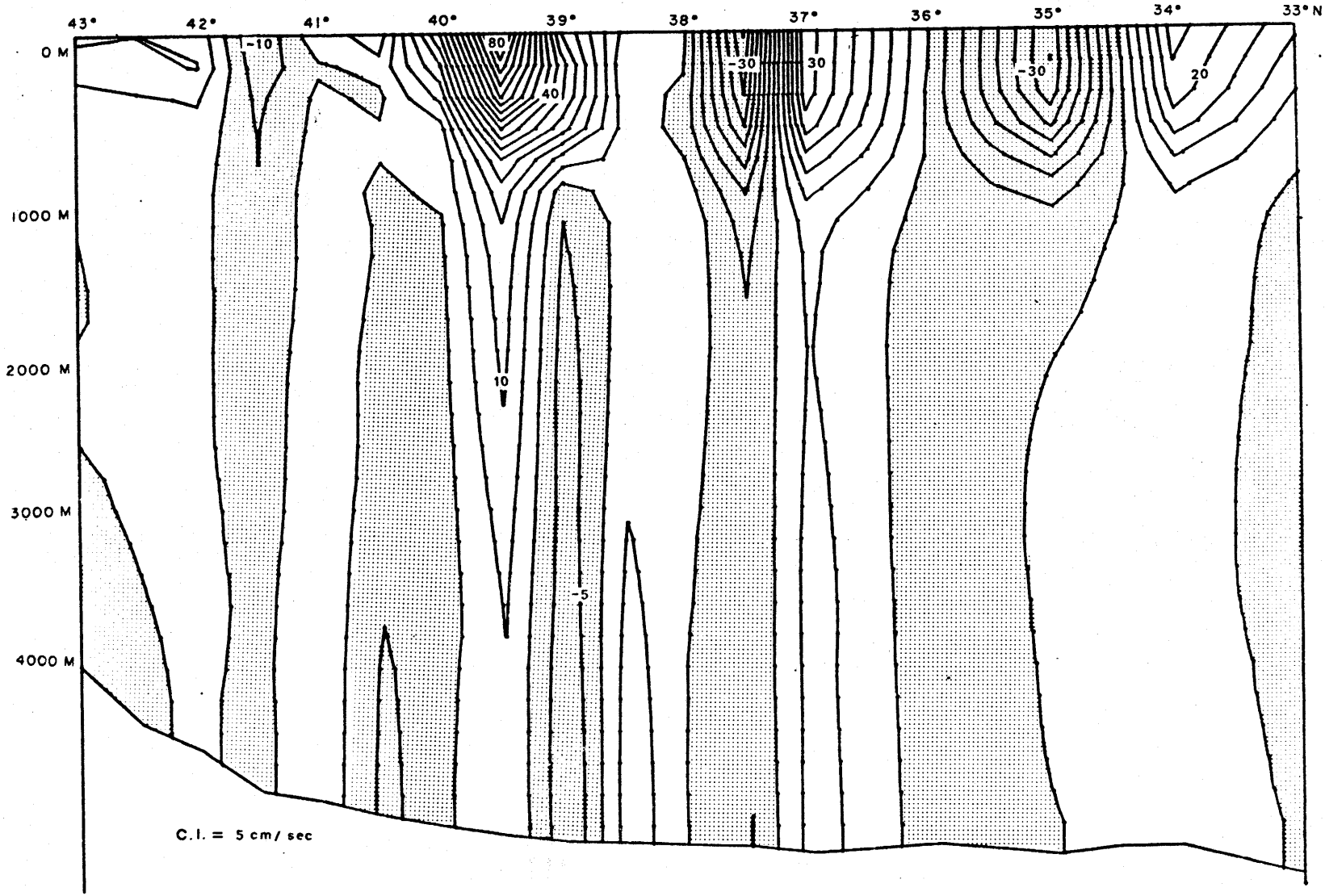
43°
42°
41°
40°
39°
38°
37°
36°
35°
34°
33° N
0 M
1000 M
2000 M
3000 M
4000 M
-10
80
40
-30
30
-30
20
10
-5
C.I. = 5 cm/ sec

Figure 3.4g

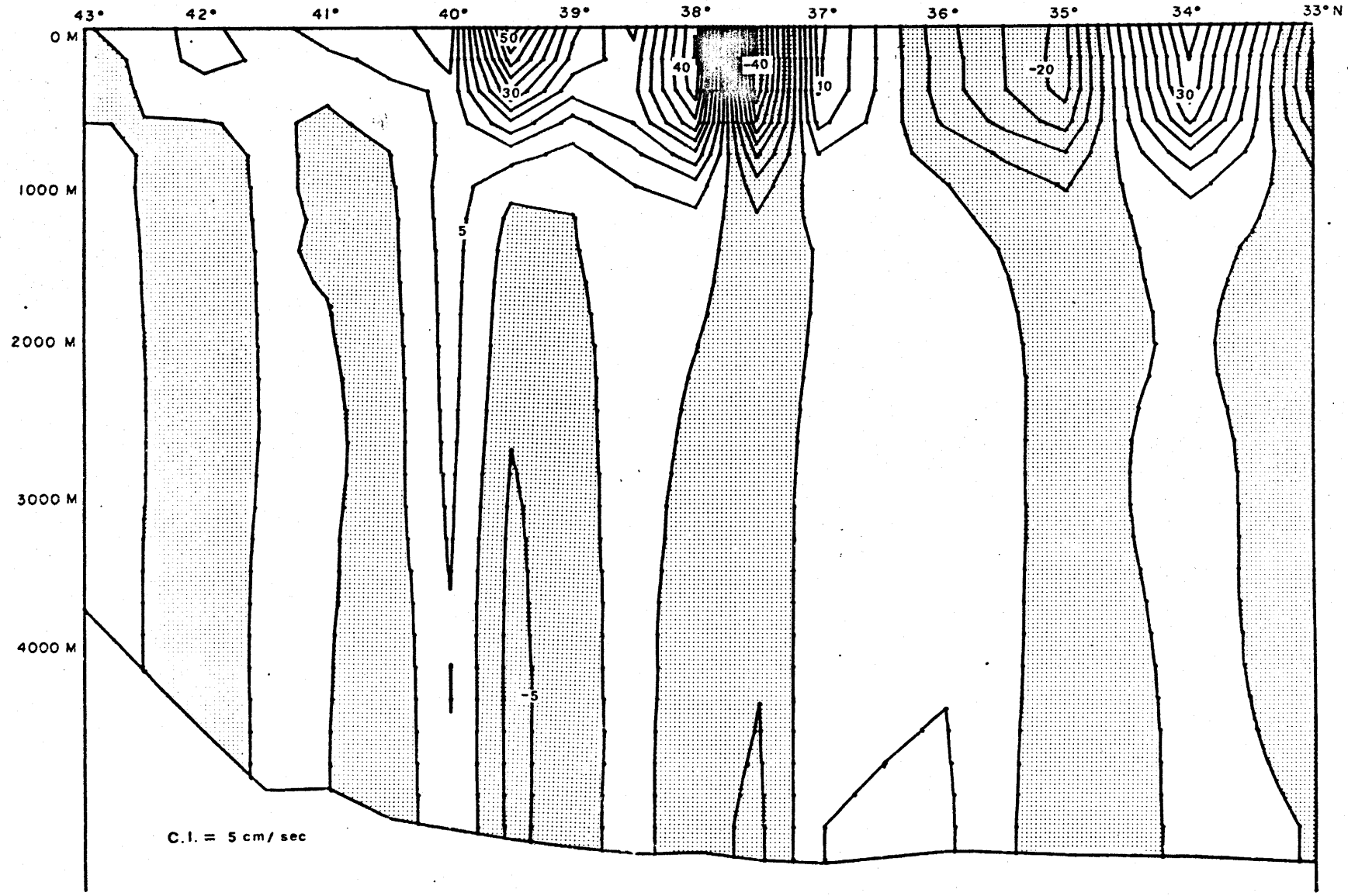
43°
42°
41°
40°
39°
38°
37°
36°
35°
34°
33° N
0 M
1000 M
2000 M
3000 M
4000 M
50
40
30
-40
10
-20
30
5
-5
C.I. = 5 cm/ sec

Figure 3.4h

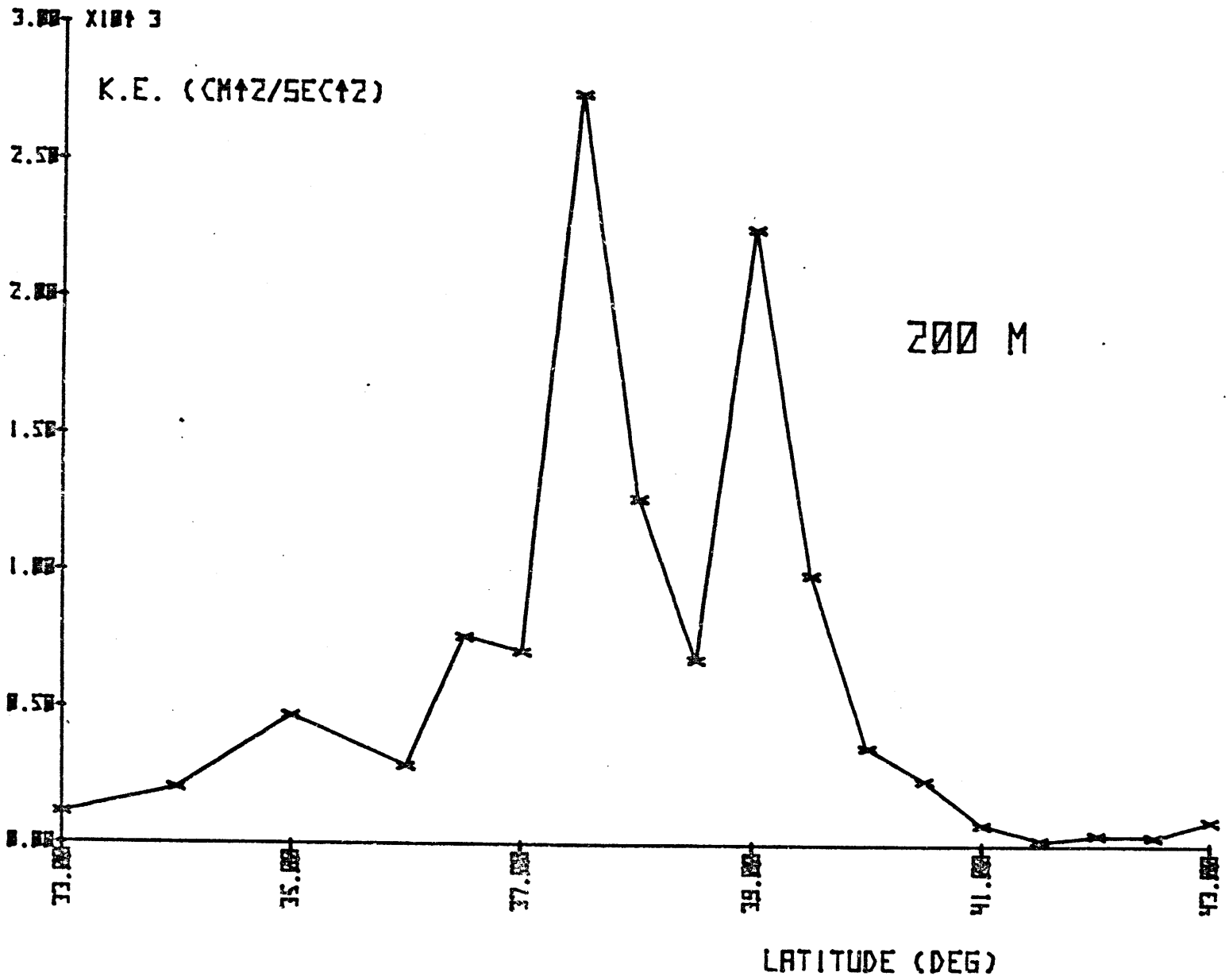

Figure 3.5a

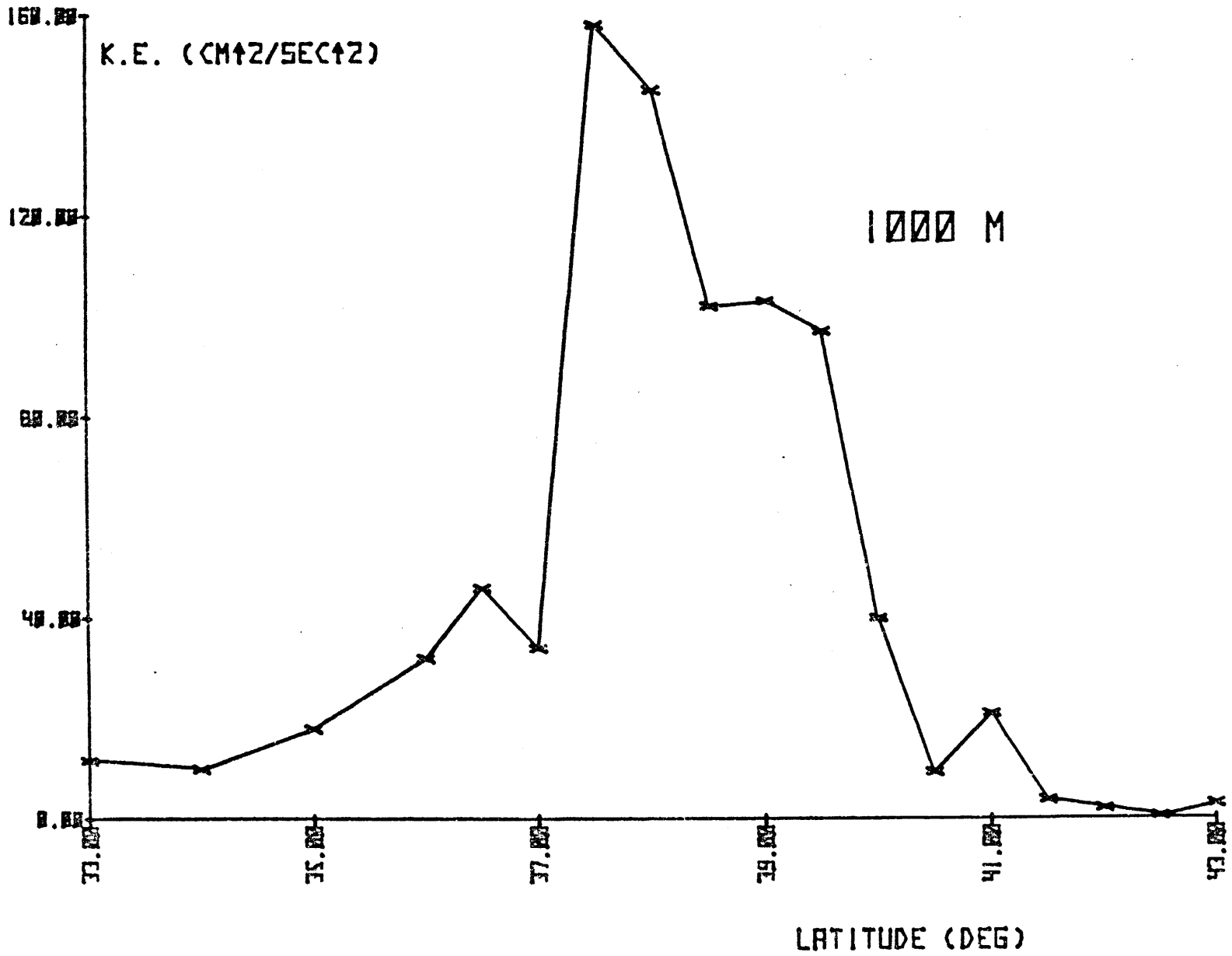

Figure 3.5b

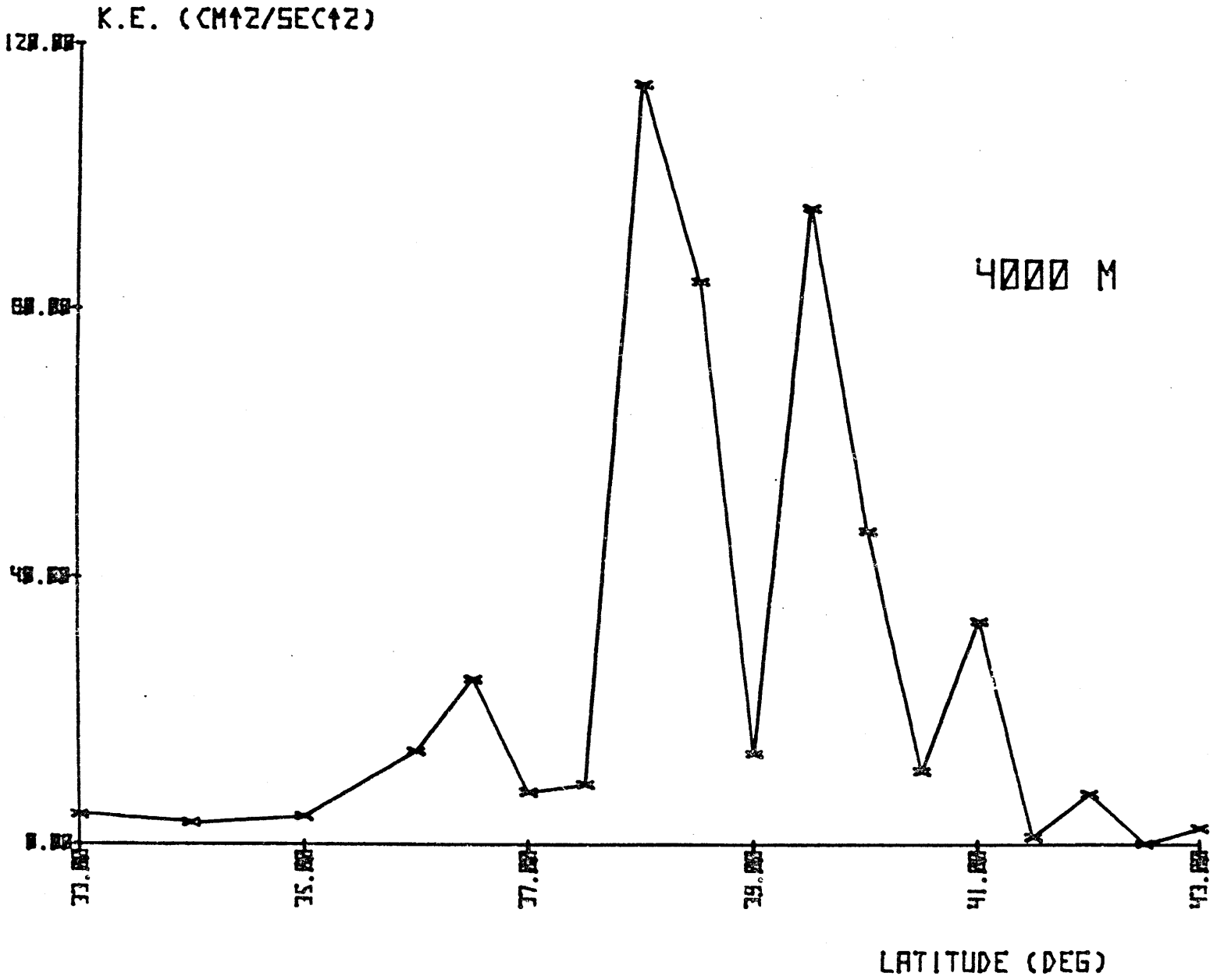

Figure 3.5c

Figure 4.1

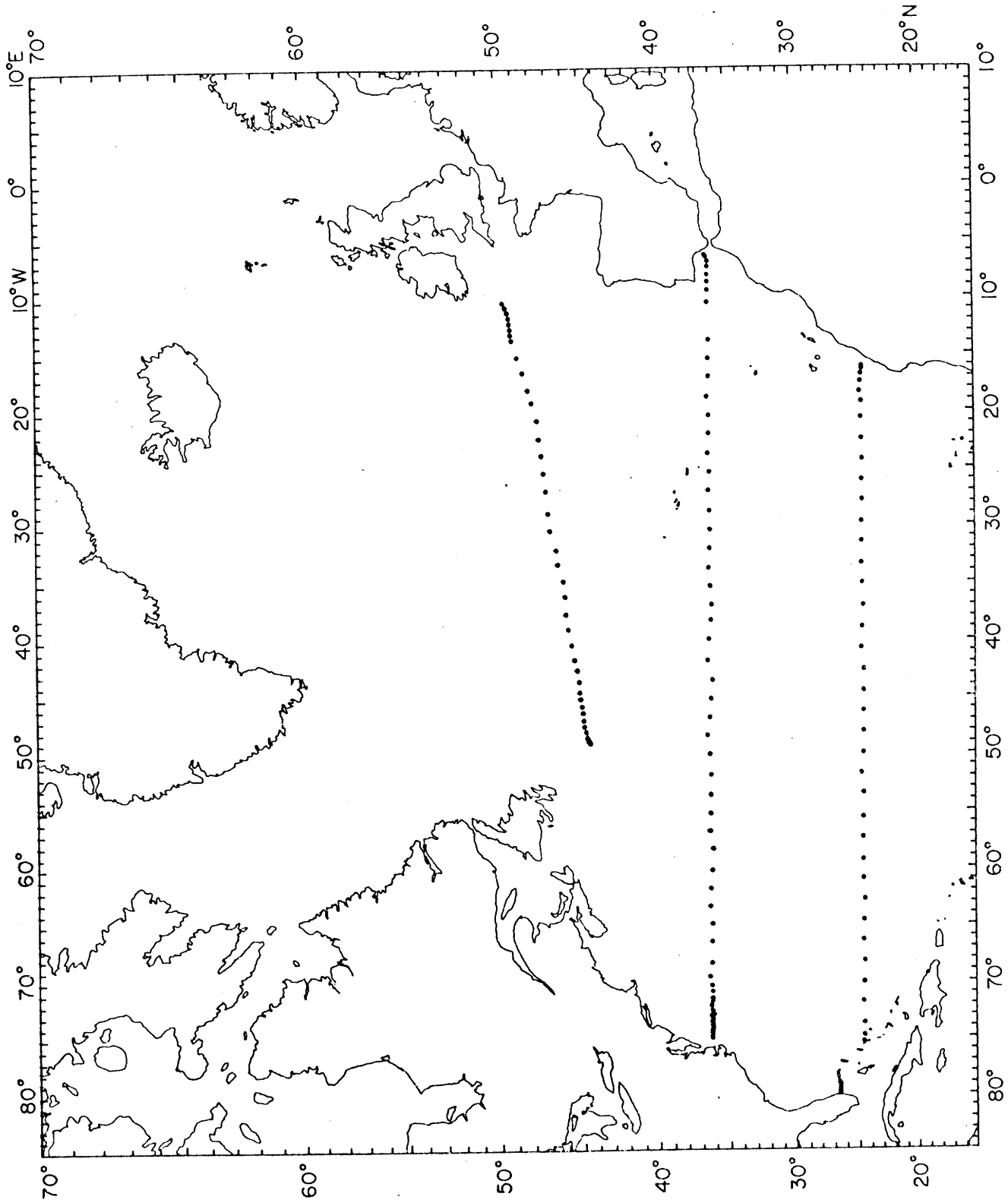

Figure 4.2

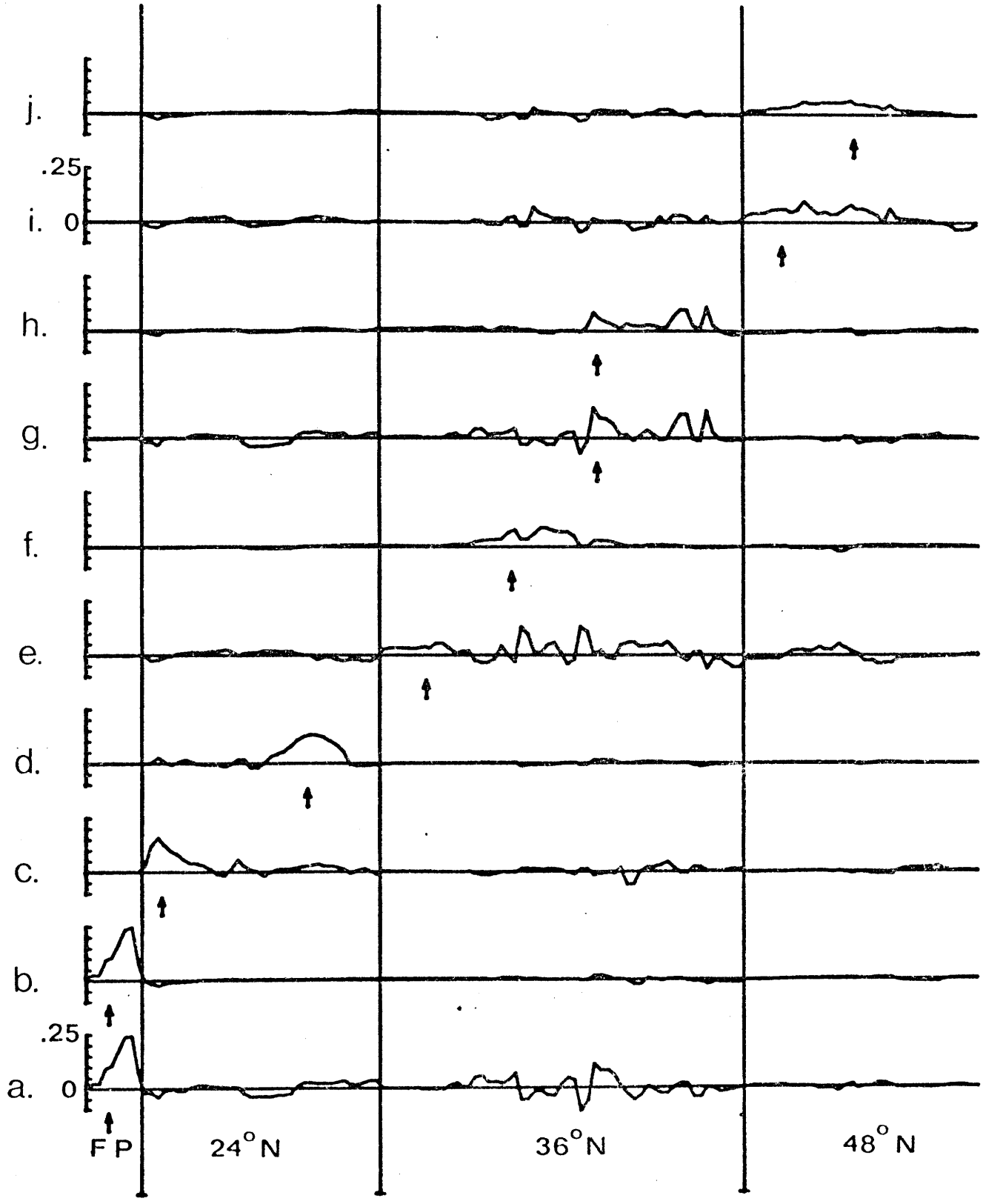

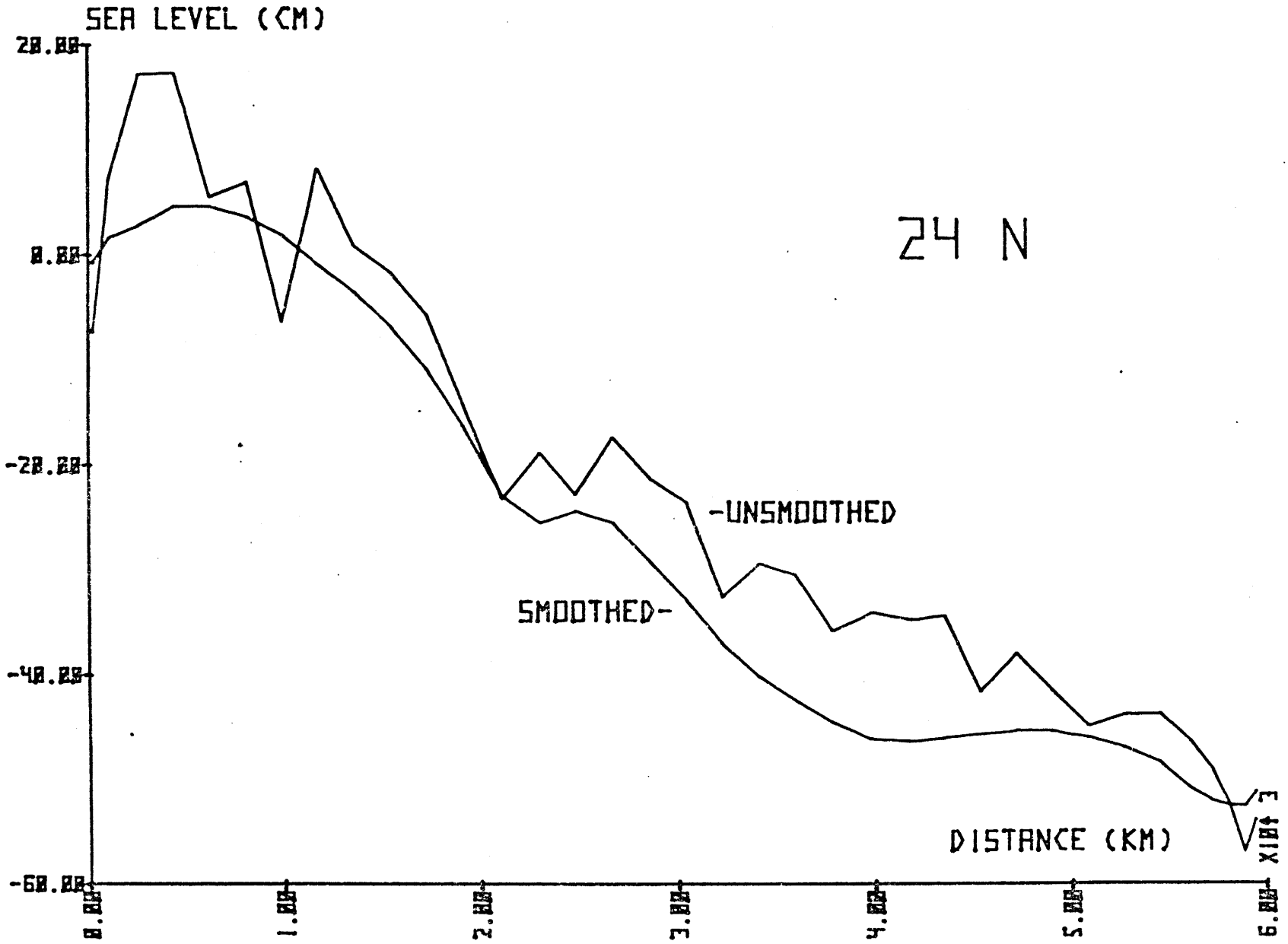
SEA LEVEL (CM)
20.00
0.00
-20.00
-40.00
-60.00
24 N
-UNSMOOTHED
SMOOTHED-
DISTANCE (KM)
0.00
1.00
2.00
3.00
4.00
5.00
6.00
X10↑3

Figure 4.3a

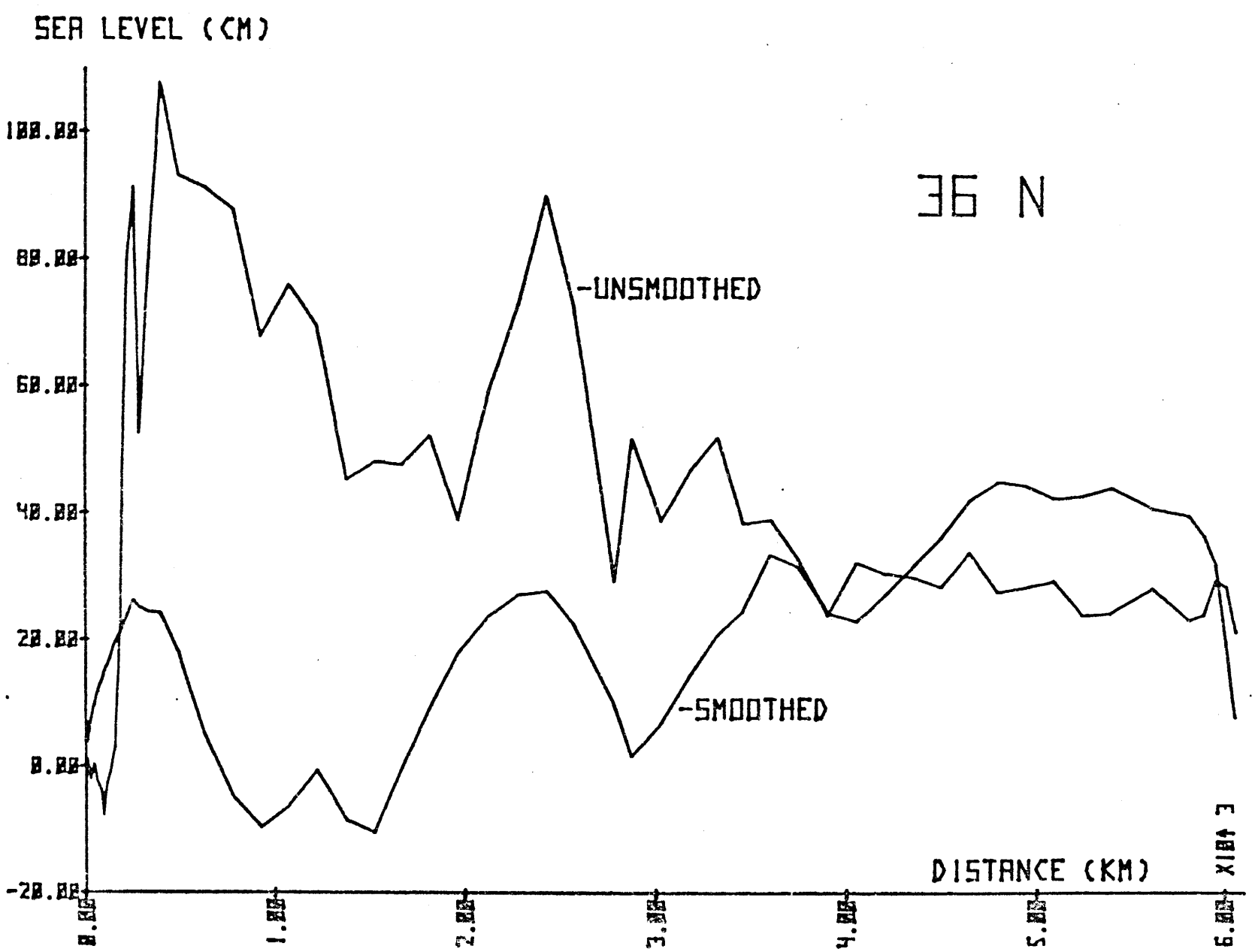
SEA LEVEL (CM)
100.00
80.00
60.00
40.00
20.00
0.00
-20.00
36 N
-UNSMOOTHED
-SMOOTHED
DISTANCE (KM)
0.00
1.00
2.00
3.00
4.00
5.00
6.00
E VBIX

Figure 4.3b

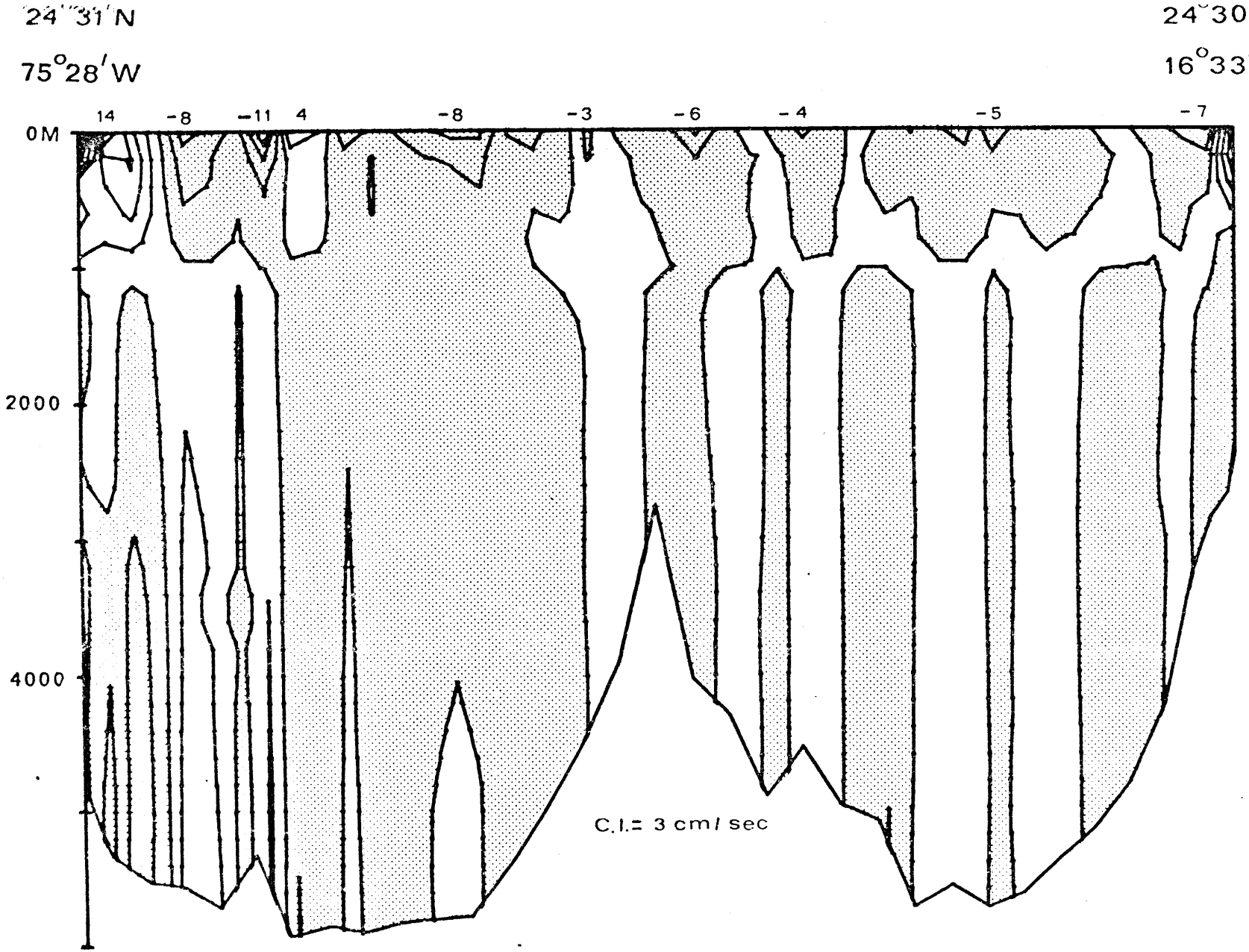
24°31'N
75°28'W
24°30'N
16°33'W
14
-8
-11
4
-8
-3
-6
-4
-5
-7
0M
2000
4000
C.I.= 3 cm/sec

Figure 4.4a

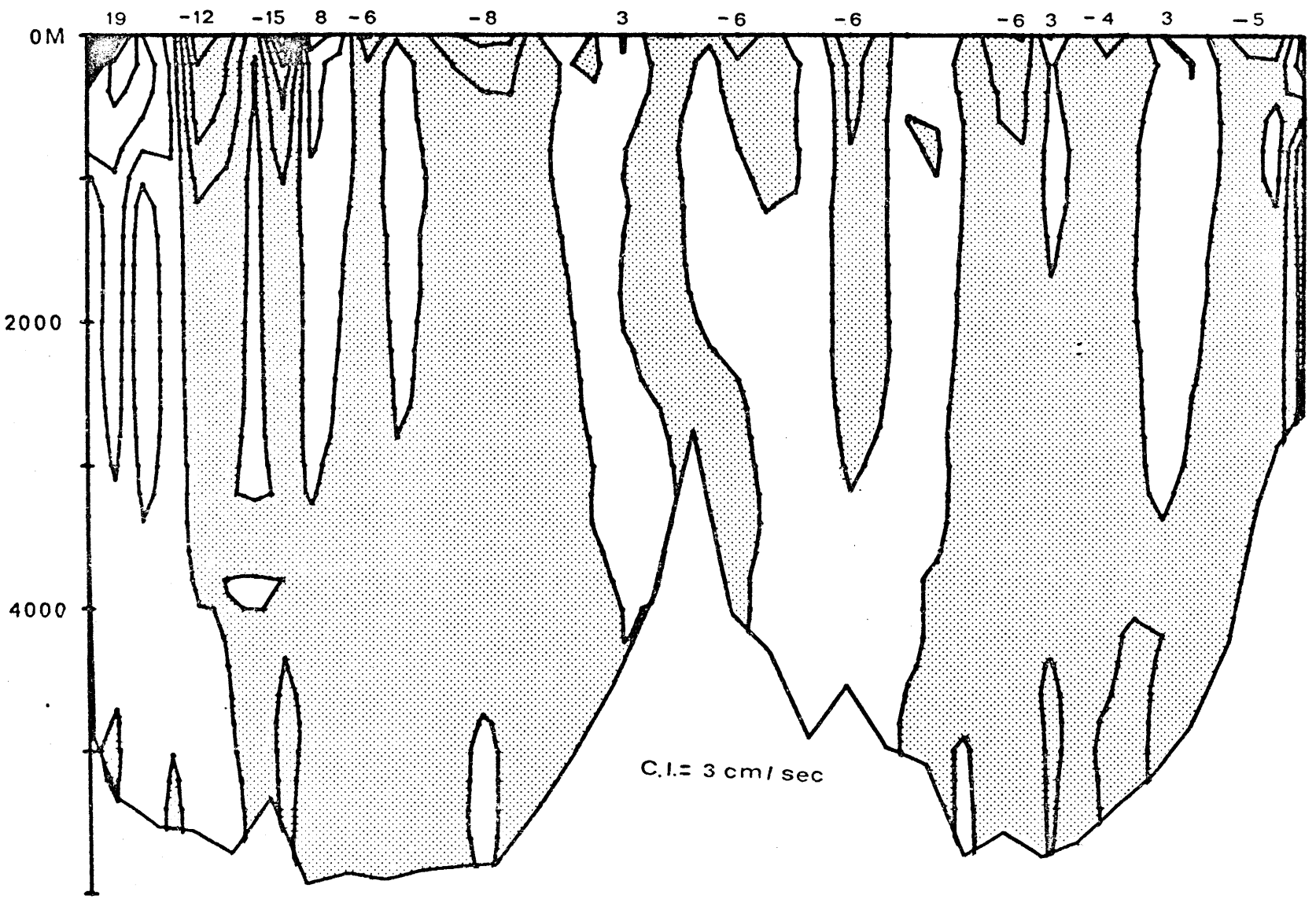
24°31′N
75°28′W
24°30′N
16°33′W
19
-12
-15
8
-6
-8
3
-6
-6
-6
3
-4
3
-5
0M
2000
4000
C.I.= 3 cm/ sec

Figure 4.4b

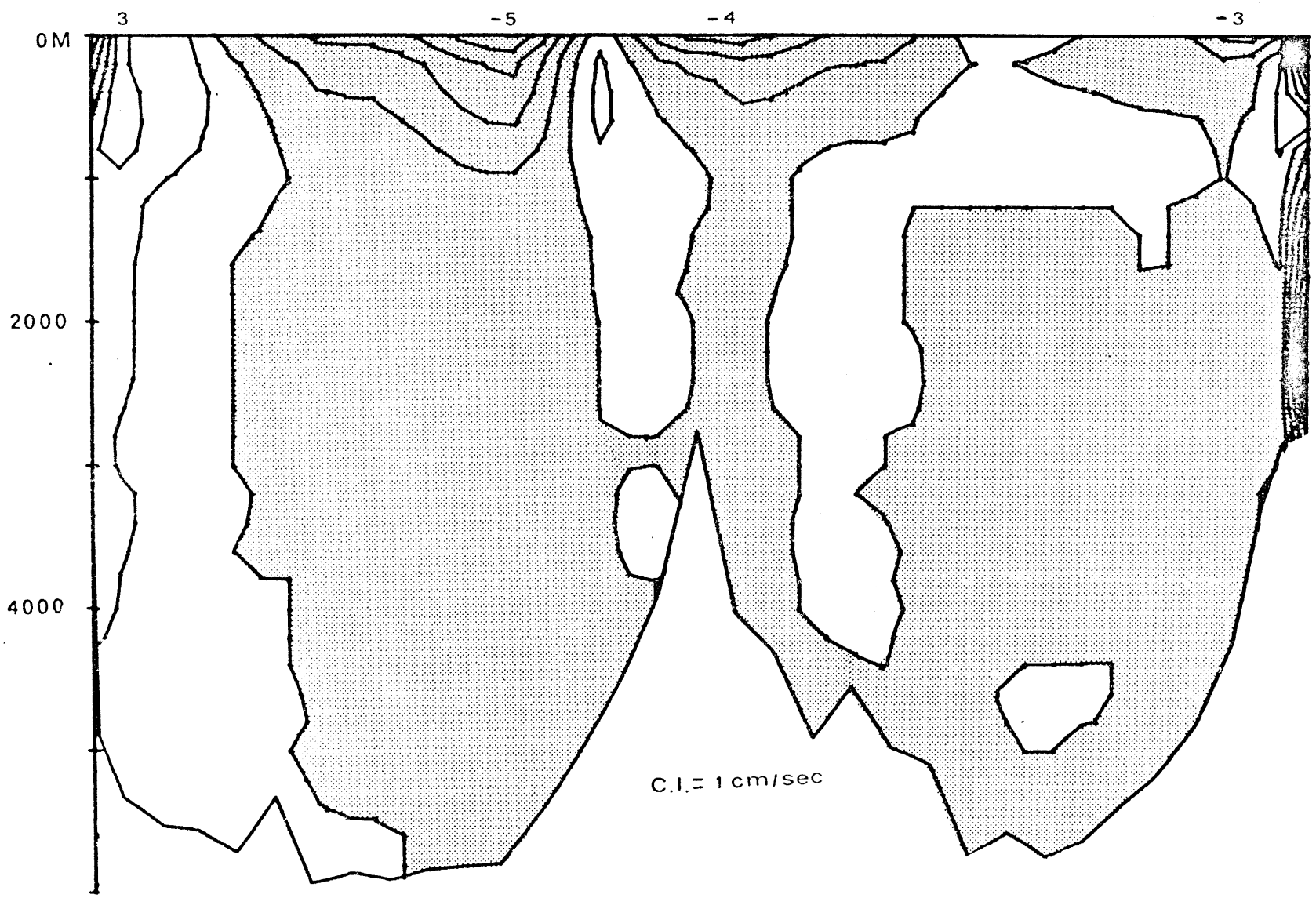

Figure 4.4c

Figure 4.5

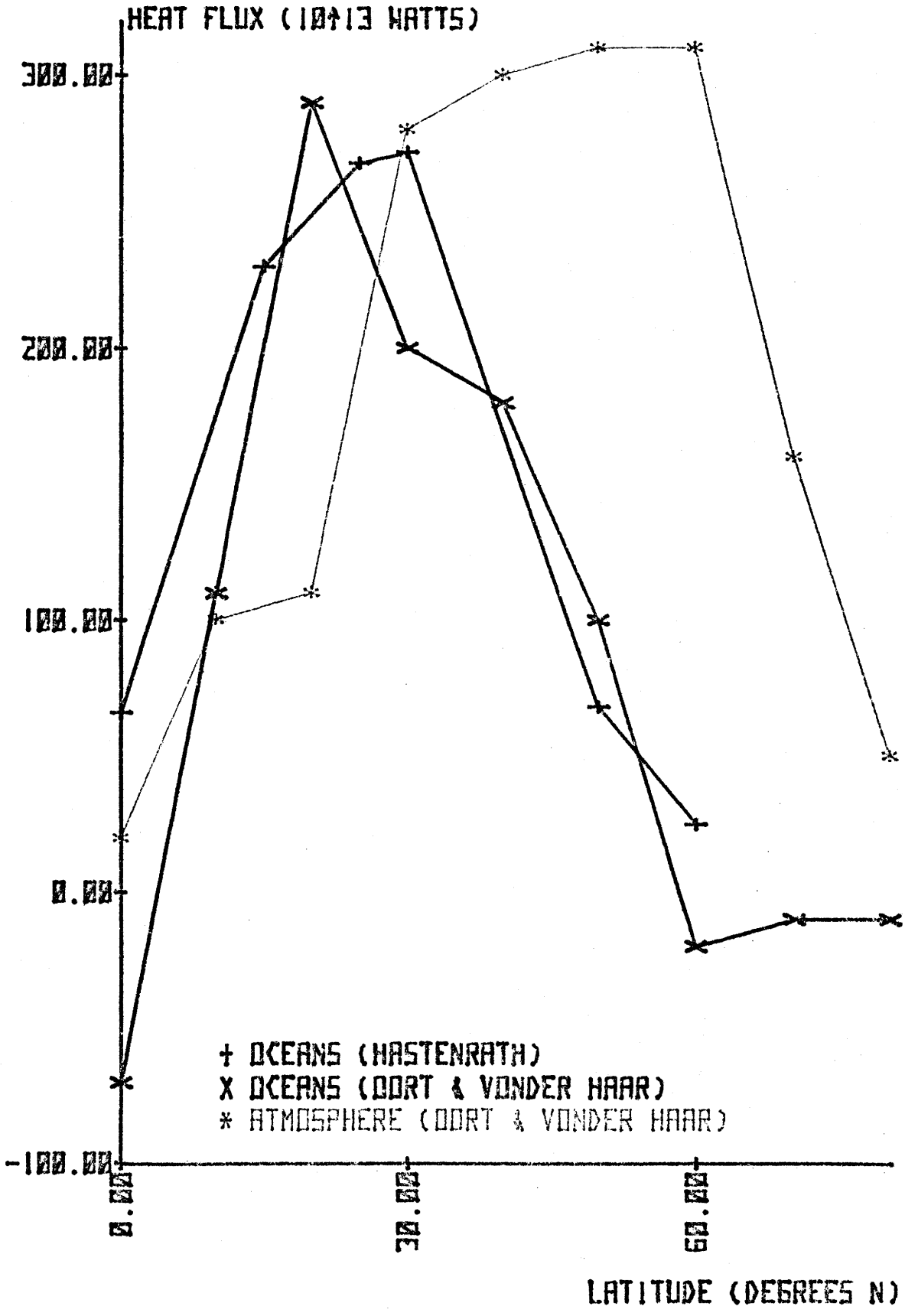
HEAT FLUX (10↑13 WATTS)
300.00
200.00
100.00
0.00
-100.00
0.00
30.00
60.00
LATITUDE (DEGREES N)
+ OCEANS (HASTENRATH)
X OCEANS (OORT & VONDER HAAR)
* ATMOSPHERE (OORT & VONDER HAAR)

Biographical Note

Dean H. Roemmich was born in Minneapolis, Minnesota in 1948. He received his B. A. degree in physics from Swarthmore College in 1970. During the years 1971-1975, he worked in the southwest Pacific, teaching general mathematics and science for two years at Tonga High School in Nuku'alofa, Tonga, and as Lecturer in Physics at the University of the South Pacific in Suva, Fiji in 1974. He also designed and coordinated teacher training programs as part of three Peace Corps training projects in the Kingdom of Tonga. He began work in the Joint Program in 1975.